Office of Naval Research
Contract N00014-67-A-0298-0012 NR-017-308
ARPA Contract SD-88

ELECTRICAL AND OPTICAL PROPERTIES OF HIGH QUALITY CRYSTALLINE V_2O_4 NEAR THE SEMICONDUCTOR-METAL TRANSITION TEMPERATURE

By
Larry A. Ladd

June 1971

Technical Report No. HP-26
Technical Report No. ARPA-41

Division of Engineering and Applied Physics
Harvard University · Cambridge, Massachusetts

MISSING PAGE
NUMBERS ARE BLANK
AND WERE NOT
FILMED

Unclassified

Security Classification

DOCUMENT CONTROL DATA - R & D

Security classification of title, body of abstract and indexing annotation must be entered when the overall report is classified

1. ORIGINATING ACTIVITY (Corporate author)

Division of Engineering and Applied Physics
Harvard University
Cambridge, Massachusetts

2a. REPORT SECURITY CLASSIFICATION

2b. GROUP

3. REPORT TITLE

ELECTRICAL AND OPTICAL PROPERTIES OF HIGH QUALITY CRYSTALLINE V_2O_4 NEAR THE SEMICONDUCTOR-METAL TRANSITION TEMPERATURE

4. DESCRIPTIVE NOTES (Type of report and inclusive dates)

Interim technical report

5. AUTHOR(S) (First name, middle initial, last name)

Larry A. Ladd

6. REPORT DATE	7a. TOTAL NO. OF PAGES	7b. NO. OF REFS
June 1971	209	161

8a. CONTRACT OR GRANT NO	9a. ORIGINATOR'S REPORT NUMBER(S)
N00014-67-A-0298-0012 and ARPA SD-88	Technical Report No. HP-26 Technical Report No. ARPA-41
b. PROJECT NO	
c.	9b. OTHER REPORT NO(S) (Any other numbers that may be assigned this report)
d.	

10. DISTRIBUTION STATEMENT

Reproduction in whole or in part is permitted by the U.S. Government.
Distribution of this document is unlimited.

11. SUPPLEMENTARY NOTES	12. SPONSORING MILITARY ACTIVITY
	Office of Naval Research

13. ABSTRACT

The object of this research is to contribute to our knowledge and understanding of the electrical and optical properties of high quality crystalline V_2O_4. This material exhibits a phase change at 65°C which is accompanied by a change in electrical resistivity of five orders of magnitude which is often referred to as a semiconductor-metal transition. Several theories had been suggested to explain the nature of this transition, but sufficient experimental evidence to determine which, if any, of these theories applied to V_2O_4 was not available at the time this research began. In particular, it was not known whether or not V_2O_4 was a Mott insulator below the transition temperature, or whether a band theory approach such as the Adler-Brooks theory might describe the transition. This research has resulted in experimental measurements and theoretical analysis which permit a tentative explanation of the transition mechanism to be made.

In the course of this investigation high quality crystals were grown and their electrical and optical properties were measured. Crystals were grown which had a larger and sharper change in resistance than had been previously reported. Their resistivity and optical transmission and reflection were carefully measured both above and below the transition temperature. The resistivity was also measured during the transition process. An optical absorption edge was observed in the low temperature state and its temperature dependence was carefully measured. The dependence of the semiconducting resistivity and the transition temperature on c-axis uniaxial stress was also determined.

A theoretical analysis of these measurements and the recent theoretical and experimental work of other investigators is presented in order to characterize the properties of the low and high temperature phases and the nature of the transition mechanism. The high temperature state appears to have a partly filled conduction band and metallic conductivity. The mean free path is short, however, and correlation effects are probably present. The low temperature phase appears to be describable in terms of one electron band theory and is characterized by the fact that the 3d electrons are localized in pair bonds. The mean free path is short and correlation effects are present, but the material is not a Mott insulator. The measurement of the temperature dependence of the energy gap shows that the number of carriers does not avalanche just before the transition temperature. This allows the Adler-Brooks theory and several other theories of the transition to be eliminated. A thermodynamic analysis is performed which shows that the transition can be characterized as being due to the difference in Helmholtz function $F=U-TS$ between two phases with different crystal structures, band structure and phonon spectrum. The change in the band structure and the pairing up of the electrons are related to the change in crystal structure. The changes in the phonon spectrum and the band structure are probably related since the electron-phonon interaction is large. A model relating the change in the phonon spectrum to the change in the number of carriers via screening effects is suggested.

DD FORM 1 NOV 65 1473 (PAGE 1)

S/N 0101-807-6801

Unclassified

Security Classification

14 KEY WORDS	LINK A		LINK B		LINK C	
	ROLE	WT	ROLE	WT	ROLE	WT
Transition metal oxides						
Insulator-metal transitions						
Mott transitions						

Office of Naval Research

Contract N00014-67-A-0298-0012

NR - 017 - 308

ELECTRICAL AND OPTICAL PROPERTIES OF HIGH QUALITY CRYSTALLINE V_2O_4 NEAR THE SEMICONDUCTOR-METAL TRANSITION TEMPERATURE

By

Larry A. Ladd

June 1971

Technical Report No. HP-26

Technical Report No. ARPA-41

The research reported in this document was made possible through support extended the Division of Engineering and Applied Physics, Harvard University, by the Office of Naval Research, under Contract N00014-67-A-0298-0012 and by the Advanced Research Projects Agency under Contract ARPA SD-88.

Division of Engineering and Applied Physics

Harvard University Cambridge, Massachusetts

ABSTRACT

The object of this research is to contribute to our knowledge and understanding of the electrical and optical properties of high quality crystalline V_2O_4. This material exhibits a phase change at 65°C which is accompanied by a change in electrical resistivity of five orders of magnitude which is often referred to as a semiconductor-metal transition. Several theories had been suggested to explain the nature of this transition, but sufficient experimental evidence to determine which, if any, of these theories applied to V_2O_4 was not available at the time this research began. In particular, it was not known whether or not V_2O_4 was a Mott insulator below the transition temperature, or whether a band theory approach such as the Adler-Brooks theory might describe the transition. This research has resulted in experimental measurements and theoretical analysis which permit a tentative explanation of the transition mechanism to be made.

In the course of this investigation high quality crystals were grown and their electrical and optical properties were measured. Crystals were grown which had a larger and sharper change in resistance than had been previously reported. Their resistivity and optical transmission and reflection were carefully measured both above and below the transition temperature. The resistivity was also measured during the transition process. An optical absorption edge was observed in the low temperature state and its temperature

dependence was carefully measured. The dependence of the semiconducting resistivity and the transition temperature on c-axis uniaxial stress was also determined.

A theoretical analysis of these measurements and the recent theoretical and experimental work of other investigators is presented in order to characterize the properties of the low and high temperature phases and the nature of the transition mechanism. The high temperature state appears to have a partly filled conduction band and metallic conductivity. The mean free path is short, however, and correlation effects are probably present. The low temperature phase appears to be describable in terms of one electron band theory and is characterized by the fact that the 3d electrons are localized in pair bonds. The mean free path is short and correlation effects are present, but the material is not a Mott insulator. The measurement of the temperature dependence of the energy gap shows that the number of carriers does not avalanche just before the transition temperature. This allows the Adler-Brooks theory and several other theories of the transition to be eliminated. A thermodynamic analysis is performed which shows that the transition can be characterized as being due to the difference in Helmholtz function $F = U - TS$ between two phases with different crystal structures, band structure and phonon spectrums. The change in the band structure and the pairing up of the electrons are related to the change in crystal structure. The changes in the phonon spectrum

and the band structure are probably related since the electron-phonon interaction is large. A model relating the change in the phonon spectrum to the change in the number of carriers via screening effects is suggested.

TABLE OF CONTENTS

LIST OF FIGURES

Chapter I

INTRODUCTION

The object of this research is to contribute to our knowledge and understanding of the electrical and optical properties of high quality crystalline V_2O_4. This material exhibits a phase chance at 65°C which is accompanied by a change in the electrical resistivity of several orders of magnitude which is often referred to as a semiconductor-metal transition. In the course of this investigation high quality V_2O_4 crystals were grown, their electrical and optical properties were measured, and the effect of stress on their electrical properties was determined. Based on these and other measurements the nature of the high and low temperature states and the nature of the phase transition are discussed.

This chapter is concerned with describing how our program of research was motivated and what type of measurements we wanted to make. Consequently only work which was published prior to the start of this project in 1966 will be mentioned, and later developments will be included in Chapter VI. The first section presents some background information on the problem of understanding the conductivity of transition metal oxides. The next section considers semiconductor-metal transitions and discusses the experimental information which was available about materials which exhibited these transitions and the theoretical models which had been presented to explain these transitions when this work was begun. The Adler-Brooks model of the transition which appeared to have been successfully applied to V_2O_3 is

discussed in detail. The next section outlines the original plan of this research program and includes the measurements we wanted to make and the theories we wanted to test. The last section of this chapter is a summary of the information which was known about V_2O_4 when this research began.

A. Conductivity in Transition Metal Oxides

In this section we will briefly discuss the failure of Bloch-Wilson band theory to adequately predict the extremely low conductivity of materials such as MnO or NiO, and we will consider whether the electron-phonon interaction or correlation effects could be responsible for the high resistivity of these materials. This section is not meant to be an exhaustive or complete review of the subject of conduction in transition metal oxides, but rather is meant to acquaint the reader with some of the problems which we felt might arise in trying to understand the conductivity of V_2O_4. A more complete discussion of the conductivity of transition metal oxides can be found in the article by David Alder in volume 21 of Solid State Physics.

In most discussions of the chemistry of the transition metal oxides, the bonding is assumed to be largely ionic [1]. In this case the oxygen 2p states become the bonding orbitals and the transition metal 4s states become the antibonding orbitals [1]. The splitting between these bonding and antibonding orbitals is approximately 20 eV, and the 3d levels are generally assumed to lie somewhere between the 2 p and 4s levels [1]. The 2p levels would thus be full, the 4s

levels empty, and the 3d levels partly filled. If the bonding were strongly ionic we would expect the 3d electrons to spend most of their time near the metal cations and the 3d energy levels could be described by crystal field theory. For materials like NiO this type of behavior is experimentally verified by the fact that sharp crystal field absorption lines have been observed [2]. For the oxides of the transition metals near the titanium end of the 3d series, however, there is evidence that the bonding is somewhat less ionic. Consider for example the LCAO calculation of the band structure of $SrTiO_3$ done by Kahn and Leyendecker [3]. They found that the calculated band structure was in agreement with measurements on $SrTiO_3$ when the charge on each oxygen ion was -1.68e rather than the fully ionized value of -2e. This reduced the splitting between the oxygen 2p levels and the titanium 4s levels from ~ 25 eV to ~ 11 eV. The titanium 3d band was then found to be located ~ 3 eV above the oxygen 2p band. Although this calculation cannot be considered as definitive, it does give some idea of the ionicity and the position of the bands to be expected in the transition metal oxides near the titanium end of the series. When the bonding is only partly ionic, we expect that the unbonded electrons would only be partially localized on the cations and that the energy levels of these 3d electrons could be described by tight binding band theory. In the rest of this section we will assume that the electrical and optical properties of the unsaturated 3d transition metals oxides can be attributed to the properties of the partially filled 3d bands and that these bands can be described

in a first approximation by using tight binding band theory.

Let us now apply Bloch-Wilson band theory to MnO. This material is antiferromagnetic and the room temperature resistivity of pure MnO is about 10^{15} Ω cm. Each manganese ion has five 3d electrons remaining after satisfying the chemical bonds. The material has the NaCl structure above the Neel temperature and a distorted NaCl structure which increases the size of the unit cell below the Neel temperature. An insulating state below T_N can be explained in terms of band theory if one assumes that the exchange splitting is greater than the crystal field splitting. Each cation would then have two fivefold degenerate sets of levels separated from each other by an energy gap. The lower set of states would be full and the upper set empty. Above the Neel temperature, however, it is impossible to explain an insulating state in terms of one-electron band theory. In this case each cation has a lower t_{2g} level which is sixfold degenerate and an upper e_g level which is fourfold degenerate. The spin orbit splitting can reduce the degeneracy of these levels, but each level must remain at least twofold degenerate due to Kramer's theorem. Thus above T_N Bloch— Wilson band theory predicts that MnO should have a partly filled band and should therefore be metallic. In the rest of this section we will consider the possible explanations of the fact that Bloch-Wilson band theory cannot be used to describe the properties of some transition metal oxides, such as MnO.

It was first realized in 1937 by DeBoer and Verwey that there were some materials such as NiO which did not obey the predictions of

Bloch-Wilson band theory [4]. They offered the qualitative explanation that the electrons were localized by the high potential barriers between cations. A mechanism for such a trapping of electrons in polar crystals by the formation of polarons was suggested by Gurney and Mott [5]. In 1938 Wigner introduced the electron-electron interaction e^2/r_{12} into the problem. He argued that the electrons potential energy would be larger than their kinetic energy at low densities and that the potential energy would be lowest if the electrons were localized in a periodic non-conducting array. In 1949 Mott discussed the case of a cubic lattice of one electron atoms with a variable lattice constant d, and he gave arguments that for large values of d the material would be an insulator and for small values of d a metal [6]. He showed that when d becomes large, the potential energy arising from the electron-electron interaction becomes quite large and cannot be included as a small correction to the electron energy which results from the periodic potential. Consequently, one-electron band theory is not a suitable description of the material and an insulating state can arise when d is large. We thus have two possible explanations of the low conductivity of materials such as MnO or NiO: polaron effects and electron-electron correlation effects.

Let us consider how polaron effects could modify Bloch-Wilson band theory. A small polaron can be considered to be an electron which is trapped in the potential well which arises from the distortion of the lattice around the electron. Polarons generally only occur in ionic materials where the electron-lattice interaction is large. In ionic

crystals the electrons interact most strongly with longitudinal optical phonons and an electron-phonon coupling constant α which measures the strength of this interaction can be defined by

$$\alpha = \frac{e^2}{2\hbar\omega_\ell}\left[\frac{2m^*\omega}{\hbar}\right]^{\frac{1}{2}}\left(\frac{1}{\epsilon_\infty} - \frac{1}{\epsilon_o}\right) \qquad [7].$$

In this expression ω_ℓ is the longitudinal optical phonon frequency, ϵ is the frequency dependenc dielectric constant, and m* is the effective mass given by Bloch-Wilson band theory. The factor $(\epsilon_\infty^{-1} - \epsilon_o^{-1})$ is present because we are interested only in the ionic contribution to the electron-lattice interaction. In the large polaron or weak coupling limit where $\alpha \leq 1$, the phonon self energy is given by $E_o = -\alpha\hbar\omega_\ell$ and the polaron effective mass is given by $m_p = m^*(1 + \frac{1}{6}\alpha)$ [7]. In the strong coupling or small polaron limit where $\alpha \geq 10$, Holstein has shown that at low temperatures a polaron band exists whereas for temperatures above one half the Debye temperature the quasi-particle bandwidth has effectively shrunk to zero and the polarons are essentially localized [8]. At low temperatures the polaron effective mass is given by $m_p = m^* \frac{1}{50}\alpha^4$ which may be quite large and the polaron self energy is given by $E_o = -0.1\ \alpha^2\hbar\omega_\ell$ [9]. At high temperatures the conduction which occurs will be by diffusive hopping between adjacent sites rather than by the correlated motion described by band theory and so the mobility may be quite small [8]. Thus at either low or high temperatures small polaron theory is capable of lowering the mobility of the conduction electrons, but polaron theory is not capable of producing an energy gap in a material that would otherwise have a partly filled band. Thus it is unlikely that polaron theory by itself could account for the extremely low conductivity of materials like MnO.

Let us now consider how correlation effects could modify Bloch-Wilson band theory. First let us note that Bloch-Wilson band theory is based on the Hartree-Fock method in which a single particle wave function is solved. In writing the Hamiltonian for a single electron, the assumption is made that the energy of an electron resulting from its interaction with all other electrons can be derived from the periodic potential caused by the other electrons average distribution of charge. If we consider the case of a crystal which is composed of atoms whose outer shell has one s electron and which has one atom per unit cell, then Bloch-Wilson band theory would predict that the crystal is metallic because it has a half filled band. Now let us make the assumption that we are dealing with a material that has narrow bands and where the tight binding or Heitler-London approximation is appropriate. In this case the overlap between orbitals will be small and the electronic energy levels will not be too different from the atomic energy levels. Consider now a particular atomic site at which is located an electron with energy E_O. A second electron placed at the same site will have an additional energy ΔE_c since a Coulomb repulsive force will have to be overcome in order to place a second electron on the same site. If the bandwidth Δ is less than ΔE_c, then at $T = 0$ there will be two bands, one full and one empty. The splitting ΔE_c between the bands arises because the energy of each electron depends on whether or not there is another electron on the same site. This interaction cannot be reduced to an effective potential energy term $V(r)$ as is required by the Hartree-Fock method. Thus this interaction cannot be incorporated into Bloch-Wilson band theory. As Mott has pointed out, these correlation effects become more important as the lattice spacing is increased, and Kohn has given a formal proof that for large enough d, a one dimensional array of monovalent atoms is non-conducting [10].

Hubbard has considered the case of a partially filled s band for which the Hartree-Fock problem has been solved. He has explicitly introduced correlation effects into band theory by considering the following simple Hamiltonian

$$H = \sum_{ij\sigma} T_{ij}\, c_{i\sigma} c^{+}_{j\sigma} + U \sum_{i}\, n_{i\uparrow} n_{i\downarrow}$$

which is written in the Wannier representation where i and j represent lattice sites and σ represents spin. The first term is the normal Hartree-Fock term and the second term is the correlation term. The constant $U = \langle ii|\frac{e^2}{r}|ii\rangle$ is the Coulomb matrix element for electrons on the same site. Thus U represents the Coulomb energy necessary to place two electrons on the same site, and the second term in the Hamiltonian just counts the number of doubly occupied sites and multiplies by U. This Hamiltonian thus only includes intra-atomic Coulomb interactions and ignores all nearest neighbor and longer range Coulomb interactions which are also important.

In the atomic limit of zero bandwidth this problem can be solved exactly by means of retarded and advanced Green's functions [11]. Two energy levels are found to exist for adding the next electron, one at energy 0 with weight proportional to the number of unoccupied atoms, and one at an energy U with weight proportional to the number of atoms already containing an electron of opposite spin. This is the sort of behavior that we would intuitively expect.

For the case of wider bands, the problem becomes quite difficult mathematically and only approximate solutions are possible. Hubbard

has written several papers analyzing the behavior of this Hamiltonian [11, 12, 13, 14]. He finds that as the Hartree Fock bandwidth increases from zero, the two energy levels described above broaden into bands. For the special case of parabolic bands he found by an approximation method that when the bandwidth Δ was such that $(\Delta/U) = 2/\sqrt{3}$, the separation between the bands is reduced to zero as is shown in Figure I-1 [13]. Similar results have been obtained by Gutzwiller [15] and Kemény [16]. We thus expect that correlation effects can give an insulating state for narrow band materials with large values of U. Since as we have already mentioned, the transition metal oxides near the nickel of the series are thought to have narrow bands, these correlation effects may account for the insulating behavior of materials such as NiO or MnO.

B. Transition Metal Oxides with Semiconductor-Metal Transitions

There are several transition metal oxides which undergo phase changes which are accompanied by large discontinuities in resistivity. This phenomenon was first observed by Foëx in 1948 on powdered samples of V_2O_3 which exhibited a sharp change in the resistivity and the sample volume near 140°K [17]. Morin observed transitions in single crystal samples of V_2O_3, V_2O_4, VO, and Ti_2O_3 in 1958 and reported the data shown in Figure I-2 [18]. Since then several other transition metal oxides and sulfides have been found to exhibit similar behavior [1]. At the time that this work began, V_2O_3 was the material which had been studied in the most detail and had been shown to have a change

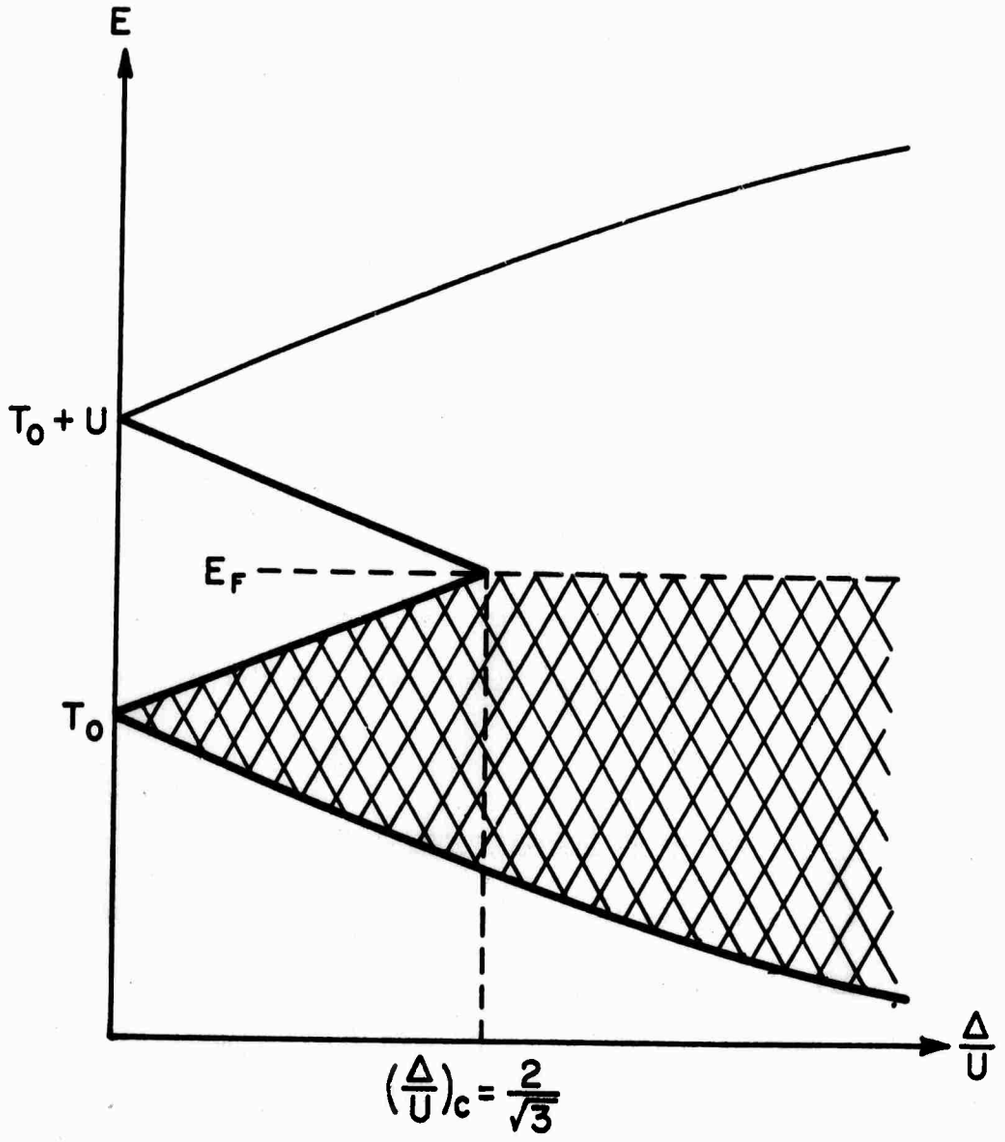

FIGURE I-1 Pseudoparticle band structure as a function of the ratio of bandwidth Δ to intra-atomic Coulomb matrix element U for the case of a single s band. (After Hubbard [13]).

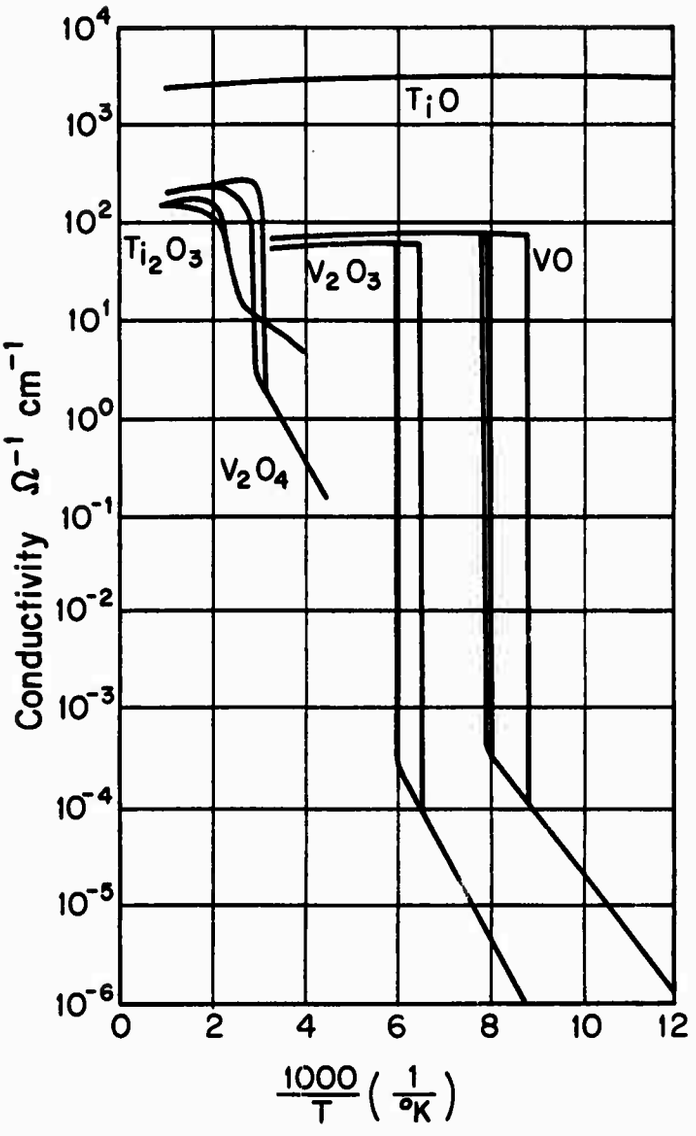

FIGURE I-2 Conductivity as a function of reciprocal temperature for the lower oxides of vanadium as measured by Morin [18].

in resistivity by a factor of 10^7 near 140°K by Feinleib and Paul [19, 20]. This material undergoes a phase change which is accompanied by a latent heat and a change in the crystal structure at the transition temperature [19, 20]. Notice in Figure I-2 that the temperature dependence of the resistivity in the low temperature phase is like that of an intrinsic or lightly doped semiconductor and in the high temperature phase is like that of a metal. Optical transmission measurements made on the material in the semiconducting state were suggestive of an energy gap of about 0.1 eV [19].

When this research began, there were several theoretical models which had been presented to try and explain semiconductor-metal transitions in transition metal oxides. Slater had proposed that a half filled band could be split into a filled and an empty band by antiferromagnetism [21]. This theory would require that the low temperature phase was antiferromagnetic and that the transition temperature was the Neel temperature. Mott had shown that if the lattice spacing of a material was reduced then a sharp semiconductor-metal transition could occur as the result of exciton effects [6], but the transition metal oxides which have these transitions do not have negative coefficients of thermal expansion. Hubbard has shown using the Hubbard Hamiltonian model that a material is a Mott insulator if $(\Delta/U) < 1.2$ where as was defined above Δ is the bandwidth and U is the Coulomb energy of two electrons on the same atom [13]. If (Δ/U) is an increassing function of temperature, then a semiconductor-metal transition could occur at the temperature where Δ/U reaches a critical value.

This model, however, does not predict a sharp transition. Another possibility is that the critical value of (Δ/U) is temperature dependent. In any case it is certainly possible for correlation effects to produce a semiconductor-metal transition. Goodenough has postulated that the transition can arise from the formation of homopolar bands between the cations at low temperature [22]. He has also suggested that the distortion which occurs in the crystal structures of V_2O_4 and V_2O_3 is compatible with cation pairing at low temperatures. For V_2O_4 in particular the c-axis cations which are evenly spaced for $T > T_c$ are quite unambiguously paired up for $T < T_c$ with spacings alternating between 0.265 nm and 0.312 nm. Considering the number of available electrons per cation, we find that such bonds could account for the lack of metallic conductivity at low temperatures of both materials.

Another simple model of a semiconductor-metal transition is band overlap. If a bandgap existed which had a large negative temperature coefficient, then the conductivity of the material would increase rapidly as the band gap reduced to zero and became negative. This would, however, produce a gradual transition. If excitons were produced -- as Mott has suggested [6] -- the transition would be sharpened somewhat, but this still would not produce a sudden transition where the resistivity changed by several orders of magnitude.

Polarons were discussed in Section A,and we noted that polaron conductivity is by polaron bands at low temperatures and by polaron hopping at high temperatures. Thus the only type of a transition that could be produced by polaron effects is from a state with low mobility at low temperatures to a state with even lower mobility at

high temperatures. This is exactly the opposite behavior from that observed in materials like V_2O_3 and shows that the transition is not caused by polaron effects.

We will consider a theory of the semiconductor-metal transition which was presented by Adler and Brooks in some detail [23, 24]. This theory assumes that ordinary band theory is appropriate and that the material has a band gap in the lower temperature state which is given by $E_g = (E_g)_o - \beta n$ where $(E_g)_o$ is the band gap at $T = 0$, n is the carrier concentration in the conduction band, and β is a constant. Thermodynamically it can be shown that such a relationship is always valid at low temperatures if the band gap has any stress or pressure dependence [25]. If the value of β is large enough, Adler and Brooks show that a semiconductor-metal transition can result. They also show how a large value of β can occur in a material where the semiconductor-metal transition is accompanied by a crystalline distortion which results in a pairing up of the cations below the transition temperature.

Let us sketch out some of the features of their theory by considering a one dimensional chain of hydrogen atoms which are paired up as is shown in Figure I-3. If the potential at each atom is considered to be a negative delta function, then the band structure can be calculated and is shown in Figure I-3. When the distortion parameter $\epsilon = 0$, we have a half filled band, and when $\epsilon \neq 0$ a gap is introduced in the density of states. When the bandwidth is small, it can be shown that an energy gap proportional to ϵ is produced. Since filled states are lowered in energy and unfilled states are raised, we see that the

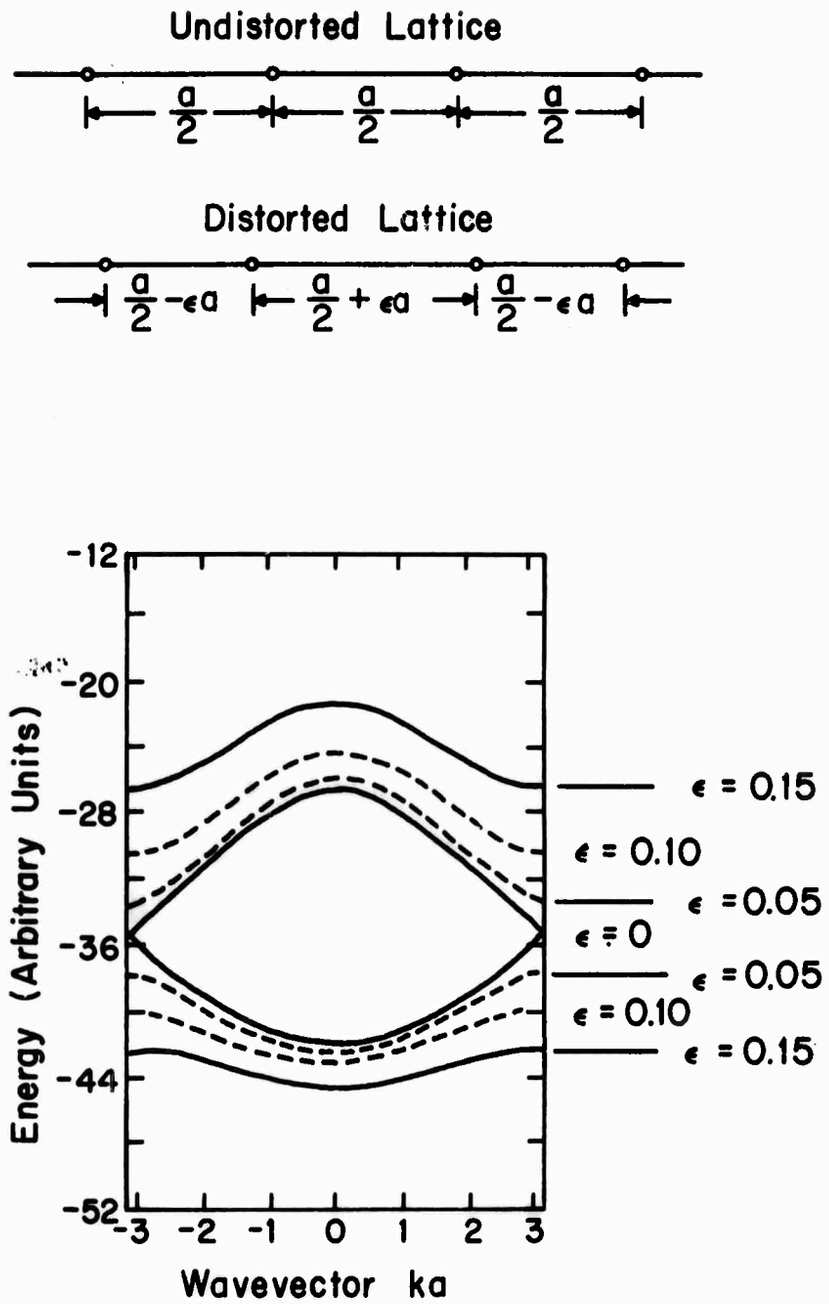

FIGURE I-3 The distortion parameter ϵ and the dependence of E(k) on ϵ in one dimension as calculated by Adler and Brooks [23].

distorted configuration has the lower energy and is more stable. If we investigate the nature of the wave functions in the two bands, we find that the lower band is a bonding band and the upper band is an antibonding band. If we now assume that the distortion ϵ is caused by the formation of chemical bonds, then the distortion will be proportional to the number of bonded electrons, or $\epsilon = \epsilon_0\left(1 - \frac{n}{N}\right)$ where n is the number of electrons in the conduction band and N is the number of states in the conduction band. We can thus say that $E_g \sim \epsilon \sim \left(1 - \frac{n}{N}\right)$ or $E_g = (E_g)_0 - \beta n$. Adler and Brooks have also shown that a similar carrier dependence of the energy gap can arise from antiferromagnetism [23,24].

Let us now consider the consequences of such a carrier dependent energy gap. Qualitatively one can argue that as the temperature increases, the number of carriers in the conduction band increases and this in turn causes the band gap to shrink. But a smaller band gap also causes the number of carriers in the conduction band to increase. Thus $\frac{dn}{dT}$ increases with temperature and at a critical temperature T_0, $\frac{dn}{dT} \to \infty$ and the band gap disappears suddenly which gives rise to a semiconductor-metal transition. At the same time as the temperature increases from about 0.8 T_0 to T_0, the energy gap shrinks by perhaps 25% or more. Adler and Brooks have shown rigorously that such behavior does occur for the case of narrow band materials where the bandwidth is less than the band gap at T = 0. They have also shown that the ratio $(E_g)_0/kT_0$ is an increasing function of bandwidth and that their narrow band analysis is valid up to the point where $(E_g)_0/kT_0 \sim 10$. In the narrow band limit they have also shown that the ratio $(E_g)_0/kT_0$ is a constant independent of external stress

or pressure. They thus predict that $\frac{d\,\ell n(E_g)_o}{dx}$ should be equal to $\frac{d\,\ell n(T_o)}{dx}$ where x is an external parameter such as stress or pressure.

This theory has been applied to V_2O_3 and was found to be in good agreement with the measurements of Feinleib and Paul [19, 20]. Using the X-ray data of Warekois [26], the low temperature distortion of V_2O_3 was interpreted by Goodenough [22] as resulting in a pairing up of each cation with two other cations. Thus it was reasonable to investigate whether the Adler-Brooks theory is applicable. Using the value of 0.1 eV for the energy gap which was estimated by Feinleib and Paul [20], the ratio $(E_g)_o/kT_o$ was found to be 8.3 which means that the narrow band analysis is appropriate. Feinleib and Paul measured the uniaxial stress and hydrostatic pressure dependence of the transition temperature and the resistivity. If the mobility is assumed to be relatively independent of stress and pressure, then the ratio $(E_g)_o/kT_o$ is found to be unchanged by the application of either stress or pressure. Thus the predictions of the Adler-Brooks theory were found to be confirmed by these measurements on V_2O_3.

The above original version of this theory has been generalized to consider the transition from a thermodynamic point of view, and two types of transitions have been found to be possible [23]. If the free energy of the metallic state does not fall below the free energy of the semiconducting state for temperatures below T_o, then a second order transition similar to that described above occurs at T_o. There is also, however, the possibility that a first order transition will occur at some temperature $T_c < T_o$ if the free energy of the metallic state

falls below the free energy of the semiconducting state at T_c. They have shown that a crystalline distortion induced transition is only expected to occur for narrow band materials for which the ratio $(E_g)_o/kT_o \leq 10$ and that such a transition is expected to be first order and to occur at a temperature T_c slightly below T_o. This refined analysis was still in accord with the interpretation that the transition in V_2O_3 is a crystalline distortion induced transition since the transition is first order and the ratio $(E_g)_o/kT_o$ was estimated to be approximately 8.3.

Although the above interpretation of V_2O_3 seemed very reasonable at the time this research began, it should be noted that recent experiments show that V_2O_3 is antiferromagnetic below the transition temperature. Reexamination of the optical data also shows that the energy gap can be interpreted to be as large as 0.3 eV. Thus, if we still want to apply the Adler-Brooks theory to V_2O_3, the theory would have to be modified so that the band gap could be considered to arise from both antiferromagnetism and the crystalline distortion, and the optical, stress, and electrical measurements would have to be reinterpreted.

We see that there were several theoretical ideas which had been presented to explain semiconductor-metal transitions in materials like V_2O_3. We felt that the models which might fit the experimental data on V_2O_3 were the antiferromagnetism model of Slater, the model of

a correlation induced transition, Goodenough's cation pairing model, and Adler and Brooks model of a carrier dependent energy gap. Of all these models, the Adler-Brooks model was the only one which could be quantitatively tested, and we felt that a test of this theory on another material would be a very suitable research project. The next section deals with the original plan of this investigation.

C. Design of Our Research Program

This research program was designed to investigate the semiconductor-metal transition in a transition metal oxide. We wanted to be able to characterize the nature of the high and low temperature states and also to try and understand the dynamics of the transition. In particular, we wanted to test the Adler-Brooks theory of the transition since this theory seemed to be very promising.

In order to begin this investigation we needed high quality crystals of a material that exhibited a semiconductor-metal transition, and we wanted to pick a material where the Adler-Brooks theory seemed likely to apply. This limited the initial selection to VO, V_2O_3, and V_2O_4 [27]. There were no commercially available crystals of any of these materials which were of high quality, and so we decided to grow our own samples. The material V_2O_4 was picked since it had a convenient transition temperature of 65°C and since it seemed to be the easiest of the three materials to grow. It had also been suggested that the Adler-Brooks theory might apply to V_2O_4 in the narrow band limit so that a quantitative check of the theory might be possible [27].

Once high quality crystals were available we wanted to make careful measurements of the resistivity. We thought that both the temperature dependence of the resistivity above and below T_c and the shape of the resistivity versus temperature curve during the transition might be informative.

We hoped to make both reflectivity and transmission measurements on high quality samples. The reflectivity measurements would help us to compare and characterize the high and low temperature states, and transmission measurements would enable us to determine the band gap in the low temperature state. We also hoped to measure the temperature dependence of the energy gap as a direct check on whether the Adler-Brooks theory of the transition applied to V_2O_4 and more generally to see if the energy gap disappeared suddenly at T_c.

We wanted to make stress and pressure measurements since we knew that the dimensions of the crystal axes changed at the transition temperature and we thought that some interesting effects might possibly occur. We planned to measure the stress and pressure dependence of the transition temperature and the resistivity. In the process we would also be able to see if the ratio $(E_g)_o/kT_o$ was independent of external stress and pressure as is predicted by the Adler-Brooks theory.

D. Preliminary Information About V_2O_4

This section will be a summary of the information we had about V_2O_4 when this investigation began. A semiconductor-metal transition at 340°K was first observed in V_2O_4 by Jaffray and Dumas in 1953 [28]. In 1958 Morin reported resistivity measurements on small single crystals of V_2O_4 which were grown hydrothermally [18], the data for which are shown in Figure I-2. Larger crystals which show a change in resistivity by a factor of 10^4 at the transition temperature were grown by Sasaki and Watanabe [29] and by Sobon and Greene [30]. The latent heat had been measured with values reported between 700 and 1000 cal/mol [31]. Magnetic measurements had failed to show any evidence of antiferromagnetism [31, 32, 33]. The pressure dependence of the transition temperature was known to be quite small [34, 35], and the pressure dependence of the semiconducting resistivity had been measured [34]. The phase diagram and phase boundaries had been determined for the phases between V_2O_3 and V_2O_5 by electrical and magnetic measurements [32, 36]. The X-ray lines observed for phases between V and V_2O_3 had been reported by Wilhelm and Krimm [37] and the X-ray analysis for the phases between V_2O_3 and V_2O_4 had been reported by Andersson [38]. A total of eleven phases had also been shown to exist in the composition range from VO to V_2O_5 by Andersson [38].

The crystal structure of the low and high temperature phases had been determined by Andersson [39] and Westman [40]. Westman had also shown that the structural transitions occur at the same temperature as the electrical transition. Figure I-4 shows the crystal structure

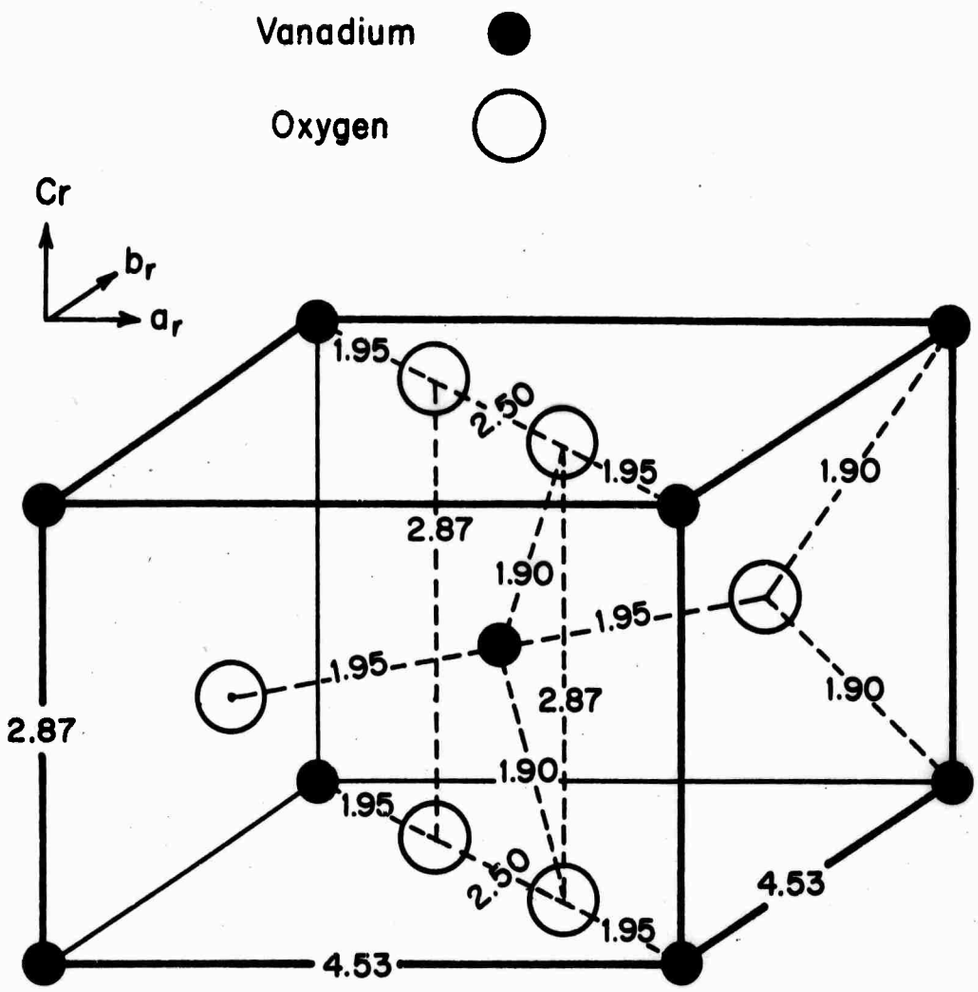

FIGURE I-4 The crystal structure of V_2O_4 in the high temperature rutile phase. Distances are in angstroms. (After Westman [40]).

in the high temperature rutile phase. Notice that the vanadium atoms form a body centered tetragonal structure. The vanadium atoms in the body center position are surrounded by six oxygen atoms which form a distorted octahedron. From the bonding distances which are included in the figure we can see that the distortion of the octahedron is not too great. The environment of the body center and the corner cations is identical except for a rotation of 90° around the c-axis. Every oxygen atom has four nearest neighbors -- one oxygen and three vanadium atoms.

Below the transition temperature the size of the unit cell is doubled and the crystal axes are different. Figure I-5 shows the relation between the crystal axes in the high and low temperature structures. The displacement of the vanadium atoms when the temperature is lowered through the transition is also shown [41]. The vanadium atoms move more than the oxygen atoms and the pairing up of the vanadium atoms is the biggest change. Below T_c the spacing of alternate pairs of vanadium atoms along the rutile c-axis is 0.265 nm and 0.312.

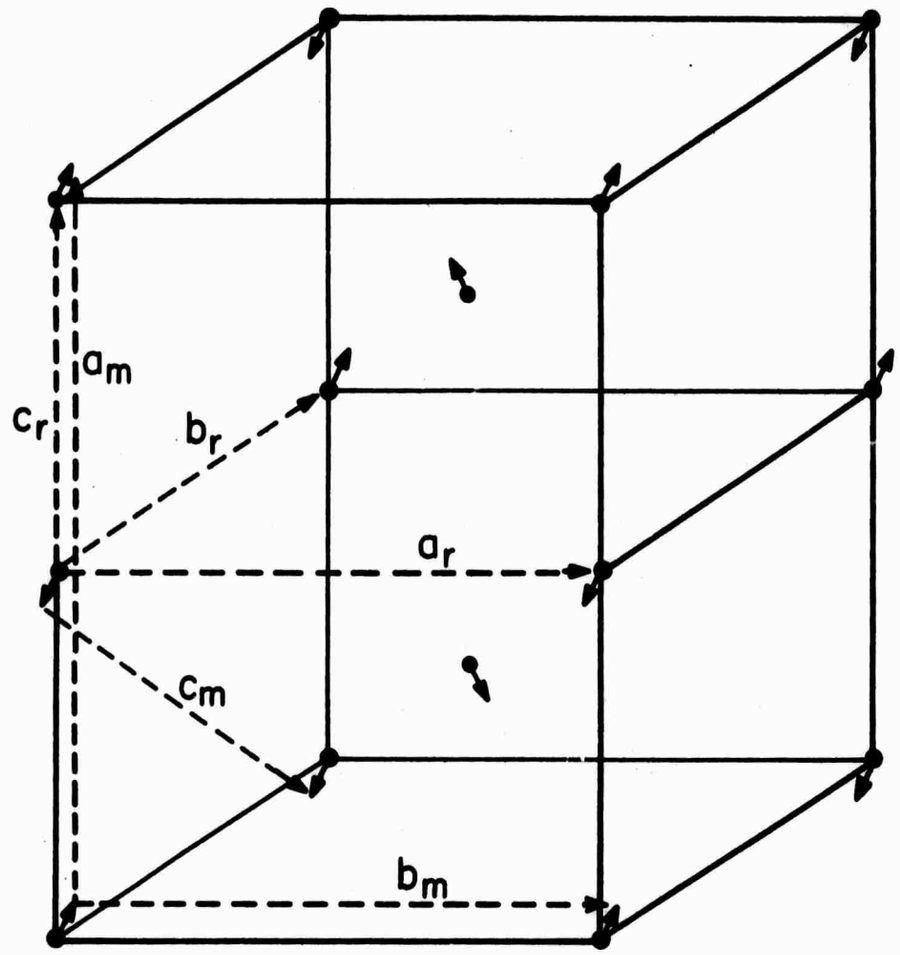

FIGURE I-5 The relationship between the high temperature rutile and low temperature monoclinic structures. The displacement of the vanadium ions in the transformation is shown. (After Magneli and Anderson [41].)

Chapter I

REFERENCES

[1] D. Adler, Solid State Phys., 21, 1 (1968).

[2] R. Newman and R.M. Chrenko, Phys. Rev., 114, 1507 (1959).

[3] A.H. Kahn and A.J. Leyendecker, Phys. Rev., 135, 1321 (1964).

[4] J.H. DeBoer and E.J. W. Verwey, Proc. Phys. Soc. (London) A49, 59 (1937).

[5] R.W. Gurney and N.F. Mott, Proc. Phys. Soc. (London) A49, 32 (1937).

[6] N.F. Mott, Proc. Phys. Sox. (London) A62, 416 (1949).

[7] C. Kittel, Quantum Theory of Solids, p. 140. John Wiley & Sons, New York, 1963.

[8] T. Holstein, Ann. Phys. (n.Y.) 8, 325,343 (1959).

[9] G.R. Allcock, Advan. Phys., 5, 412 (1956).

[10] W. Kohn, Phys. Rev., 133, 171 (1964).

[11] J. Hubbard, Proc. Phys. Soc. (London) A276, 238 (1963).

[12] J. Hubbard, Proc. Phys. Soc. (London) A277, 237 (1964).

[13] J. Hubbard, Proc. Phys. Soc. (London) A281, 401 (1964).

[14] J. Hubbard, Proc. Phys. Soc. (London) A285, 542 (1965).

[15] M.C. Gutzwiller, Phys. Rev., 137, A1726 (1965).

[16] G. Kemény, Ann. Phys. (N.Y.) 32, 69 (1964).

[17] M. Foëx, Compt. rend., 223, 1126 (1946), 227, 193 (1948).

[18] F.J. Morin, Phys. Rev. Lett., 3, 34 (1959).

[19] J. Feinleib and W. Paul, Phys. Rev., 155, 841 (1967).

[20] J. Feinleib, Tech. Rep. No. HP-11, Gordon McKay Laboratory, Harvard University, 1963 (unpublished).

[21] J.C. Slater, Phys. Rev., 82, 538 (1951).

[22] J.B. Goodenough, Phys., Rev., 117, 1942 (1960).

[23] D. Adler and H. Brooks, Phys. Rev., 155, 826 (1967).

[24] D. Adler, Tech. Rept. No. ARPA-12, Div. of Eng. and Appl. Phys., Harvard University, 1964 (unpublished).

[25] T. Figielski, Phys. Status. Solidi, 3, 1876 (1963).

[26] E.P. Warekois, J. Appl. Phys., Suppl., 31, 3465 (1960).

[27] D. Adler, H. Brooks, J. Feinleib, and W. Paul, Phys. Rev., 155, 851 (1967).

[28] J. Jaffray and A. Dumas, J. Recherches Centre Natl. Recherche Sci. Labs. Bellevue (Paris) 5, 360 (1953-1954).

[29] H. Sasaki and A. Watanabe, J. Phys. Soc. Jap., 19, 1748 (1964).

[30] L.E. Sobon and P.E. Greene, J. Am. Ceram. Soc., 49, 106 (1966).

[31] T. Kawakubo and T. Nakagawa, J. Phys. Soc. Jap., 19, 517 (1964).

[32] K. Kosuge and T. Takada, J. Phys. Soc. Jap., 18, 318 (1963).

[33] J. Umeda, H. Kusumoto, K. Narita, and E. Yamada, J. Chem. Phys., 42, 1458 (1965).

[34] C.H. Newman, A.W. Lawson, and R.F. Brown, J. Chem. Phys., 41, 1591 (1964).

[35] S. Minomura and H. Nagasaki, J. Phys. Soc., Jap., 19, 131 (1964).

[36] S. Kachi, T. Takada, and K. Kosuge, J. Phys. Soc. Jap., 18, 1839 (1963).

[37] W. von Wilhelm and L. Krimm, Zeit. für Anorg. and All. Chem., 250, 42 (1942).

[38] G. Andersson, Acta. Chem. Scand., 8, 1594 (1954).

[39] G. Andersson, Acta. Chem. Scand., 10, 623 (1956).

[40] S. Westman, Acta. Chem. Scand., 15, 217 (1961).

[41] A. Magnéli and G. Andersson, Acta. Chem. Scand., 9, 1378 (1955).

Chapter II

CRYSTAL GROWTH

The growth of V_2O_4 single crystals suitable for optical and stress measurements was one of the central problems of this thesis. Crystals were quickly grown by the slow cooling method which were not thought to be large or strong enough for these measurements. While efforts were being made to grow better crystals by this method and by the vacuum reduction method, apparatus was designed and built to make measurements on small samples. We were ultimately successful in growing crystals which could be measured with our new apparatus.

This chapter will discuss the methods of growing V_2O_4 crystals which have been reported by others and the methods that we used. These methods are evaluated in terms of how easily single crystals with good mechanical and electrical properties can be obtained. Since we were studying the semiconductor-metal transition in V_2O_4, we wanted crystals which had a sharp transition and a large discontinuity in resistance. The ratio of resistances in the semiconducting and metallic states, R_s/R_m, will be referred to as the resistance ratio.

Crystal growth is a complicated process, with many variables, and we were more concerned with obtaining crystals which were satisfactory for our purposes than with investigating in detail the growth process. Thus our work on crystal growth gives

information on how to grow high quality V_2O_4 crystals, but we do not pretend to have exhaustively analyzed the conditions of growth or to have optimized all the growth parameters.

A. Previous Methods of V_2O_4 Growth

Much of the earlier work on V_2O_4 was done by studying powder samples or sintered bars. For X-ray analysis or magnetic susceptibility measurements this is satisfactory, but single crystals are desirable for electrical or optical measurements. Before this research began, there were four main methods which had been used to grow single crystals of V_2O_4. We were able to modify one of these methods to give crystals which were better in terms of the criteria mentioned above than any previously reported. These four methods will now be discussed.

1. Hydrothermal Growth

The original paper by Morin [1] describing transition metal oxides with semiconductor-metal transitions included V_2O_4. These samples were grown hydrothermally at Bell Telephone Laboratories by Guggenheim [2]. Two terminal resistivity measurements were made on samples 0.1 mm on a side. The resistivity ratio R_s/R_m was almost 100 at the transition temperature of 350°K. There was a hysteresis of about 20°C and the transition temperature varied by about 15°C for different samples. See Figure II-1.

The hydrothermal technique involves growing crystals at high temperatures and pressures in sealed pressure systems. Many

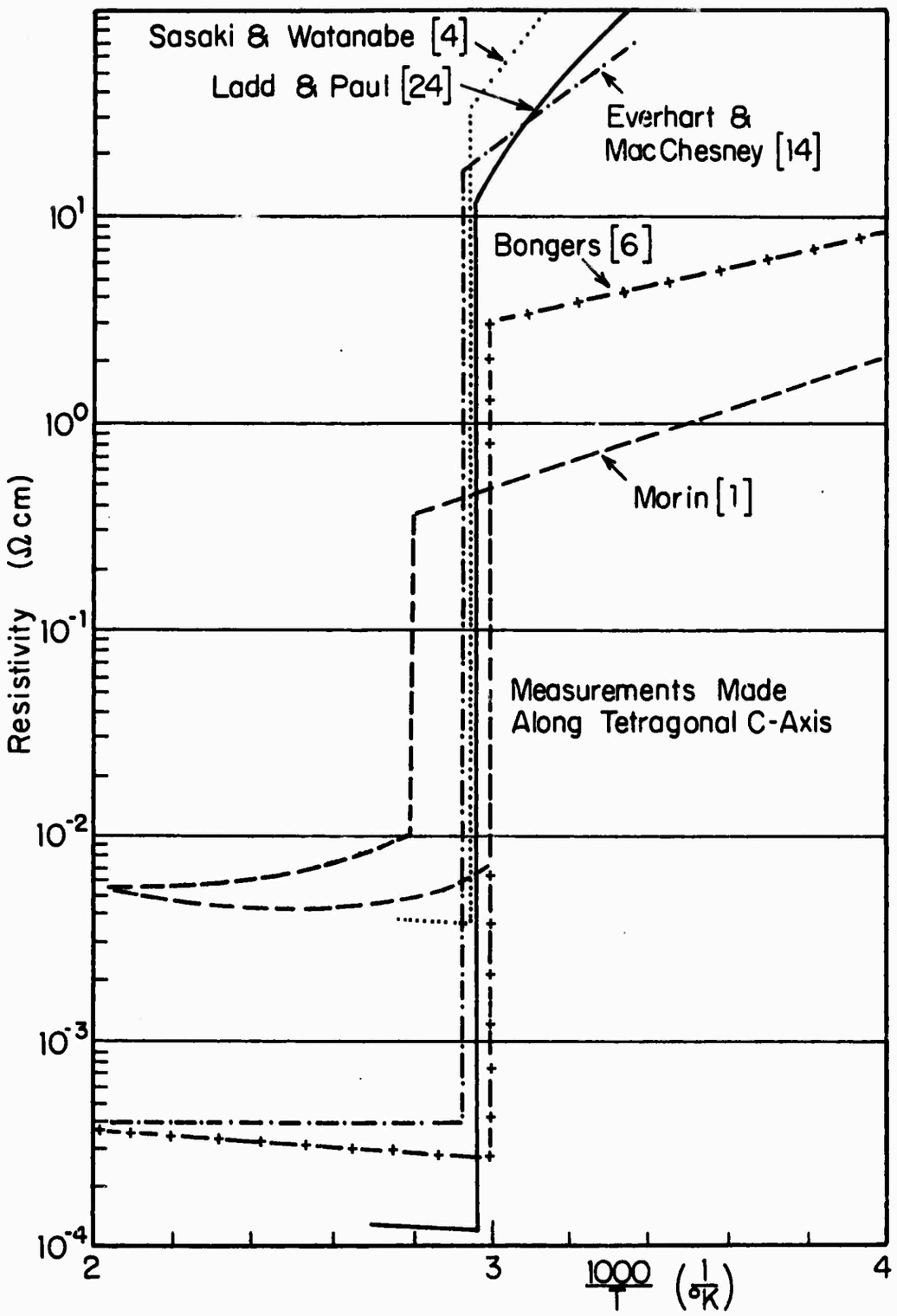

FIGURE II-1 Resistivity versus temperature for V_2O_4 crystals as reported by various authors.

materials are more soluble in common solvents such as acids and bases when the temperature and pressure are increased. The nucleation and growth processes are also quite sensitive to temperature and pressure. The usual technique consists of having undissolved nutrient material sitting at the bottom of a solvent-filled pressure system. The top of the container is kept cooler than the bottom so that the nutrient material goes into solution and migrates by convection currents to the top of the container where it is deposited on seed crystals. Quartz crystals several inches long can be grown in NaOH at a rate of 1 mm/day in this manner when the pressure is 2000 atmospheres and the temperature is 350°C.

V_2O_4 crystals were grown by putting a mixture of V_2O_3 and V_2O_5 powder in the bottom of the container and then filling it with NaOH. The temperature was 400°C at the bottom and 380°C at the top, and the pressure was 1330 atmospheres. In ten days, dark blue octahedral crystals of size up to 0.8 mm on an edge were grown. The apparatus to maintain 1330 atmosphere and 400°C for several days is both expensive and hard to keep running. Fortunately, the methods described below give better crystals and are easier to work with.

2. Slow Cooling of V_2O_4 in a V_2O_5 Flux

Sobon and Greene [3] grew crystals of V_2O_4 by a slow cooling method. V_2O_4 was dissolved in molten V_2O_5 and the solution was

cooled slowly from 1000°C to 700°C where the V_2O_5 solidified. The solubility of the V_2O_4 increases with temperature and so if the solution is saturated at 1000°C, crystals will grow as the temperature is lowered. The V_2O_5 flux was contained in a platinum crucible, and after the run was over the V_2O_4 crystals were recovered mechanically from the solidified V_2O_5. No reaction was reported between the platinum crucible and the V_2O_5 flux. When a mixture of 25% V_2O_4 and 75% V_2O_5 was used and the cooling rate was 4°C/hour, they reported single crystals of size up to 2 mm X 2 mm X 10 mm which had a resistivity ratio $R_s/R_m = 3\ 10^3$. The crystals were prismatic bars with the tetragonal c-axis in the long direction. The transition temperature was 343°K. No details as to the strength of the crystals or hysteresis at the transition were reported.

3. Vacuum Reduction of V_2O_5 to V_2O_4

Sasaki and Watanabe [4] placed V_2O_5 in a platinum crucible in a furnace at 1000°C and flowed oxygen-free nitrogen gas past the crucible for one week. The oxygen partial pressure was low enough so that the reaction $2\ V_2O_5 \rightarrow 2\ V_2O_4 + O_2\uparrow$ occurred. Once the V_2O_5 became saturated with V_2O_4, the additional V_2O_4 which formed was crystallized out of solution. The crystals were mechanically separated from the V_2O_5 flux. Prismatic crystals of size up to 0.5 mm X 0.5 mm X 3 mm were obtained which had a resistance ratio $R_s/R_m = 6\ 10^3$. The transition took place over a temperature interval of 0.5°C. No data were reported on hysteresis. See Figure II-1.

4. Methods Used to Grow V_2O_4 Needles

Needles of V_2O_4 0.1 mm X 0.1 mm X 3 mm in size were grown by heating V_2O_4 powder at 850°C in a vacuum for one day [5]. The needles had a resistivity ratio $R_s/R_m = 10^4$ and the transition occurred over an interval of 0.1°C. For increasing temperature the transition took place at 339°K and there was as much as 15°C hysteresis.

Bongers [6] developed a vapor transport method which gave small needles of V_2O_4. A sealed quartz tube was filled with HCl vapor at a pressure of 20 mm of Hg and 0.5 grams of V_2O_3 were placed at one end. The V_2O_3 was heated to 1100°C for 10 days while the other end was kept at a temperature of 850°C. Small needles of V_2O_4 grew at the cold end and could be removed after cooling the tube. The crystals were prismatic bars of maximum size 0.3 mm X 0.15 mm X 6 mm. They had a resistance ratio $R_s/R_m = 10^4$. No information was given on hysteresis or the mechanical properties of the crystals.

5. Comments on the Above Methods

When we began this research project, we felt it would be convenient for us to try only methods two and three above. Most of the apparatus for the slow cooling method was available in the laboratory, and this method had yielded large V_2O_4 crystals with good electrical properties in terms of the previously mentioned criteria. The vacuum reduction method also seemed to be promising

since it looked to be fairly easy to try and gave high quality crystals. The hydrothermal method did not seem at all attractive due to the experimental cost and difficulty and the poor quality of the crystals produced. The methods used to grow needle-like crystals were rejected since we needed much larger samples than it seemed likely we could produce by these techniques. We thought that both the slow cooling and the vacuum reduction methods could be modified to change the growth conditions and grow better crystals than had been previously reported.

B. Growth by Slow Cooling of V_2O_4 in a V_2O_5 Flux

Our best crystals were grown by the slow cooling method. A solution of V_2O_4 in molten V_2O_5 is cooled slowly from 1050°C, and the V_2O_4 crystallizes out of solution as the temperature is lowered. The V_2O_4 crystals then have to be reclaimed from the V_2O_5 flux which solidifies at 700°C. This method requires a suitable furnace, a temperature controller, crucibles to contain the V_2O_5, a way to reclaim the V_2O_4 crystals from the flux, and a way to evaluate the quality of the V_2O_4 crystals produced. In this section each of the above will be discussed.

A suitable furnace was available in the laboratory. It is constructed out of firebricks, has glo-bar heating elements, and it will operate to a temperature of 1100°C. The hot chamber is a completely enclosed cylinder 7.5" high by 3.75" in diameter. Figure II-2 shows the location of the heating elements, the hot

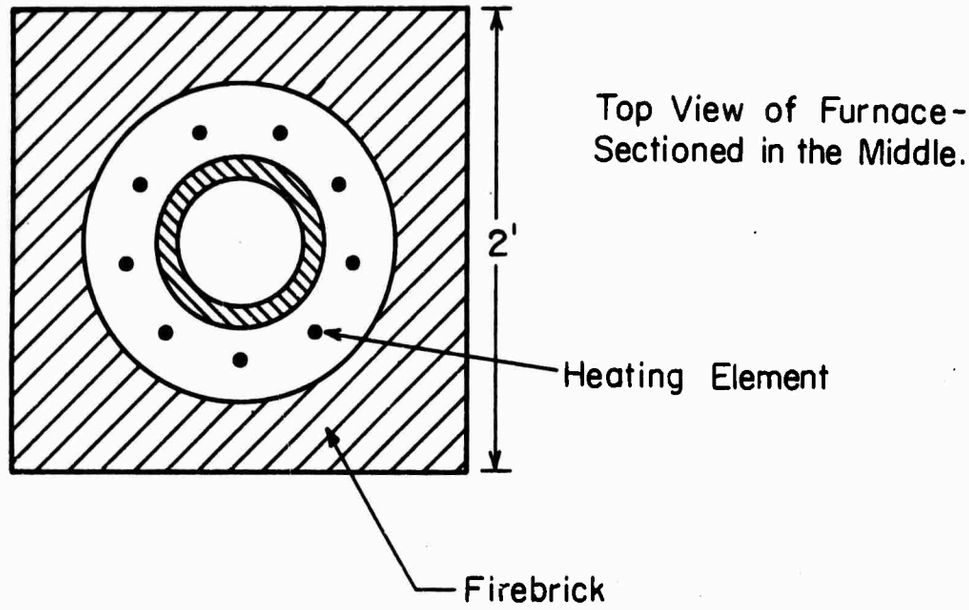

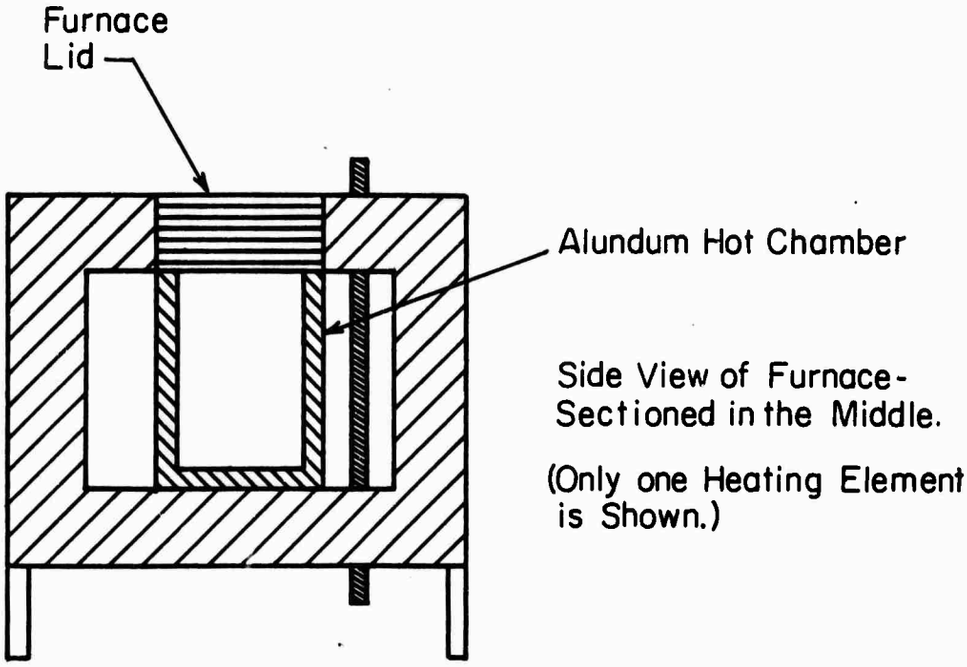

FIGURE II-2 The furnace used for V_2O_4 crystal growth.

chamber, and the access lid. The heat enters from the sides, but since the chamber walls radiate strongly above 700°C, there are only small temperature differences of 10°C or less within the hot chamber. Temperatures are measured by placing a chromel-alumel or platinum-platinum 10% rhodium thermocouple through the lid of the furnace into the middle of the hot chamber.

The desired cooling rate is maintained in the furnace by the following temperature control system: a proportioning cam program controller produces an error signal by comparing a reference voltage to the voltage produced by the thermocouple in the furnace [7]. The reference voltage is produced by a cam which can be programmed as desired. The error signal is processed by a proportioning control unit [8,9]. There are adjustments to control the time constant and the sensitivity, and to correct for the integrated error signal in order to get smooth accurate temperature control. We have a rebuilt unit and sometimes there were temperature fluctuations of up to $\pm$ 3°C in the furnace. The cooling rate is about 3°C/hour, so this is a fairly large fluctuation. The output of the proportioning control unit goes to a silicon-controlled-rectifier power supply which drives the furnace [9]. The furnace requires about 1 kilowatt of power to reach 1100°C. In order to reduce noise in the building, a special circuit which only turns the silicon-controlled rectifiers on or off at zero voltage had to be installed [10]. This unit has a timing circuit which is based on 100 cycles

of line voltage. If the proportional control unit calls for 45% of full power, then the circuit will alternately turn on the heater current for 45 cycles of line voltage and turn off the heater current for 55 cycles of line voltage. All the switching is done when the instantaneous value of line voltage is zero.

Sobon and Greene grew their crystals in platinum crucibles. We at first tried growth in quartz tubes, but since V_2O_5 is a devitrifying agent for quartz we were somewhat constrained from making long runs at high temperatures. We wished to use a high initial temperature in order to get more V_2O_4 into solution before growth began. It was found that if a starting temperature of 1050°C was used and the growth period was 5 days, 2 mm thick quartz tubing would be half eaten through. For longer runs, a lower starting temperature had to be used. Using quartz tubes had the advantage that we could vary the crucible size and shape easily and we could remove the crystals by breaking the crucible if necessary. We also made some growth runs using platinum crucibles inside of quartz tubes.

We prepared the quartz crucibles from a 6" length of 16 mm X 20 mm tubing. One end was sealed and a 6" length of smaller quartz tubing was joined to the other end. A mixture of 25% V_2O_4 and 75% V_4O_5 was poured into the crucible until it was filled to 1" from the top of the big tube. The crucible was then evacuated with a mechanical pump and heated to drive off water vapor. Some glass wool in the vacuum lines kept the powder from getting into the pump. The small quartz tube was then sealed under this vacuum close to

the end of the big tube. We used V_2O_5 powder from Fisher Scientific which was 99.9% pure and V_2O_4 powder from Alfa-Inorganics which had about 2% impurities. After the runs the V_2O_5 flux filled the bottom 1.5" of the tube. The tube was green and scaly where it was in contact with the flux. Fortunately, this process produces good, pure V_2O_4 crystals. The impurities seem to be segregated in the V_2O_5 flux by selective crystallization.

Some of the smaller crystals from a platinum crucible growth run whose larger crystals had typical values of T_c and R_s/R_m were analyzed spectrographically by the Jarrell-Ash analytical laboratory in Waltham, Massachusetts. The impurity level was found to be less than 10^{-3}% for all impurities with the possible exception of silicon. The 10^{-2}% level of silicon which was detected may be due to small quartz chips which were mixed in with the crystals which were analyzed. These chips can get into the crucible during the tube cutting operation. A small quartz chip could have easily been overlooked among the crystals which were analyzed. A recent paper claims that a level of silicon impurities too small to be measured by spectroscopic analysis can increase the resistance ratio R_s/R_m by a factor of ten [11]. The authors grew their crystals in a V_2O_5 flux by vacuum reduction and claim that adding a small amount of silicon to the flux increases the resistivity ratio of their samples from $R_s/R_m = 4\ 10^3$ to $R_s/R_m = 4\ 10^4$. It is possible that this effect may be present in our samples, but somewhat unlikely since we obtain the

same resistivity behavior for samples grown in platinum crucibles and for samples grown in quartz tubes. A typical platinum crucible growth run was also chemically analyzed for the vanadium content at the Massachusetts Institute of Technology central analytical laboratory. The stoichiometry was shown to be $V_{2+x}O_4$ where $|x| \leq 0.02$.

When we began crystal growth two methods had been reported for separating the V_2O_4 crystals from the V_2O_5 flux: mechanical separation and dissolving the V_2O_5 with dilute ammonia. We have made two improvements in this area. First, when the slow cooling run is almost over and the temperature is about 700°C, the tube is turned upside down and allowed to cool to room temperature in the turned off furnace. The V_2O_5 runs to the bottom of the tube and the V_2O_4 crystals remain attached to the walls at the tope of the tube. Some V_2O_5 remains on the crystals due to surface tension and viscosity effects. This can be removed by a solution of H_2O_2 and HNO_3 in water. The tube is cut open and the end with the crystals is placed in a 200 ml beaker of water. About 10 ml of 30% H_2O_2 and 10 ml of concentrated HNO_3 is added. V_2O_5 will dissolve in HNO_3, but the addition of H_2O_2 speeds up the process. After a few hours the reaction is complete and the solution is completely reacted and must be renewed. After three or four soakings the V_2O_4 crystals are lying freely at the bottom of the tube. The usual result is a few large and fairly weak crystals of size 1 mm × 1 mm × 10 mm and many smaller and stronger crystals. They

were nearly always rectangular bars which had shiny natural faces and prismatic ends. The long direction is the tetragonal c-axis. Figure II-3 shows the crystals from one run.

In evaluating the crystals, we were quite interested in size and strength. We originally felt that we needed crystals of 1 mm width to make the transmission measurements, but we found that we were able to measure samples that were somewhat smaller. Clearly we wanted as strong samples as possible for measurements under uniaxial stress. Crystalline V_2O_4 is quite hard and strong, and the problem is to get a sample with no voids or flaws. Growth was fastest along the c-axis, and so quite often there were narrow cavities in this direction. There was also a problem of polycrystallinity and faults in the crystal structure. For this reason, most of the larger crystals which we grew were weak and broke up into many smaller and stronger crystals.

Since the purpose of this investigation was to try to understand the nature of the semiconductor-metal transition in V_2O_4, we were interested in studying the properties of crystals which had a sharp transition and a large R_s/R_m ratio. We found, however, that these desired electrical properties correlated with good mechanical properties, so that we could carry out our primary selection on the basis of size and strength alone.

X-ray back reflection measurements have been made and we have observed that instead of single spots, there are clusters of dots for each reflection. This has been attributed to domain effects [12].

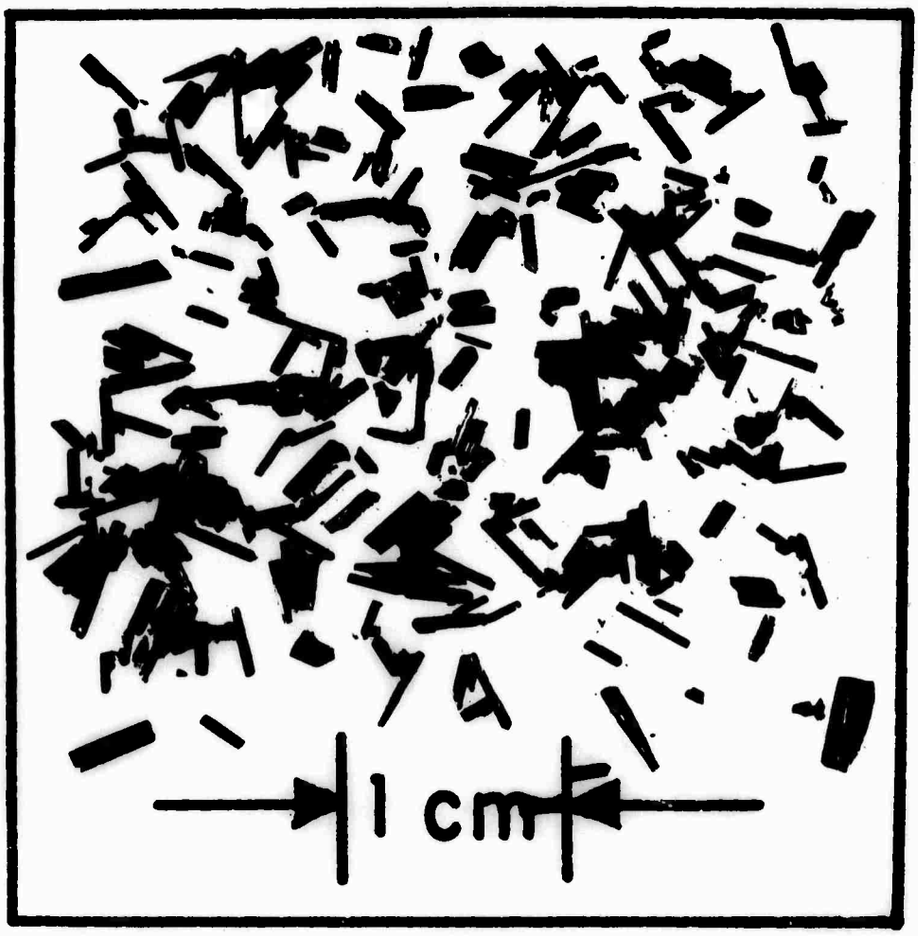

FIGURE II-3 Picture of crystals from typical quartz tube run.

Domains are believed to arise from the fact that when the crystal transforms from the tetragonal to the monoclinic phase, an individual a-axis in the tetragonal state can either elongate or contract. Thus the transformation can distort the crystal in different ways at different parts of the crystal. This is one of the reasons that many crystals tend to be weak and break apart easily.

C. Variation of the Growth Parameters for the Slow Cooling Method

The growth parameters for the slow cooling method were varied in order to obtain larger crystals. Some of the variables that affect nucleation and growth are initial composition and temperature, rate of cooling, and temperature gradient. These parameters were systematically varied in the hope of getting better crystals.

One of the variations we tried was to change the composition of the V_2O_4-V_2O_5 mixture in the tubes. Sobon and Greene claimed that in a mixture containing 25% by weight of V_2O_4, the V_2O_4 would be completely dissolved at 1000°C. We obtained larger and stronger crystals when we changed the composition to 15% V_2O_4. When more V_2O_4 was used then we found a residue at the bottom of the tubes.

Another variation was to try to change the temperature gradient. Moving the tube up to the middle of the chamber reduced the temperature gradient and generally gave smaller crystals which grew from the sides of the tube. Putting the tube at the bottom of the chamber gave the best results. Here the crystals grew from the bottom of the tube. The temperature gradient at the bottom of the hot chamber

is about 10°C/inch at 1000°C. During this variation the initial temperature was kept at 1050°C which we found to be an optimum starting temperature for the system.

The original cooling rate of about 3°C/hour which gave a five-day cooling period was varied in both directions. A three-day growth period gave larger crystals which were quite weak. A nine-day growth period yielded crystals which were somewhat larger and weaker. These crystals were strong enough for reflectivity measurements, but usually broke during stress measurements or when being lapped thin for transmission measurements.

Quartz tubes could not be used for the nine-day runs since the walls of the tube would be eaten through by the flux before the run was over. We tried platinum plating the quartz tubes, but the coatings were not good enough. We finally bought a 50 cc size platinum crucible. The crucible is sealed inside a 6" length of 46 mm X 50 mm quartz tubing which is joined to a 2' length of 16 mm X 20 mm quartz tubing at one end as shown in Figure II-4. The 16 mm X 20 mm tube projects through the lid of the furnace and a ground joint at the end of this tube seals the system from the atmosphere.

Since the powder shrinks so much upon melting, the following procedure is used to fill the crucible. The tube containing the crucible is placed into the furnace at 1000°C, and an 8 mm X 12 mm quartz tube is placed inside of the 16 mm X 20 mm quartz tube with its bottom inside the crucible. Then 97 grams of the powder is

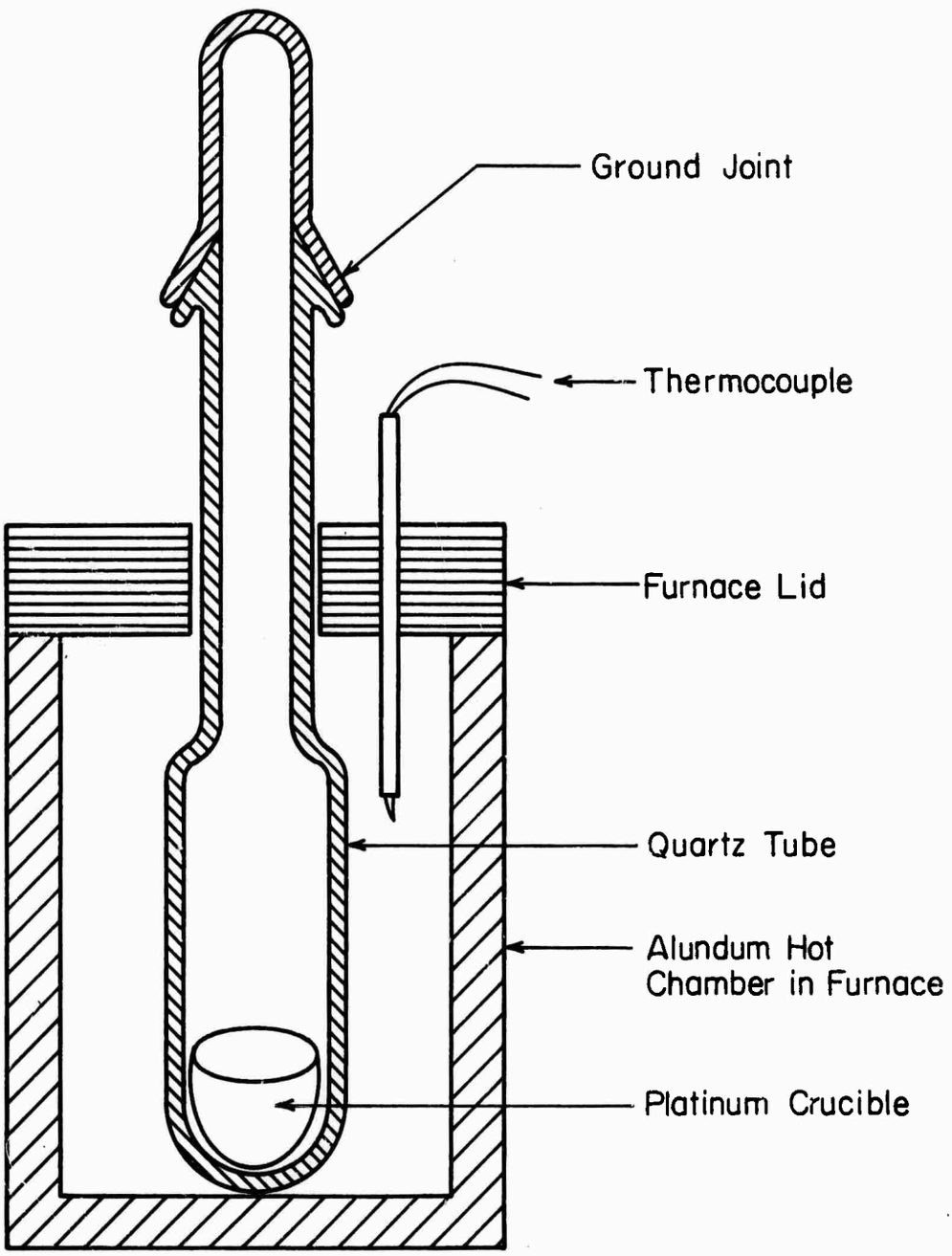

FIGURE II-4 Schematic diagram of the quartz tube in the furnace for a platinum crucible growth run.

slowly dropped down the 8 mm X 12 mm tube and melted into the crucible. The 8 mm X 12 mm tube is removed and the ground joint is put in place to close the system from the atmosphere.

Attempts to grow seed crystals into larger crystals were only partially successful. If the seed crystal is not introduced when the V_2O_4-V_2O_5 solution is saturated, the seed will dissolve. If the seed is not placed where the temperature gradient is suitable, growth will not occur. The better seed crystals are also quite small and hard to handle -- especially at around 1000°C. Seed growth was most easily tried on the platinum crucible runs since the quartz tube came out through the lid of the furnace. The seed was lowered into the crucible through the 16 mm X 20 mm quartz tube on the end of a platinum wire. We found that the seed crystals either dissolved or did not grow as well as the crystals growing on the bottom of the crucible.

We got our strongest crystals from the following conditions: a 15% V_2O_4 and 85% V_2O_5 mixture, a 5-day growth period, an initial temperature of 1050°C, and growth in a 16 mm X 20 mm quartz tube placed on the bottom of the furnace hot chamber. We were able to get strong crystals which were 1 mm^2 in cross section and 5 mm long by this method. These crystals also have better electrical properties than any previously reported.

D. Growth by Reducing V_2O_5 to V_2O_4

We grew crystals by a vacuum reduction method similar to that of Sasaki and Watanabe [4]. A vacuum system was used to lower the oxygen partial pressure to the desired level rather than flowing nitrogen gas over the V_2O_5 flux. This was first tried in quartz tubes at a temperature of 900°C. It was found that a pressure of 0.4 Torr gave a suitable growth rate. The quartz tube was placed in a vertical tube furnace and the pressure was controlled by a mechanical pump and a needle valve. This pressure regulation system was not very satisfactory, for the growth rate is quite sensitive to pressure. The original mixture contained 15% V_2O_4 so that we would not have to wait so long before the solution became saturated and growth began. One could use quartz tubes for up to one month at 900°C. Small chunky crystals which were quite strong were grown in this manner.

This vacuum reduction method worked much better with platinum crucibles. The temperature was raised to 950°C where the proper pressure was 1.0 Torr. This pressure could be obtained and regulated by using a diffusion pump, a needle valve, and a sensitive manostat as indicated in Figure II-5. In a week or two we were able to grow crystals which were 2 mm X 2 mm in cross section and which were strong enough for our reflectivity or resistivity measurements. This method has the advantage that one can continue growth for a long time and thus get large crystals while maintaining a slow

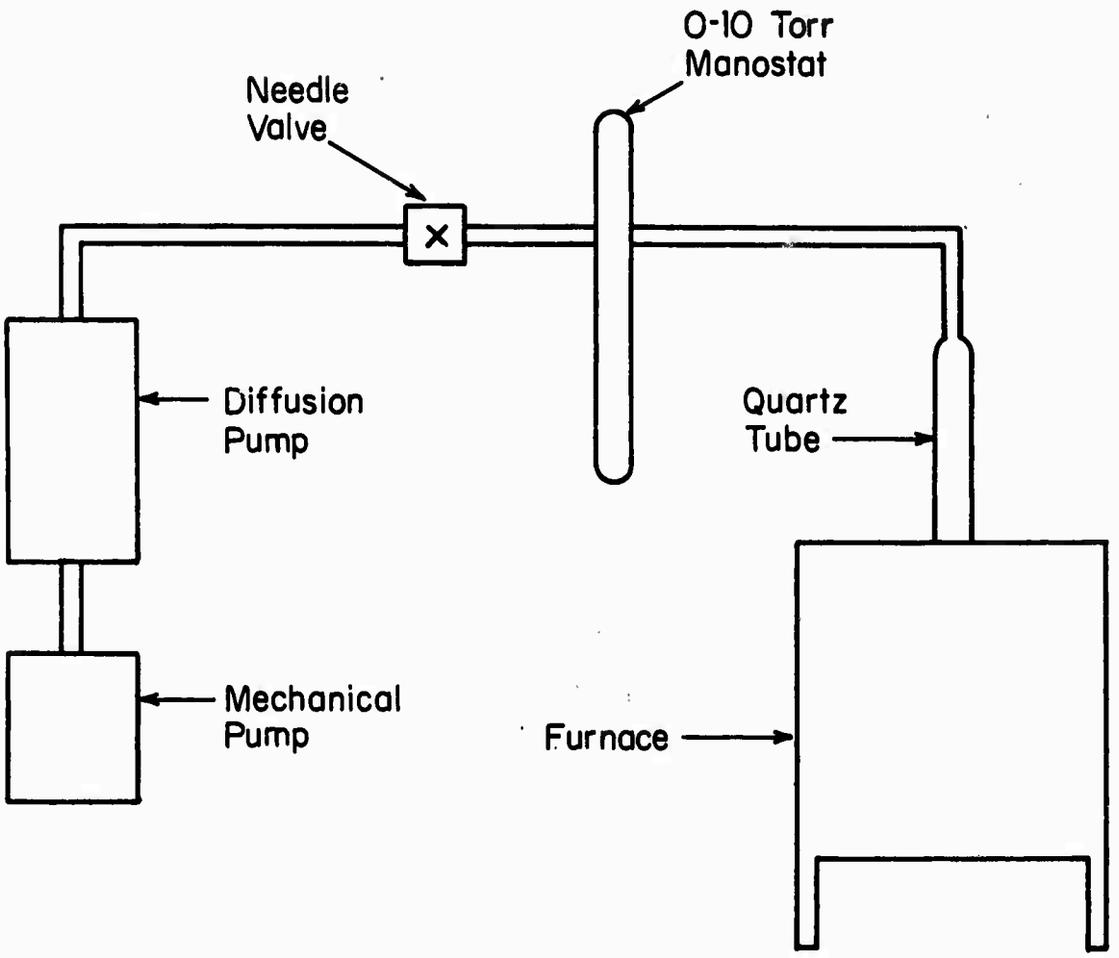

FIGURE II-5 Schematic diagram of the pressure control system for the vacuum reduction method of crystal growth.

growth rate. The main disadvantage is the very long time required for each run. If several furnaces were available, this method would be more suitable and one could optimize growth conditions. The recent work of Guggenheim on this method is discussed in the next section [11].

E. Recently Developed Methods of Growth

While this work has been in progress, other researchers have grown V_2O_4 crystals by vapor transport and by vacuum reduction of V_2O_5. Much work has also been done on the growth of thin films which can be used for both optical and electrical measurements. We will discuss these crystal and film growth methods in this section.

1. The Reduction of V_2O_5 to V_2O_4

Kitahiro, Watanabe, and Sasaki [13] have developed a method of growing needles of V_2O_4. They placed a sealed quartz tube with V_2O_5 at the bottom and Ti powder at the top in a vertical furnace so that the top of the tube was at 700°C or 800°C and the bottom was at 1000°C. After five days needles of V_2O_4 of size 0.1 mm × 0.2 mm × 8 mm had grown from the sides of the tube. The crystals had a resistance ratio $R_s/R_m = 2.7\ 10^4$ and the transition took place within 1°C. Although the crystals are easy to reclaim in this method, they are inferior in size and electrical properties to those we grew by slow cooling.

Guggenheim and his coworkers at Bell Telephone Laboratories [11,14] have developed the method of reduction of V_2O_5 to V_2O_4 to give large chunky crystals 1 cm on a side. A platinum crucible is placed in a furnace at high temperature and nitrogen gas is passed over the crucible to reduce the oxygen partial pressure. The growth temperature is 1250°C to 1350°C and the growth period is about one week. This method is very similar to the vaccum reduction growth method which we used, the main difference being that their growth temperature was about 300°C higher. This allowed them to operate at a much higher and more convenient oxygen partial pressure. Their method, however, requires a high temperature furnace and platinum crucibles which have special lids which have gas inlet and gas outlet tubes built into them. These items were not readily available in our laboratory. This method gives crystals which are larger than the ones we have grown, but apparently not as strong, since they had more difficulty preparing optical transmission samples than we did [15]. Their samples have a hysteresis of about 1°C and a resistance ratio R_s/R_m of up to 10^5. Their transition temperature is 67°C, about 1°C or 2°C higher than for our samples.

2. Vapor Transport Methods of V_2O_4 Growth

Takei and Koide [16,17] have developed a method which can be used to grow V_2O_5, V_2O_4, V_3O_5, and V_2O_3 crystals. This method involves the vapor phase decomposition of vanadium oxychloride ($VOCl_3$)

with water vapor. As indicated in Figure II-6, two quartz tubes are placed one inside of the other in a furnace. $VOCl_3$ vapor and nitrogen flow through the central tube, and hydrogen, water vapor, and nitrogen flow through the outer tube. A dish shaped piece of quartz covers the end of the central tube and serves as a reaction chamber. When the two gas mixtures meet, the water and $VOCl_3$ undergo the reaction $2VOCl_3 + 3H_2O \rightarrow V_2O_5 + 6HCl$. Due to the presence of hydrogen, lower oxides of vanadiums and water are produced. By controlling the oxygen partial pressure one can produce V_2O_3, V_2O_4, V_3O_5, or V_2O_5. Prismatic bars of V_2O_4 were grown at 800°C. In 24 hours crystals 0.8 mm × 0.8 mm × 15 mm in size were grown. The resistance ratio R_s/R_m is 10^4 for these crystals, but no information is given on hysteresis. This method is convenient since the crystals can be reclaimed easily and since different oxides can be produced with the same apparatus.

Bando, Nagasawa, Kato, and Takada [18] have developed a vapor transport method which yields high quality V_2O_4 crystals with a resistance ratio R_s/R_m of almost 10^5. A tube is placed in a furnace with one end at 1040°C and the other end at 920°C. The tube has V_2O_4 at the hot end and contains a small amount of $TeCl_4$. The reaction at the hot end of the tube is $VO_2 + TeCl_4\uparrow \rightarrow VCl_4\uparrow + TeO_2\uparrow$. At the cold end the reverse reaction occurs and crystals 3 mm on a side can be grown in a period of three days. The amount of hysteresis for these crystals is not mentioned.

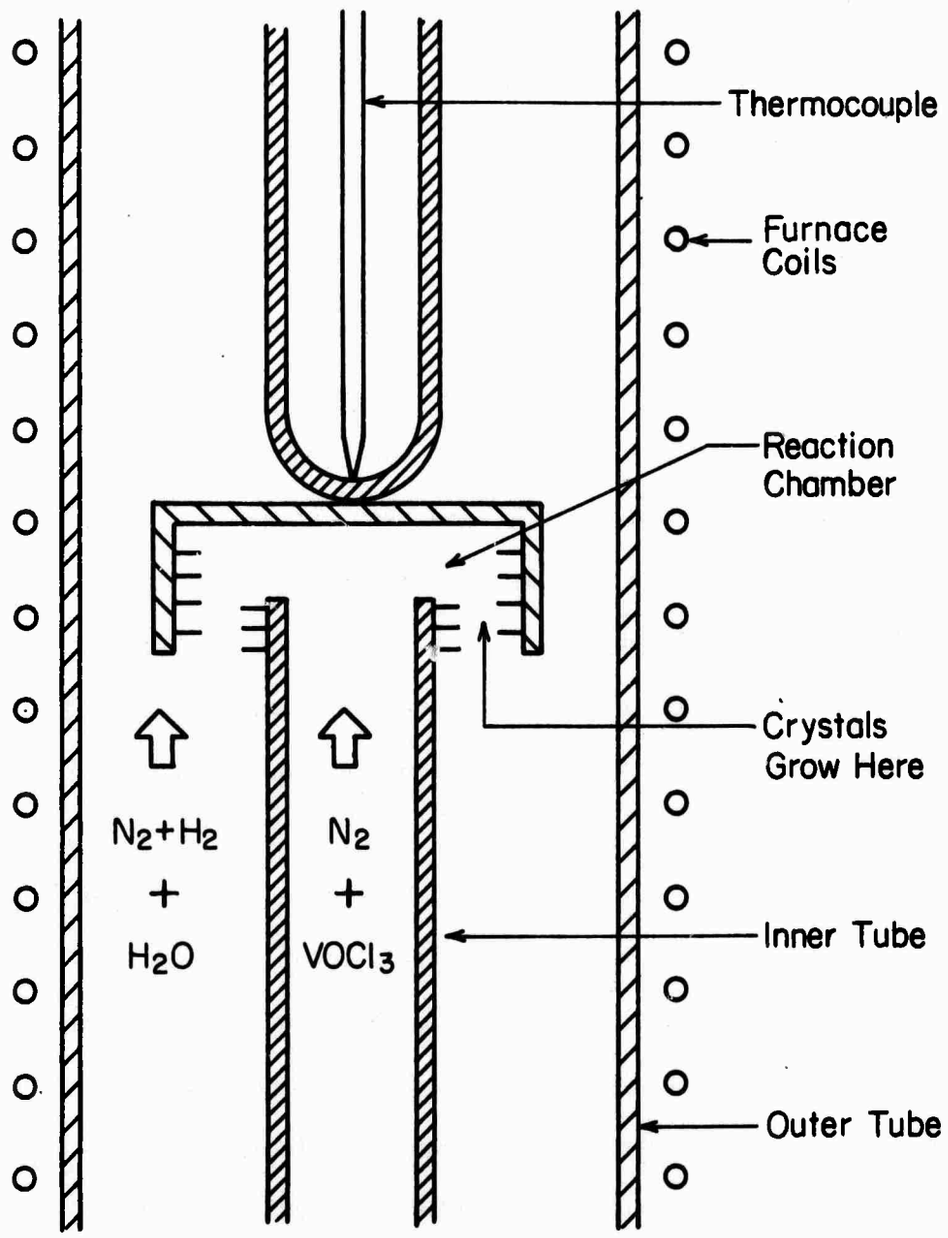

FIGURE II-6 Schematic diagram of the furnace interior for the vapor transport crystal growth method of Takei and Koide [16, 17]

3. Methods to Grow Thin V_2O_4 Films

The simplest way to get a thin film of V_2O_4 is to make a film of vanadium and oxidize it, or to make a film of V_2O_5 and reduce it. Polycrystalline V_2O_4 films were grown by the latter method which have a resistance ratio R_s/R_m of 10^3 and a hysteresis of 7°C to 8°C [19]. Similar results have been obtained for polycrystalline films made by annealing amorphous sputtered V-O films at 450°C in an oxidizing atmosphere [20] and by oxidizing evaporated vanadium films [21].

Epitaxial V_2O_4 films have been grown by Fuls, Hensler, and Ross by sputtering vanadium in an atmosphere of argon doped with oxygen [22]. Growth was on a sapphire substrate heated to 400°C. The sputtering gas pressure was $2\ 10^{-2}$ Torr. These films had a resistance ratio R_s/R_m of 10^3 and a few degrees of hysteresis.

Koide and Takei have used the method of hydrolysis of vanadium oxychloride described in the preceding section to grow epitaxial films on rutile which have a resistance ratio R_s/R_m of 10^2 and a few degrees hysteresis [17,23]. This method can also be used to grow epitaxial V_2O_3 films.

The electrical properties of these thin films are not as good as those of single crystals, but the films are useful for making optical measurements because they are thin enough so that the absorption coefficient above the band gap can be measured and they have large good surfaces for reflectivity measurements. Their large surface area also makes them useful for Hall effect measurements.

Chapter II

REFERENCES

[1] F.J. Morin, Phys. Rev. Lett. 3, 34 (1959).

[2] R.A. Landise and J.W. Nielsen, "Hydrothermal Crystal Growth," Solid State Physics 12, 149 (1961).

[3] L.E. Sobon and P.E. Greene, J. Am. Ceram. Soc. 49, 106 (1966).

[4] H. Sasaki and A. Watanabe, J. Phys. Soc. Jap. 19, 1748 (1964).

[5] C.H. Neuman, A.W. Lawson, and R.F. Brown, J. Chem. Phys. 41, 1591 (1964).

[6] P.F. Bongers, Solid State Comm. 3, 275 (1965).

[7] Electronik Proportioning Cam Program Controller, Model R15214116-01-01-0-150-024-53 202, Brown Instruments Div., Minneapolis-Honeywell Co., Philadelphia, Pa.

[8] Three Mode Electro-O-Volt Control Unit, Brown Instrument Div., Minneapolis Honeywell Co., Philadelphia, Pa.

[9] Power Pac Solid State Power Controller Model PC-230-40-DC-MC, Research Incorporated Controls Co., Minneapolis, Minn.

[10] Zero Voltage Firing Circuit, Model SS-ZC, Research Incorporated Controls Co., Minneapolis, Minn.

[11] J.B. MacChesney and H.J. Guggenheim, J. Phys. Chem. Solids 30, 225 (1969).

[12] P.J. Fillingham, J. App. Phys. 38, 4823 (1967).

[13] I. Kitahiro, A. Watanabe, and H. Sasaki, J. Phys. Soc. Jap. 21, 196 (1966).

[14] C.R. Everhart and J.B. MacChesney, J. App. Phys. 39, 2872 (1968).

[15] A.S. Barker, Private Communication, Bell Telephone Laboratories, Murray Hill, New Jersey.

[16] H. Takei and S. Koide, J. Phys. Soc. Jap. 21, 1010 (1966).

[17] H. Takei, Jap. J. App. Phys. 7, 827 (1968).

[18] Y. Bando, K. Nagasawa, Y. Kato, and T. Takada, Jap. J. App. Phys. 8, 633 (1969).

[19] J. MacChesney, J. Potter, and H. Guggenheim, J. Electrochem. Soc. 115, 52 (1968).

[20] G. Rozgonyi and W. Polito, J. Electrochem. Soc. 115, 56 (1968).

[21] R.J. Powell, C.N. Berglund, and W.E. Spicer, Phys. Rev. 178, 1410 (1969).

[22] E.N. Fuls, D.H. Hensler, and A.R. Ross, App. Phys. Lett. 10, 199 (1967).

[23] S. Koide and H. Takei, J. Phys. Soc. Jap. 22, 946 (1967).

[24] L. Ladd and W. Paul, Solid State Comm. 7, 425 (1969).

Chapter III

RESISTIVITY MEASUREMENTS

The resistivity of our V_2O_4 crystals was measured as a function of temperature both near the transition and at lower temperatures. A sample holder and temperature control system were designed and constructed to make these measurements. The apparatus and the measurements will be discussed in this chapter and the interpretation of the measurements will be included in Chapter VI.

A. The Sample Holder and Temperature Control System

1. The Bayley Electronics and New Temperature Sensor

We required a temperature control system which was sufficiently sensitive and stable to permit study of the detailed variation of both resistivity and optical transmission at closely regulated temperatures near the semiconductor-metal transition, and which would operate from 100°K to 400°K. We wanted to be able to set and regulate the temperature to about 0.01°C near the transition. The temperature sensing probe also had to be small enough to fit into an optical dewar.

Several types of temperature control systems were considered. Two important components of a temperature control system are the sensing probe and the controlling electronics. Thermocouples are often used as sensing probes, but their low output signal demands very sensitive, low-noise, stable d.c. amplification in the

controlling electronics. Nevertheless, thermocouples are easily calibrated, stable, and can be readily built into different pieces of equipment.

Another commonly used sensing probe is a resistor with a large temperature coefficient of resistance which can be used as one element of a Wheatstone bridge circuit. Direct current amplification can be used in the sensing circuit when the temperature coefficient of the resistance is large enough, but it is difficult to find a small sized resistance probe which has a large temperatue coefficient over the entire temperature region of interest. Another technique, which we adopted, is to use a metallic resistor which has a linear temperature coefficient and use a.c. voltages in the bridge and detection circuits. The use of a.c. amplification increases the sensitivity and stability of the system.

We were able to construct such a system by using the electronics from a Bayley temperature controller which we had in the laboratory [1]. Its original temperature sensor is a three foot long metal probe which can be placed in a temperature bath. When the temperature of the sensor falls below the set point of the instrument, a relay connected to a plug on the instrument front panel closes. If one of the heater leads is connected through this plug, then the Bayley will switch on the heater current until the temperature of the sensor rises back up to the set point.

A simplified circuit diagram is shown in Figure III-1. The original probe contains a nickel resistor which is one of the elements in a Wheatstone bridge circuit. The error signal from the bridge is amplified and then applied to the grid of a triode. The circuit is designed so that the amplified error signal and the plate voltage of the triode are in phase when the probe resistance is too small to balance the Wheatstone bridge circuit. The resulting plate current of the triode then turns on the relay which can be used to switch on the heater current. Since the voltage across the bridge circuit is at 60 Hz, the instrument is sensitive to grounding and pickup problems. The 500 Ω resistor is a 10 turn potentiometer which can be adjusted to control the temperature set point. Fine control is obtained by the 1 Ω variable resistor shown in the circuit diagram. With the original probe which has 80 Ω resistance at room temperature, the range of the Bayley is from -200°C to 100°C.

We wanted to make two new probes for the Bayley controller, so that it could be used for both our resistance and optical measurements. We wanted two flat nickel wire resistors about $\frac{1}{2}$" by $\frac{1}{4}$" in size with a room temperature resistance of 80 Ω. The small size is necessary because one of the resistors must fit on the optical dewar sample holder. To make such a resistor would have been difficult, but we were able to purchase three "stickon" nickel surface resistors of size $\frac{1}{4}$" by $\frac{3}{8}$" and 100 Ω

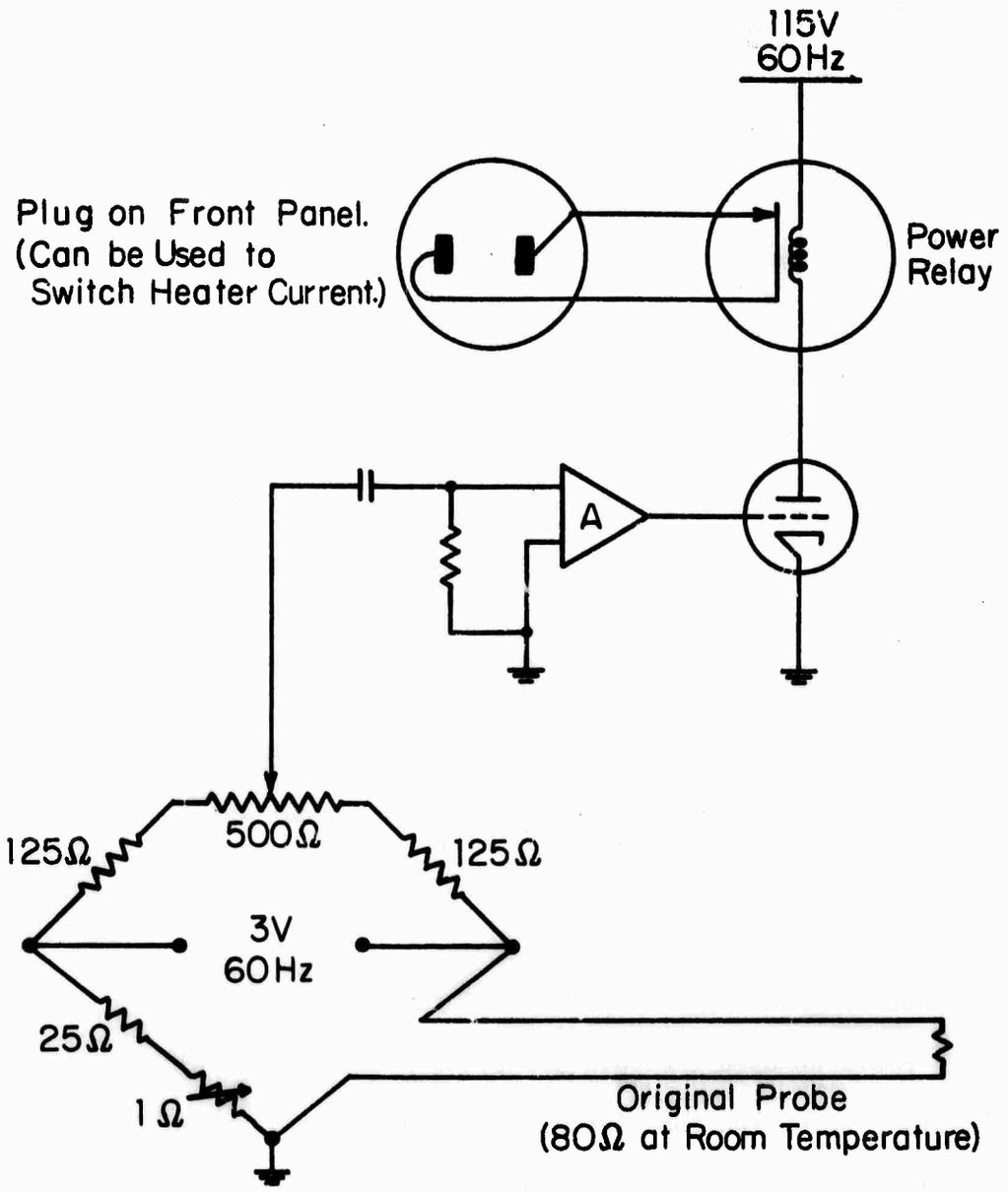

FIGURE III-1 Schematic diagram of the electronics in the Bayley temperature controller.

room temperature resistance from the RdF Corporation in Hudson, New Hampshire. They are made from 0.0008" diameter nickel wire, are covered with bakelite, and have a total thickness of 0.008".

The resistance probes are wired as shown in Figure III-2. We note that one of the 125 Ω resistors has to be shunted in order to compensate for the increased resistance of the new probes. The connections between the probe and the Bayley have to be made with shielded cable which includes a capacitance lead to prevent unwanted phase shifts in the bridge circuit.

2. Resistivity Sample Holder and Dewar

The resistance sample holder consists of a spool shaped piece of copper 1" in diameter to which the new Bayley temperature sensor is attached as shown in Figure III-3. On top of this holder there are eight insulated terminals which are used as the tie points for the sample leads, the heater leads and the temperature sensor leads. There is also a piece of sapphire which is used to electrically isolate the sample from the copper block while maintaining good thermal contact. The sample was cemented to the sapphire and the sapphire was cemented to the copper block with General Electric No. 7031 varnish which is often used as a low temperature thermally conducting cement. Number 40 enameled copper wire is wound around the center portion of the copper block to form a heating coil. The room temperature resistance of the coil is 300 Ω.

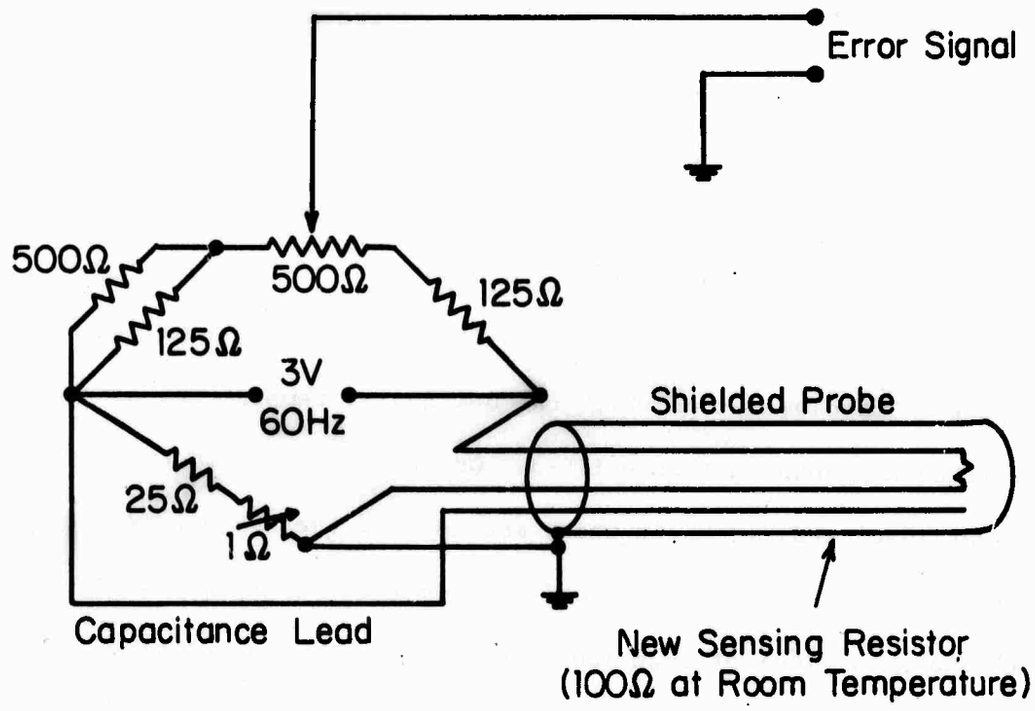

FIGURE III-2 Circuit diagram of Bayley bridge circuit with new sensing resistor.

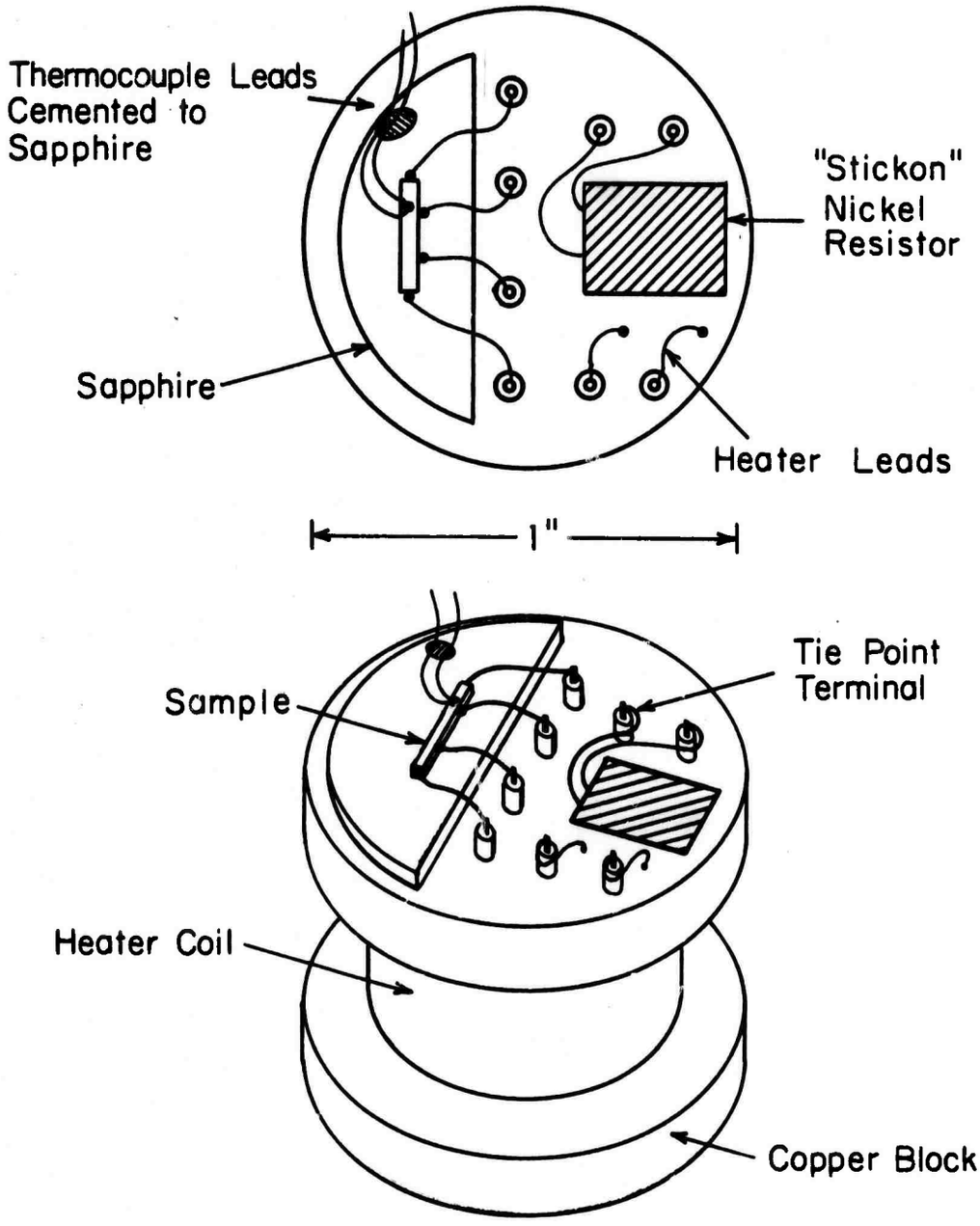

FIGURE III-3 Top and perspective views of sample holder for resistance measurements.

This sample holder is designed to fit into the bottom end of an eighteen inch long evacuable tube as shown in Figure III-4. The bottom of the tube where the sample holder is placed is made of copper and the sides are thin walled stainless steel tubing only 0.010" thick. During operation the sample holder is placed inside the tube, the lid is fastened in place, the tube is evacuated with a diffusion pump to 10^{-5} Torr, and then the tube is lowered half way into a cooling bath such as liquid nitrogen or ice water. The heater coil on the sample holder can heat the sample to a temperature which is 100°C above that of the bath. During operation the heat generated in the heating coil flows through the center of the sample holder and out the bottom plate of the tube. Since there is no heat flow through the top of the sample holder, there should be no large temperature gradients near the sample.

The sample holder is screwed to the bottom plate of the tube as shown in Figure III-4 to give consistent thermal contact. The bottom of the sample holder was relieved until only a ring $\frac{1}{16}$" wide was in contact with the bottom plate of the tube in order to adjust the heat leak to the desired value.

Figure III-4 shows the shield which fits over the sample holder when it is being mounted in the tube. There is a slot on one side for passage of the wires from the sample holder. The shield is attached to the sample holder by one screw as indicated. On the top of the shield there is a hexagonal socket into which a long rod fits so that the sample holder can be screwed in place inside the tube.

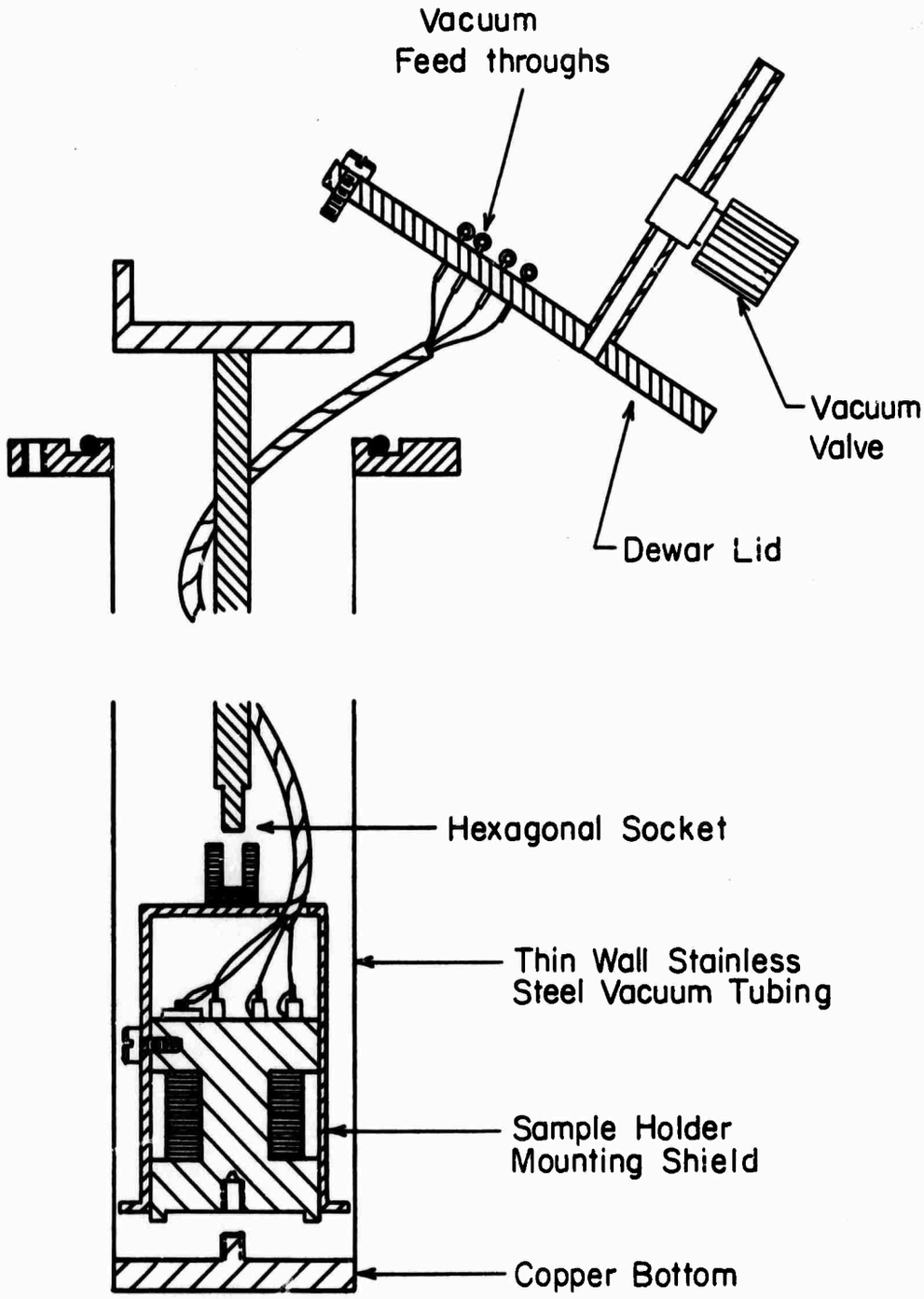

FIGURE III-4 Schematic diagram showing how resistivity sample holder is mounted in dewar tube.

A copper-constantan thermocouple is used to measure the sample temperature. The internal junction of the thermocouple is cemented to one end of the sample, and the external junction is placed in an ice bath. The thermocouple measuring circuit has to be isolated from the sample circuit to prevent electrical interference. The thermocouple voltage is measured with a Leeds and Northrup model K-3 potentiometer and model M galvanometer. We used 0.005" diameter thermocouple wire and cemented a portion of the thermocouple lead wires an inch back from the junction to the piece of sapphire on which the sample was mounted in order to reduce the heat leak to the sample, and ensure accurate temperature measurement.

3. The Heater Circuit and System Performance

Figure III-5 shows a schematic of the heater circuit electronics. Two variacs are hooked up in series to provide coarse and fine control of the heater current. The fine control variac is turned on and off by the Bayley controller. Since the Bayley bridge circuit operates on 60 Hz, the heater current has to be rectified and filtered in order to eliminate interaction between the control and heater circuits. Isolation transformers on the input side of both variacs eliminate grounding problems.

The temperature control provided by this system has been satisfactory even though the sensitivity of the Bayley is temperature dependent. When the sample temperature is increasing, the Bayley will switch off the heater at a temperature T_2 which is

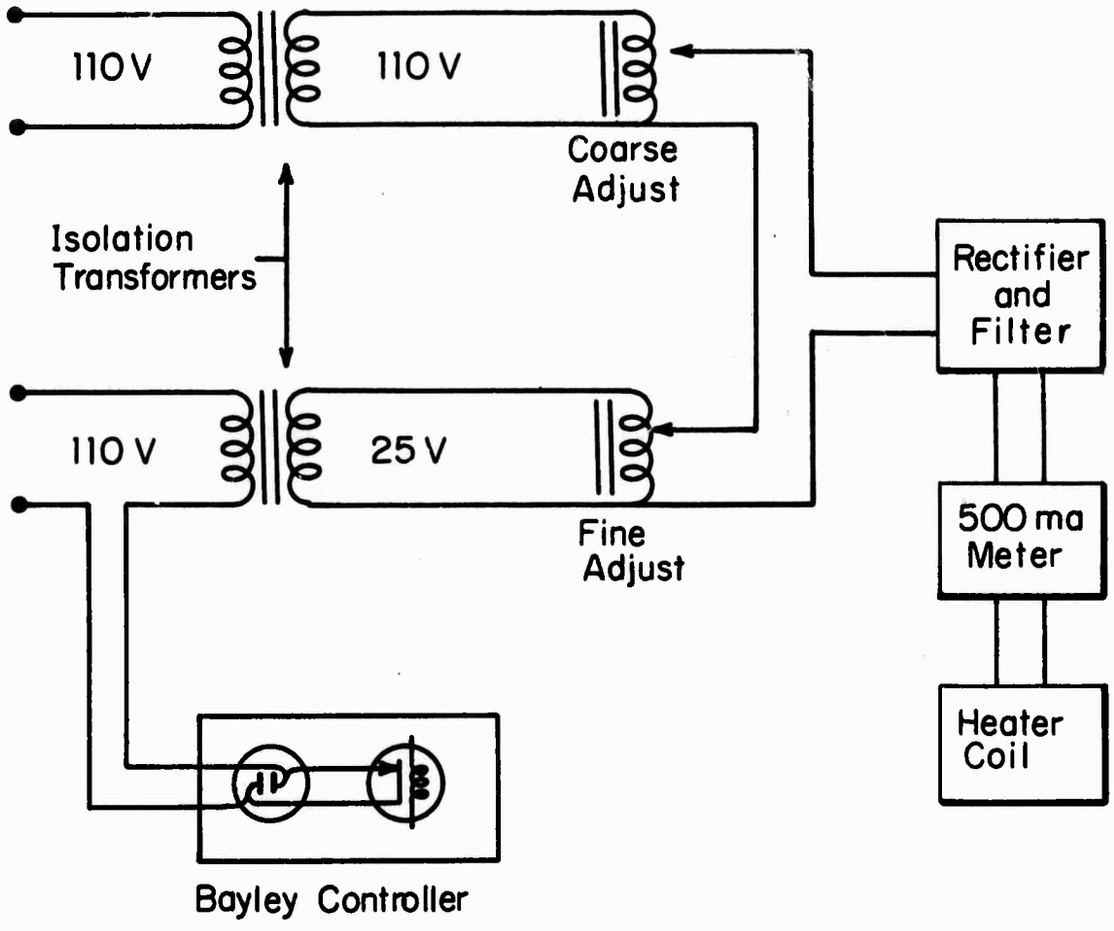

FIGURE III-5 Schematic diagram of the heater circuit electronics.

higher than the temperature T_1 at which the heater is switched on when the sample temperature is decreasing. We are calling this temperature difference $(T_2 - T_1)$ the sensitivity of the Bayley. As the resistance of the probe decreases from 131 Ω at 80°C to 12 Ω at 80°K, the sensitivity decreases from 0.02°C to 0.3°C. By looking at Figure III-1 we can see that the sensitivity should be approximately proportional to the probe resistance since it takes a minimum error voltage to activate the Bayley circuitry which closes the power relay. The temperature of the sample can be regulated to $\pm$ 0.03°C near the transition temperature. This control is achieved by setting the coarse and fine adjust variacs so that the "on" and the "off" periods of the control relay are both equal to ten seconds.

One drawback of this system is that it takes a few minutes to change the temperature of the sample holder and adjust the voltages for each new temperature. This time could be reduced by having a proportional control system rather than an on-off type controller. There were also difficulties due to the fact that the bridge circuit runs on a 60 Hz voltage which makes the instrument sensitive to pickup and grounding problems. These difficulties are manageable, and the measurements were successfully made, but a proportional control system run at a frequency other than 60 Hz would be much easier to use.

B. Measurements of the Resistivity Near the Transition Temperature

Four terminal resistivity measurements were made using a Leeds and Northrup type K-3 potentiometer and a Leeds and Northrup type M galvanometer. We wanted to make measurements with at least a precision of 1% or better, so this apparatus could not be used to measure sample resistances of above 10^6 Ω or below 10^{-2} Ω. For each measurement the temperature was stabilized and then the sample current and the voltage across the sample potential leads were determined.

Figure III-6 shows how our measurements compare with those of other researchers. The original work of Morin [2] is included as well as the more recent results of Sasaki and Watanabe [3], Bongers [4], and Everhart and MacChesney [5]. This figure shows very dramatically the variation in electrical properties of crystals grown by different authors. Morin's original data show a resistance ratio $R_s/R_m = 10^2$ for samples with a 20°C hysteresis. The hysteresis is much smaller in more recent measurements. There is a variation of about 10°C in the transition temperature for the measurements shown. For our samples the transition always occurred within one degree of 338°K. We note that the values of resistivity measured vary by about two orders of magnitude for both the high and low temperature phases. Please note, however, that many of the resistivity measurements have been made on small irregularly shaped samples and the absolute values of resistivity may be in error by a factor of two or more. Our observed resistivity ratio is as large as any value

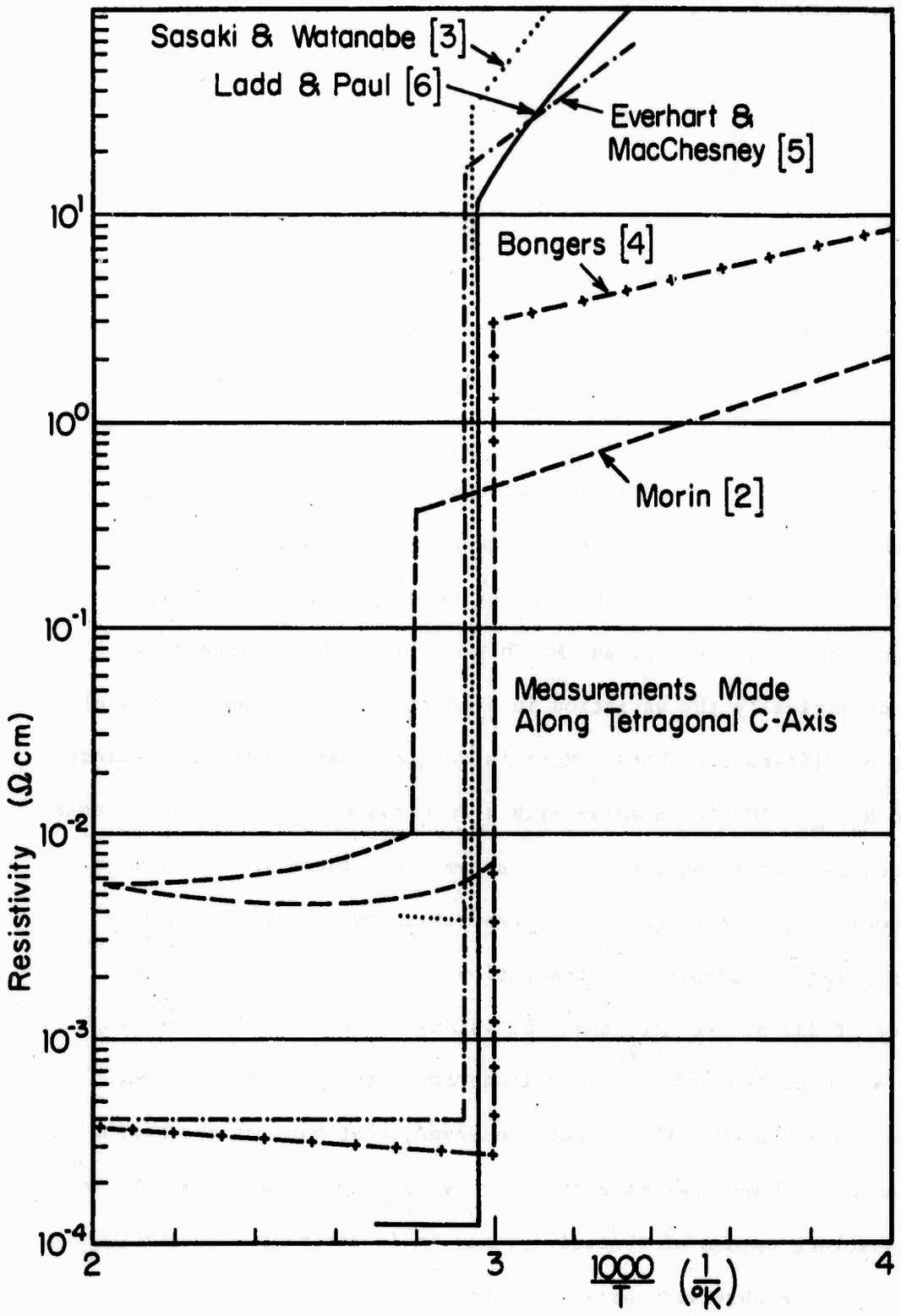

FIGURE III-6 Resistivity versus temperature for V_2O_4 crystals as reported by various authors.

in the literature [6]. For our good samples this ratio was always within $\pm$ 20% of 10^5. The variation in slope of the resistivity plot in the semiconducting phase also shows a lot of variation. We can interpret this slope as an activation energy when it is not temperature dependent. We see that the activation energy measured by Sasaki and Watanabe is four times as high as that measured by Bongers. Our curve shows an even larger slope, but it is temperature dependent and so cannot be interpreted as an activation energy. Our samples show a small positive temperature coefficient of resistivity above the transition temperature-behavior very similar to that of an ordinary metal. As can be seen in Figure III-6, this behavior has also been observed by Sasaki and Watanabe [3] and by Bongers [4].

We have also observed that in the metallic state the potential drop between the voltage leads was somewhat unstable and would suddenly increase or decrease by as much as 25%. We think that this may be due to relaxation effects associated with stresses at the sample contact interface or stresses in the bulk material. We know that there are stresses on the contacts since they come off after repeated thermal cycling. Since the contact area is large with respect to the contact spacing and the contact resistance is appreciable in the metallic state, fluctuations in the distribution of the contact resistance caused by relaxation of the stresses at the contacts could cause the observed behavior. Similarly bulk effects associated with cracks in the sample and relaxations of bulk stress could also cause the observed behavior. In the semiconducting state we sometimes

observed that the resistance would rise just before the transition. This behavior can be observed in Figure V-2, and we think that it is also associated with the existence of cracks and stresses in the sample or stresses at the sample contact interface.

We found that by careful control of the temperature we could make measurements during the transition process. After stabilizing the temperature, the resistance might change by as much as a factor of ten in five minutes, but then the crystal would reach equilibrium and the resistance would become stable. The transition occurred over a temperature interval of from 0.5°C to 0.1°C for different samples. For each crystal the shape of the resistivity versus temperature curve did not change as the sample was cycled through the transition temperature several times. The hysteresis varied from sample to sample between the values of 1.0°C and 0.4°C. The shape of the resistivity versus temperature curve was the same whether going through the transition from higher or lower temperatures as is shown in Figure III-7, and can be interpreted as a result of the nucleation and growth properties of the two phases of V_2O_4. The transition can be thought of as being sharp for any microscopic region of the crystal, and the resistivity of the crystal as a whole then depends upon how much of the crystal is in each phase. The exact temperature at which each microscopic region dV of the crystal undergoes the transition will depend upon the local density and types of imperfections in the crystal and upon the stresses between the domain in which dV is located and neighboring domains. Thus the shape of the resistivity

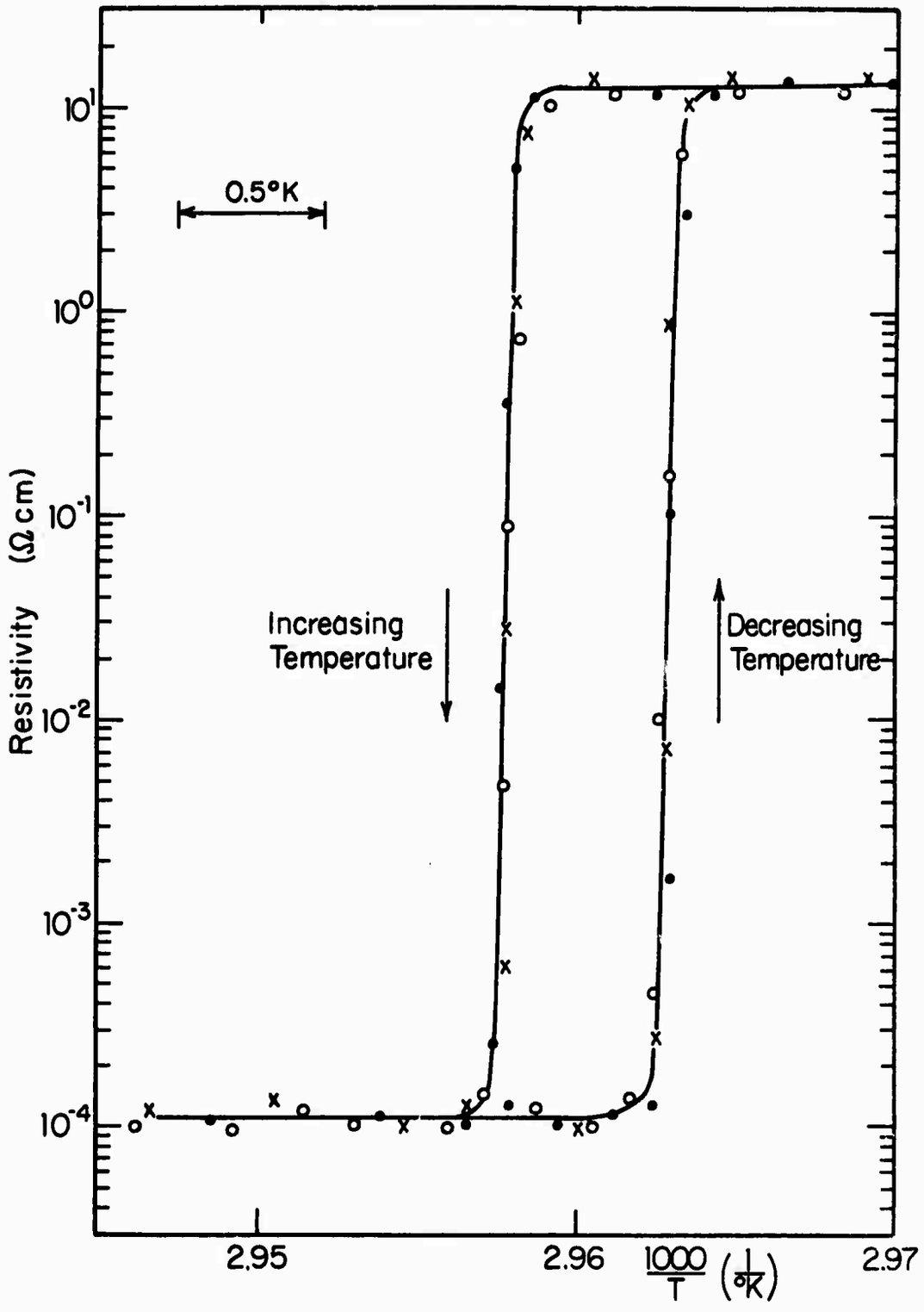

FIGURE III-7 Resistivity versus temperature near the transition temperature for one V_2O_4 crystal cycled three times through the transition.

versus temperature curve near the transition temperature is very sensitive to the structural properties of the crystal being measured and would be expected to vary somewhat from sample to sample.

C. Measurements of the Resistivity at Low Temperature

We made resistivity measurements down to 120°K. At lower temperatures the leakage currents between the current contacts were larger than the current passing through the sample. We had to take special precautions in cleaning our apparatus and cementing down the samples even to make measurements at 120°K. We cemented down only one end of the sample in order to eliminate leakage currents through the cement. The thermocouple was cemented to the same end of the sample that was cemented to the sapphire, and no cement touched the middle portion of the sample.

The contact resistance was small enough that two terminal measurements were adequate. A comparison of the results of two and four terminal measurements made between the transition temperature and 0°C showed that no significant errors were introduced. We used a Keithley Model 810B nanoammeter to measure the current through the sample. The circuit consisted of a battery, the nanoammeter, and the sample in series.

Figure III-8 shows the results of the low temperature measurements. The slope of the resistivity logarithm versus 1/T plot can be interpreted as an activation energy in regions where the slope is

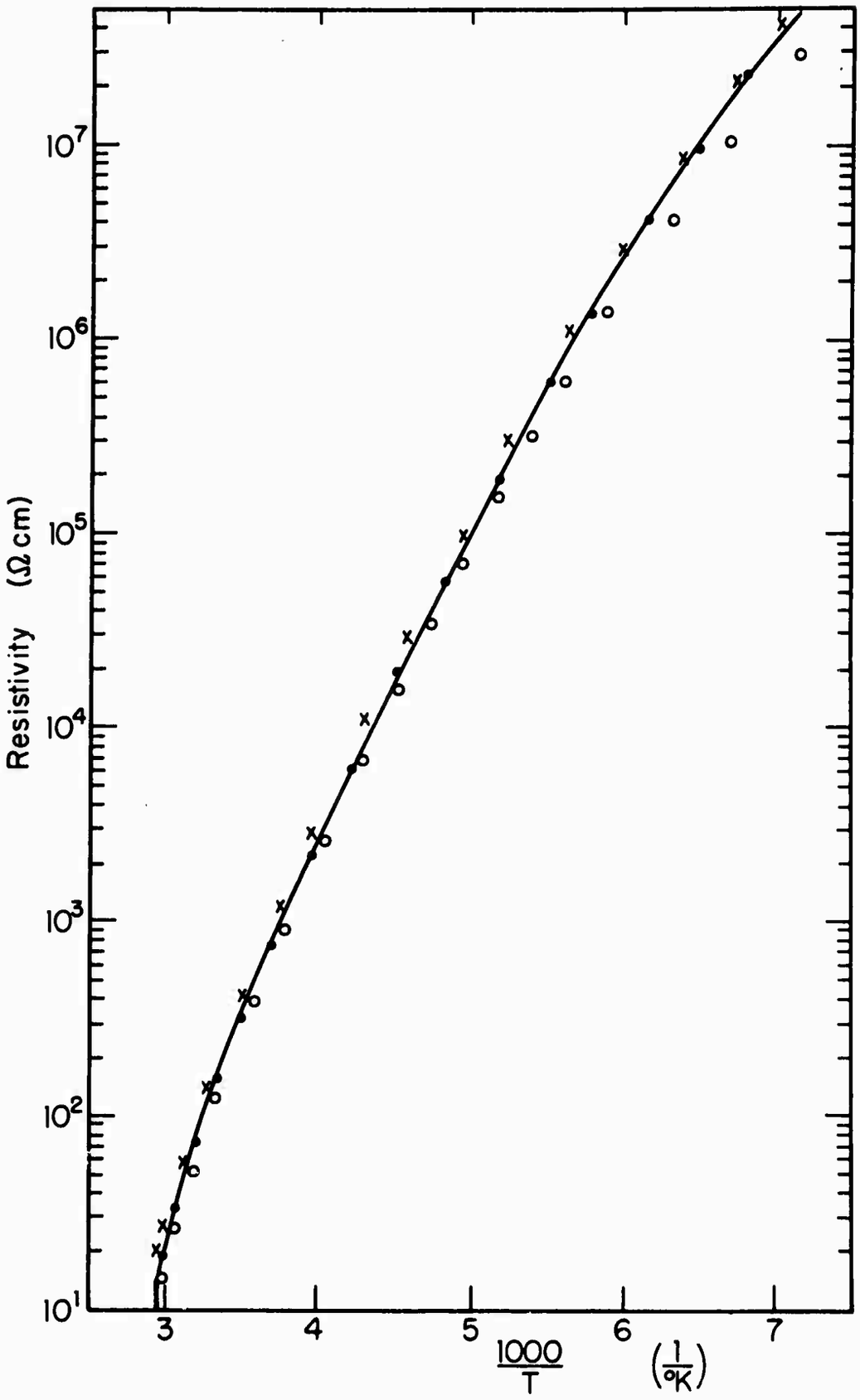

FIGURE III-8 Resistivity versus temperature for three V_2O_4 crystals at low temperature.

not changing too rapidly. We can see that as the temperature is lowered, the apparent activation energy decreases. This type of behavior is very similar to that of a doped semiconductor. This explanation and other alternative explanations of the conductivity of the low temperature phase will be considered in detail in Chapter VI.

Chapter III

REFERENCES

[1] Bayley Instrument Company, Danville, California, Precision Temperature Controller, Model 231.

[2] F.J. Morin, Phys. Rev. Lett. 3, 34 (1959).

[3] H. Sasaki and A. Watanabe, J. Phys. Soc. Jap. 19, 1748 (1964).

[4] P.F. Bongers, Solid State Comm. 3, 275 (1965).

[5] C.R. Everhart and J.B. MacChesney, J. App. Phys. 39, 2872 (1968).

[6] L. Ladd and W. Paul, Solid State Comm. 7, 425 (1969).

Chapter IV

OPTICAL MEASUREMENTS

In order to make reflection and transmission measurements on our V_2O_4 crystals as a function of temperature, a spectrometer in the laboratory was completely rebuilt. A multiple light source modification was made so that the light sources could be changed more easily, the sample optics were redesigned so that both reflection and transmission measurements could be made on small samples, a dewar sample holder was constructed which could be used with the temperature control system described in Chapter III, five high detectivity detectors were adapted to our system so that high sensitivity measurements could be made for wavelengths from 250 nm to 25 μm, and electronics compatible with these new detectors were incorporated in the system. This spectrometer was used to measure the reflectivity above and below the transition temperature and the temperature dependence of the transmission in the low temperature phase. This chapter will discuss the design and operation of the spectrometer and the measurements that were made.

A. Spectrometer Design and Operation

1. The Original Spectrometer Design

The spectrometer originally consisted of a Perkin-Elmer Model 112 single beam double pass infrared spectrometer and exit beam optics which could be used for either a pressure experiment or a

Faraday rotation experiment [1]. The optical schematic of the light source and monochromator is shown in Figure IV-1. Light from the source is focused on the entrance slit S_1 after passing through a 13 Hz chopper and being reflected from mirrors M1 and M2. Inside the monochromator the light is columnated by the parabolic mirror M3, passes through the prism once, is reflected by the Lettrow mirror M4, passes through the prism again, and then is focused on the exit slit by the parabolic mirror. The dispersed light can then be focused on an internal thermocouple detector T or mirror M6 can be displaced allowing the light to pass out of the monochromator to an external optical arrangement. The wavelength of the dispersed beam which passes through the exit slit S is adjusted by rotating the Littrow mirror M4 about the vertical post on which it is mounted. The wavelength drive which turns the Littrow mirror can be operated manually or by a synchronous motor and variable speed drive assembly. We have five prisms in the laboratory which can be used in the monochromator for different wavelength regions -- CaF_2, DF Glass, NaCl, LiF, and KBr. All of our measurements were made using the CaF_2 prisms which can be used from 250 nm to 10 μm.

The original external optics used with this spectrometer were designed to make measurements on large samples and incorporated thermocouple detectors. The standard Perkin-Elmer detection electronics consisted of a 13 Hz chopper for the light beam, a thermocouple detector, and an amplifier and phase detection circuit which drove a Leeds and Northrup 10 inch strip chart recorder.

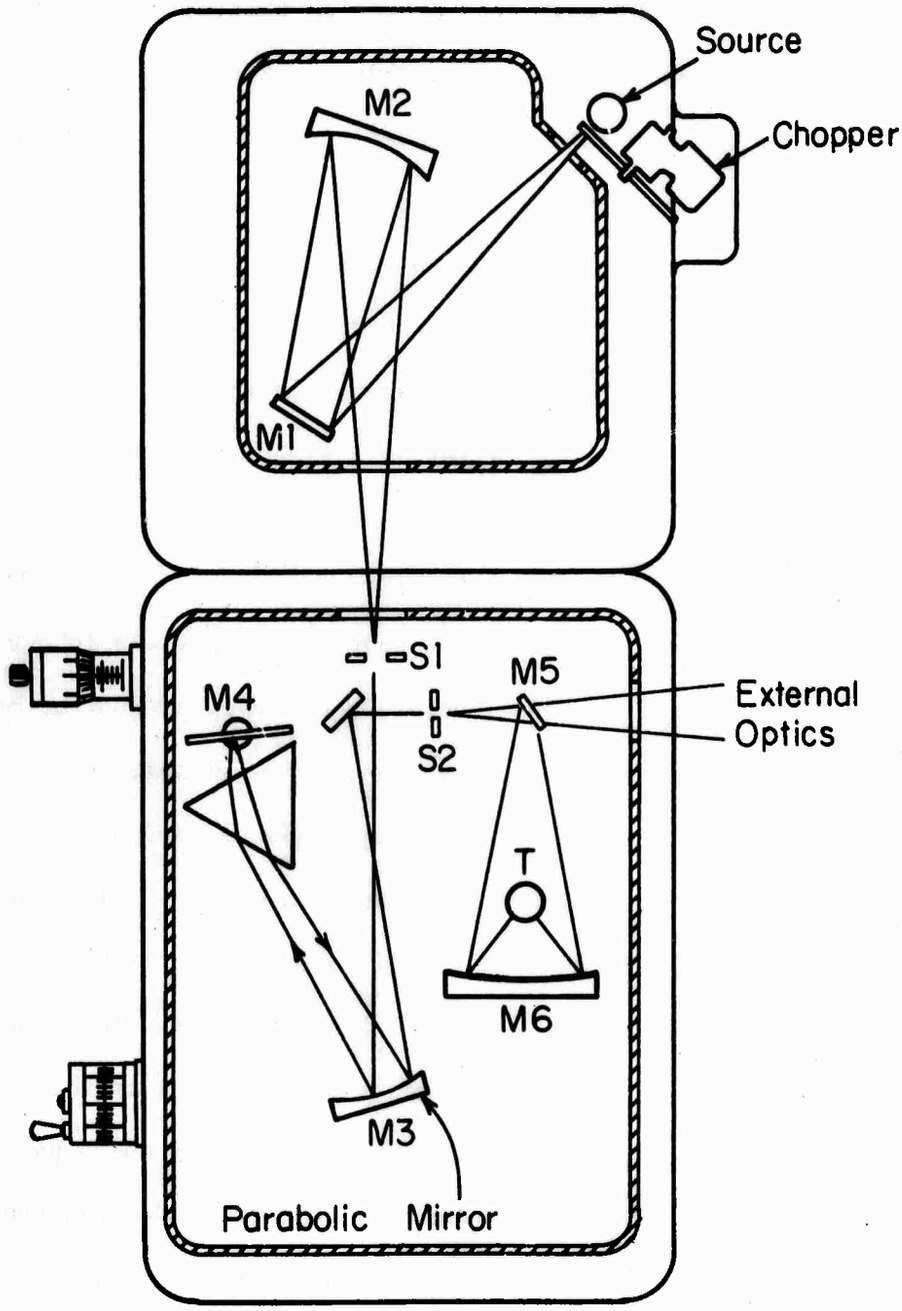

FIGURE IV-1 Perkin Elmer monochromator and light source assembly

We have rebuilt the exit beam optics so that both reflection and transmission measurements can be made on samples as small as 0.020" by 0.050" and so that five high detectivity photomultiplier and semiconductor detectors can be easily mounted in place. The electronics have also been rebuilt so as to be compatible with the higher chopping frequencies required by these new detectors and the monochromator light source assembly has been modified to permit light sources to be changed more rapidly. These modifications will be described in the following sections.

2. Multiple Light Source Assembly

The original Perkin-Elmer light source assembly was inconvenient because changing light sources involved a delay of an hour or more. We designed and built a light source assembly with which we could change between a glo-bar, a tungsten light source, and a mercury vapor calibration source by merely rotating a mirror. Figure IV-2 shows how two holes were drilled in the cover of the light source assembly to accommodate the additional light sources. The mirror M1 was placed on a rotatable mount and a slot was cut in the cover so that the mirror could be rotated by moving an arm which passed through the slot. The 13 Hz chopper was removed and a Princeton Applied Research Model BZ-1 variable speed chopper was placed just before the entrance slit. This chopper can be operated at nine speeds between the extremes of 13 Hz and 600 Hz. For a thermocouple detector it is used at 13 Hz and for the other detectors at 600 Hz.

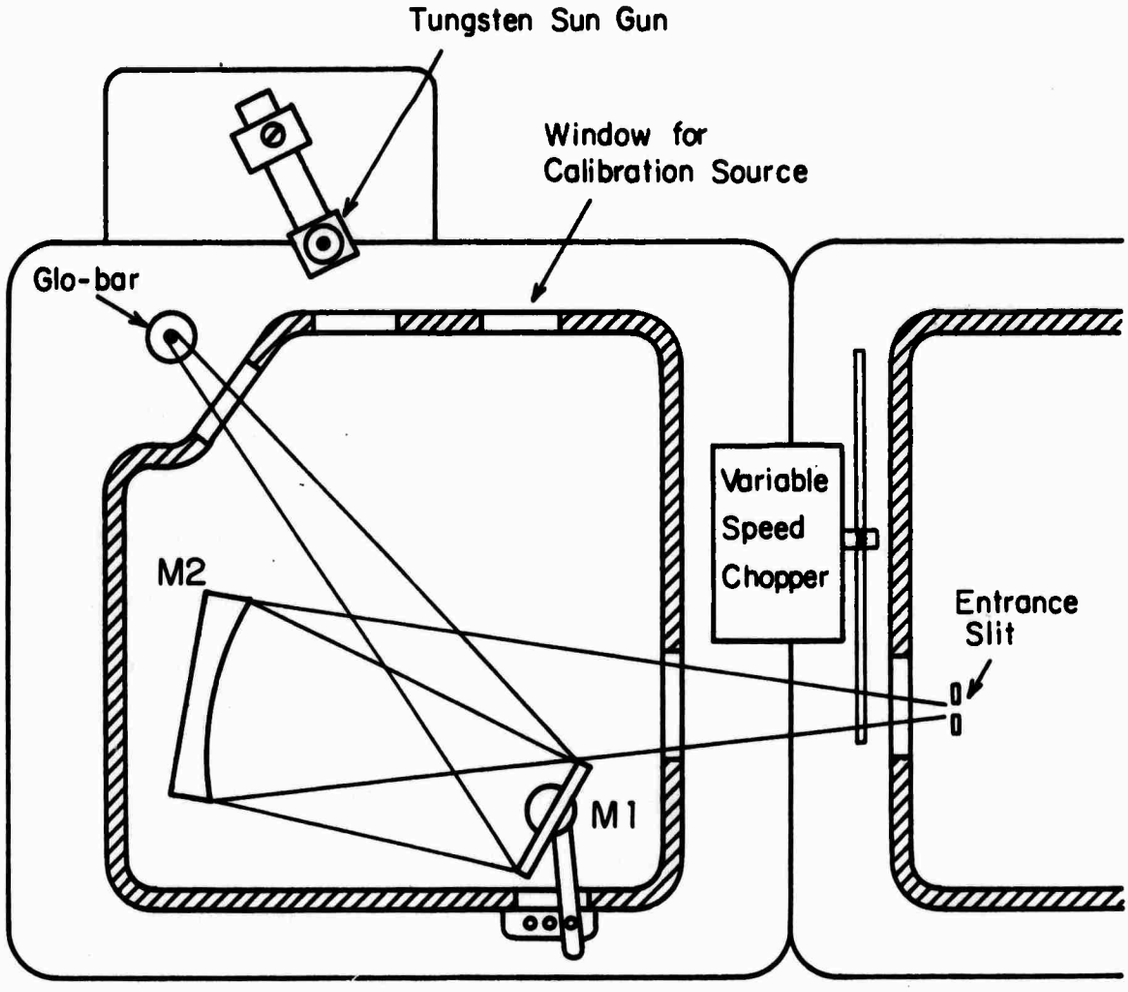

FIGURE IV-2 The multiple light source assembly and variable speed chopper.

The glo-bar was placed in the original source position and a 3200°K sun gun tungsten light source was placed in an adjustable mount in front of the adjacent window. During operation the mirror M2 was first adjusted so that the glo-bar image was in focus on the entrance slit, and then M1 was rotated and the sun gun was adjusted in its mounting so that its image was focused on the entrance slit. Both the glo-bar and the sun gun were operated at 200 watts. Any lower or higher operating voltage reduces the stability and lifetime of the sun gun. The third window was available for use with a mercury vapor calibration lamp. The spectrometer could also be used with a deuterium lamp for near ultraviolet measurements. In this case the light source assembly cover was removed and the lamp was placed on the spectrometer table at approximately the position where the word FIGURE is written in Figure IV-2. Its position has to be adjusted so that when mirror M1 is rotated the image of the light source is focused on the entrance slit. The height of all these light sources also has to be checked to make sure that the light going into the spectrometer entrance slit fills the parabolic mirror.

3. The Sample and Detector Optics

Our exit beam optical system was designed so that both reflection and transmission measurements could be made on small samples and so that cooled infrared detectors could be used. The optical system is a single beam design, so that two measurements have to be made with each sample -- an I_o measurement with the sample out of the optical path, and an I measurement with the sample in the optical path. The

reflection or transmission is then found by taking the ratio I/I_o.

The first design consideration is that the light has to be focused at both the sample and the detector since they are both small. Front surface aluminum mirrors are used throughout since they are achromatic and have high reflectivity in the visible and the infrared. One can use either on-axis or off-axis focusing with spherical mirrors. We chose an on-axis focusing system since it gives sharper images and is much easier to focus. It also requires three mirrors to focus the light on the sample instead of one, but for our measurements this was no drawback. The reflectivity of front surface aluminum mirrors is greater than 90% for all wavelengths greater than 250 nm with the exception of a small dip just below one micron. Figure IV-3 shows a schematic of the exit beam optics. Please note that part of the optical path has been drawn rotated so that the design shows more clearly. The spherical mirror just before the detector is actually mounted horizontally below the detector. This design was necessary because we wanted to be able to use cooled detectors which could be mounted vertically.

We used reducing optics to obtain a small image size at the sample and the detector. An alternative approach is to use a very small exit slit and non-reducing optics, but this method drastically reduces the light intensity at the sample. In designing reducing optics with spherical mirrors one usually has to sacrifice either light intensity or image quality because reducing optics involves low

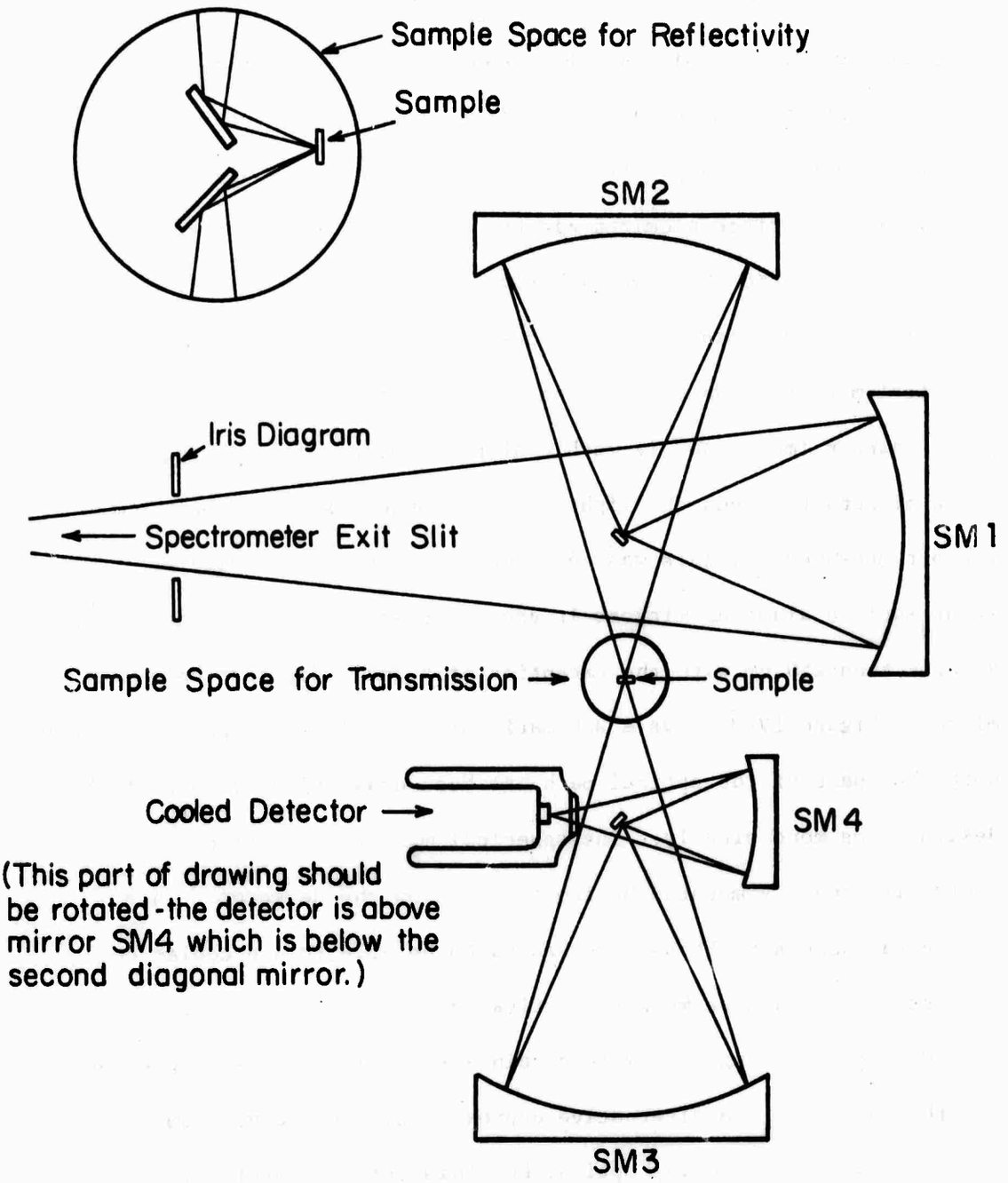

FIGURE IV-3 The sample and detector optics. The main diagram shows the configuration for transmission measurements, and the insert shows how the sample space is adapted for reflection measurements.

f-number mirrors. Thus in order to reduce spherical aberration one has to raise the system f-number by masking off most of the light beam [2]. We were able, however, to design a system that partially eliminated this problem by making the image and object distances nearly equal. For spherical mirrors the focus will be exact for any aperture if the image and object are both at the center of curvature of the mirror, thus for a given f-number the focus will always be best if the image and object distances are nearly equal. In our design all of the reduction in image size occurs at the first spherical mirror (which has an f-number of 0.92) and the image-object ratio is 3:2 in the other spherical mirrors (which have a smaller f-number of 0.69). In contrast, the f-number of the monochromator is determined by the parabolic mirror and is 3.56. The size of the image at the sample and detector is 3/8 that of the exit slit.

An iris diaphram has been placed in the exit beam of the spectrometer so that we can adjust the f-number of the exit beam optics depending upon how much light and how sharp a focus is needed. The f-number only has to be reduced by 50% in order to obtain a sharp image at the sample. Thus precision transmission measurements can be made with this spectrometer on samples as small as 0.020" by 0.050" while only masking off 50% to 75% of the light beam. Precision reflectivity measurements can be made on even smaller samples.

Figure IV-3 shows how the spectrometer is set up for both reflection and transmission measurements. For transmission the I curve

is made with the sample positioned in the light path as shown and the I_o curve is made with the sample removed from the light path. For the reflection I measurement, two mirrors are introduced into the light path and the sample is located as shown in the insert of Figure IV-3. This setup gives approximately on-axis focusing and measures the reflectivity at near normal incidence. The I_o data can be obtained either by replacing the sample with a mirror of known reflectivity or by moving the two mirrors RM1 and RM2 to the position shown in Figure IV-4. The latter method was used because it preserves the same number of reflections from the same mirrors in the I and I_o data. The necessity to correct for the reflectivity of a reference mirror is also eliminated. Since spherical mirrors SM2 and SM3 have to be refocused between the I and I_o measurements, the image of mirror SM4 also has to be refocused on the detector. The appropriate refocusing technique depends upon which detector is being used, but in all cases errors from refocusing can be reduced to ±8% or less. These refocusing errors plus drift of the light source and detector are the main sources of uncertainty in our reflectivity measurements. We feel that our reflectivity measurements are accurate to at least ±10%.

Mirror mounts similar to those used in the monochromator are used to hold the spherical mirrors. The vertical and horizontal focus at the sample can be controlled very precisely by means of spring loaded adjustment screws on mirror mounts SM1 and SM2. There is also

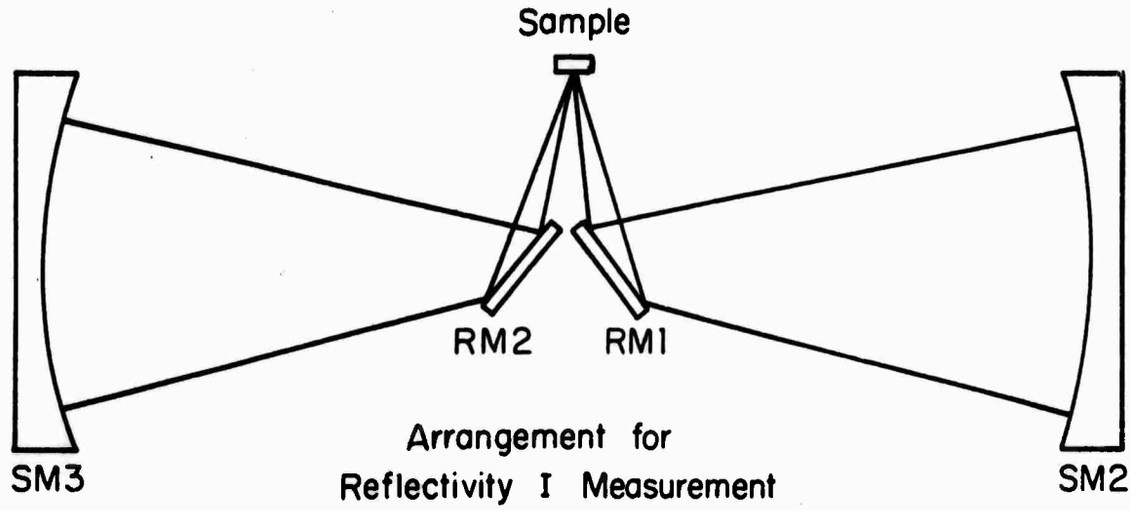

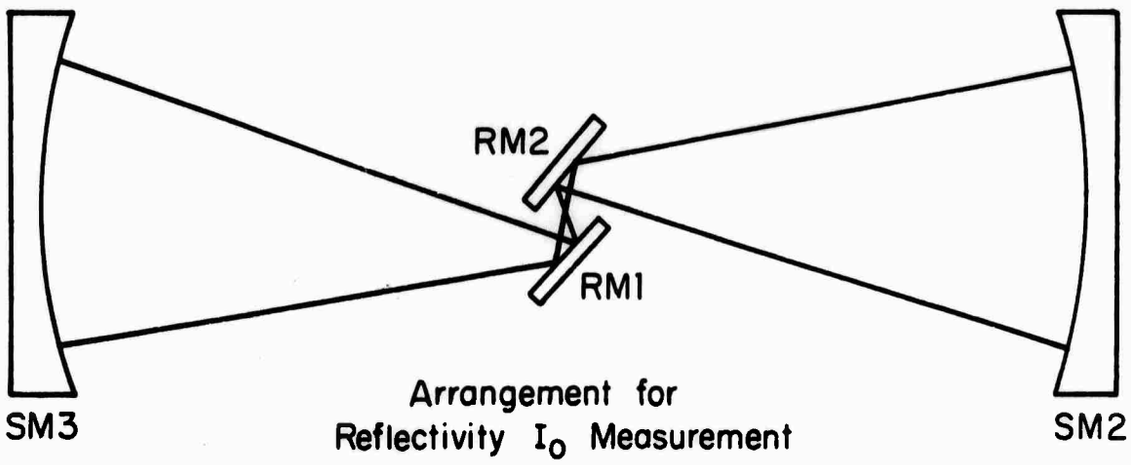

FIGURE IV-4 Schematic diagram of the arrangement used for making the I and I_0 measurements in reflectivity.

a screw adjustment on SM2 which moves the mirror toward or away from the sample so that the focal plane of the image at the sample can be adjusted to be exactly on the sample surface. There are similar adjustments on SM3 and SM4 to permit the image to be focused on the detector.

The high detectivity detectors are all mounted in holders that attach to a one inch in diameter vertical post which is located five inches to the side of the middle of mirror SM4. The detectors can be mounted in approximately the correct position on this post and then the light can be focused on them by adjusting mirrors SM3 and SM4. For the copper-doped germanium detector which requires liquid helium when in use, a special attachment has been made so that the detector can be removed from the spectrometer, filled with liquid helium, and then returned to the same position. The five high detectivity detectors which have been put in holders which fit on the spectrometer are a Ge:Cu photoconductor, an InSb photovoltaic diode, a PbS photoconductor, an S1 response photomultiplier tube, and an S13 photomultiplier tube. A thermocouple detector can also be used by replacing SM4 with a specially designed thermocouple mount. These detectors are described in detail in Section 5.

4. Sample Holder Dewar and Temperature Control System

A special dewar, illustrated in Figure IV-5, was constructed which is small enough to fit into the sample space of our spectometer and which can be used for either reflection or transmission measurements.

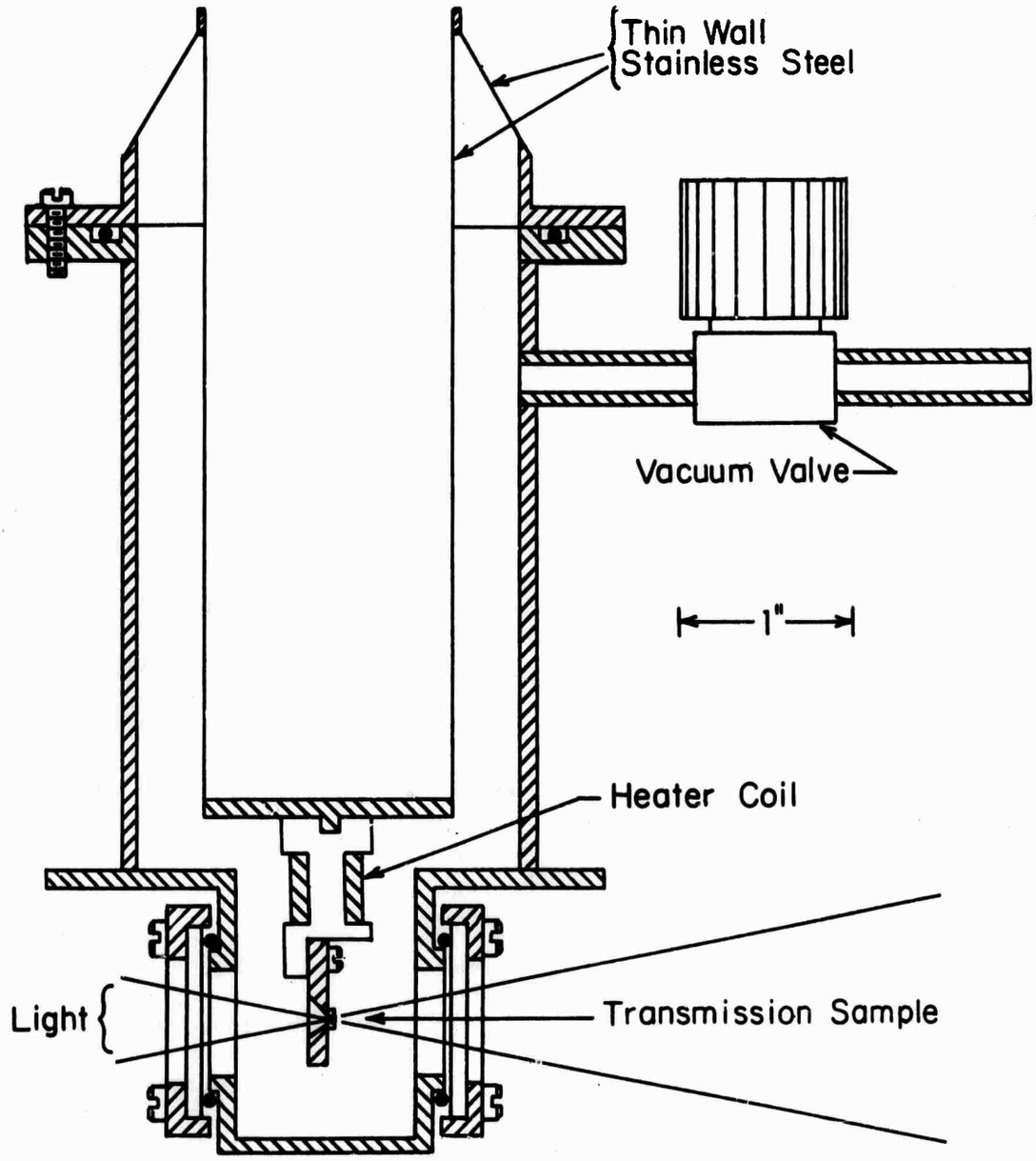

FIGURE Ⅳ-5 A schematic view of the optical dewar.

When this dewar is filled with ice water, dry ice and acetone, or liquid nitrogen, the sample holder can be heated up to a temperature approximately 150°C above the temperature of the cooling bath.

Figure IV-6 shows the construction of the heater coil and sample holder in more detail. The flow of heat in the sample holder is from the heater coil through the center portion of the copper heat sink and up through the bottom of the dewar into the cold bath. After the temperature has been stabilized there is no flow of heat in the bottom portion of the sample holder where the sensing resistor and the sample are mounted, so there are no thermal gradients in this region. The nickel temperature sensing resistor is connected to the temperature control system which is described in detail in Chapter III. The temperature of the sample is measured by a copper-constantan thermocouple which is cemented to piece A near the sample. The thermocouple leads are cemented to the copper heat sink as shown in Figure IV-6 in order to prevent any heat leak through the thermocouple wires to the sample holder and sample. The nickel temperature sensing resistor is cemented in place with General Electric No. 7031 varnish which provides fairly good thermal contact with the heat sink.

A special sample holder was designed so that we could mount samples for transmission measurements. We wanted to cement the sample over a hole in a piece of brass so that the light could pass through the sample but not around it. Our samples are usually several times longer than they are wide, so we needed small slot shaped holes. A

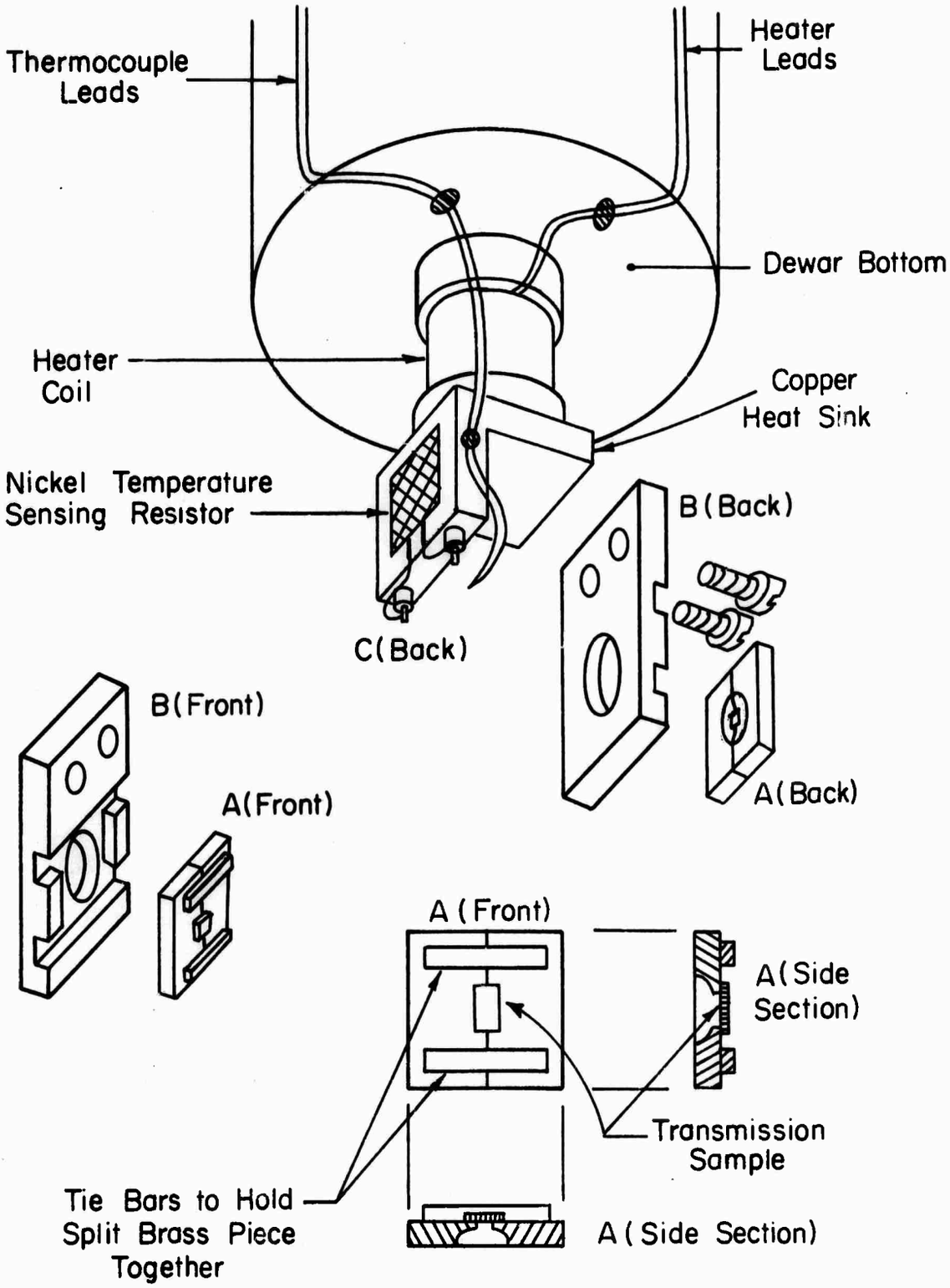

FIGURE IV-6 Optical dewar sample holder and sample mounted for a transmission measurement.

brass piece, labelled A in Figure IV-6, with such a hole was constructed by the following procedure. Two thin flat plates of brass are machined so that they fit evenly when placed together edgewise to form one larger plate. Then a small slot is milled in the edge of each plate on the surface which fits together. When the plates are again placed together edgewise they form a single plate with a slot shaped hole in the middle. Figure IV-6 shows the details of construction. Two tie bars are epoxied to the top of the plates to hold them rigidly in the proper position. Notice that the back of the plates is relieved near the hole so that the cone of light passing through the sample is not obstructed.

After a sample is mounted, piece A is cemented in place in the recess in the brass piece labelled B in Figure IV-6, and when a measurement is to be made piece B can be mounted with two screws on the sample holder heat sink labelled C. All of the B pieces are identical, but an A piece with the proper sized hole must be made for each sample. If room temperature measurements are to be made, then piece B can also be mounted on a different sample holder which is not inside a dewar. When reflectivity measurements are being made, the sample can be mounted on a solid piece A since no hole is needed.

5. The New Detection Electronics System and Detectors

The Perkin-Elmer electronics which had a chopping frequency of 13 Hz for use with thermocouple detectors was replaced by a system operating near 1 kHz which is more suitable for use with photoconductive detectors which have 1/f noise.

The new detection electronics system consists of a variable speed chopper, a lock-in amplifier, and a 10 mV strip chart recorder. The Princeton Applied Research model BZ-1 variable speed chopper can be operated at 13 Hz for thermocouple detectors and at 600 Hz for the other detectors. A reference signal from the chopper and a signal from the detector are fed into a Princeton Applied Research Model HR-8 lock-in amplifier and phase detected. The phase and frequency must be adjusted for each detector. The output of the lock-in amplifier goes to a Leeds and Northrup Model G Speedomax 10 inch strip chart recorder which was part of the original Perkin-Elmer spectrometer.

The circuit diagram, chopping frequency, region of spectral response, and maximum signal level for each of the detector is shown in Figure IV-7. The semiconductor and photomultiplier detectors would be operated at 1500 Hz if the variable speed chopper could be operated at a higher speed. The region of spectral response listed is for the system as a whole and includes the wavelength dependence of the light source, prism, mirrors, and detector. By the region of spectral response we mean the region over which the signal at the recorder is greater than 1% of the peak value. This definition gives a first approximation to the useful wavelength range for using these detectors in this spectrometer. If the semiconductor detectors are operated above the maximum signal level indicated, their response becomes non-linear and errors are introduced in the measurement, whereas if the photomultiplier detectors are operated with output

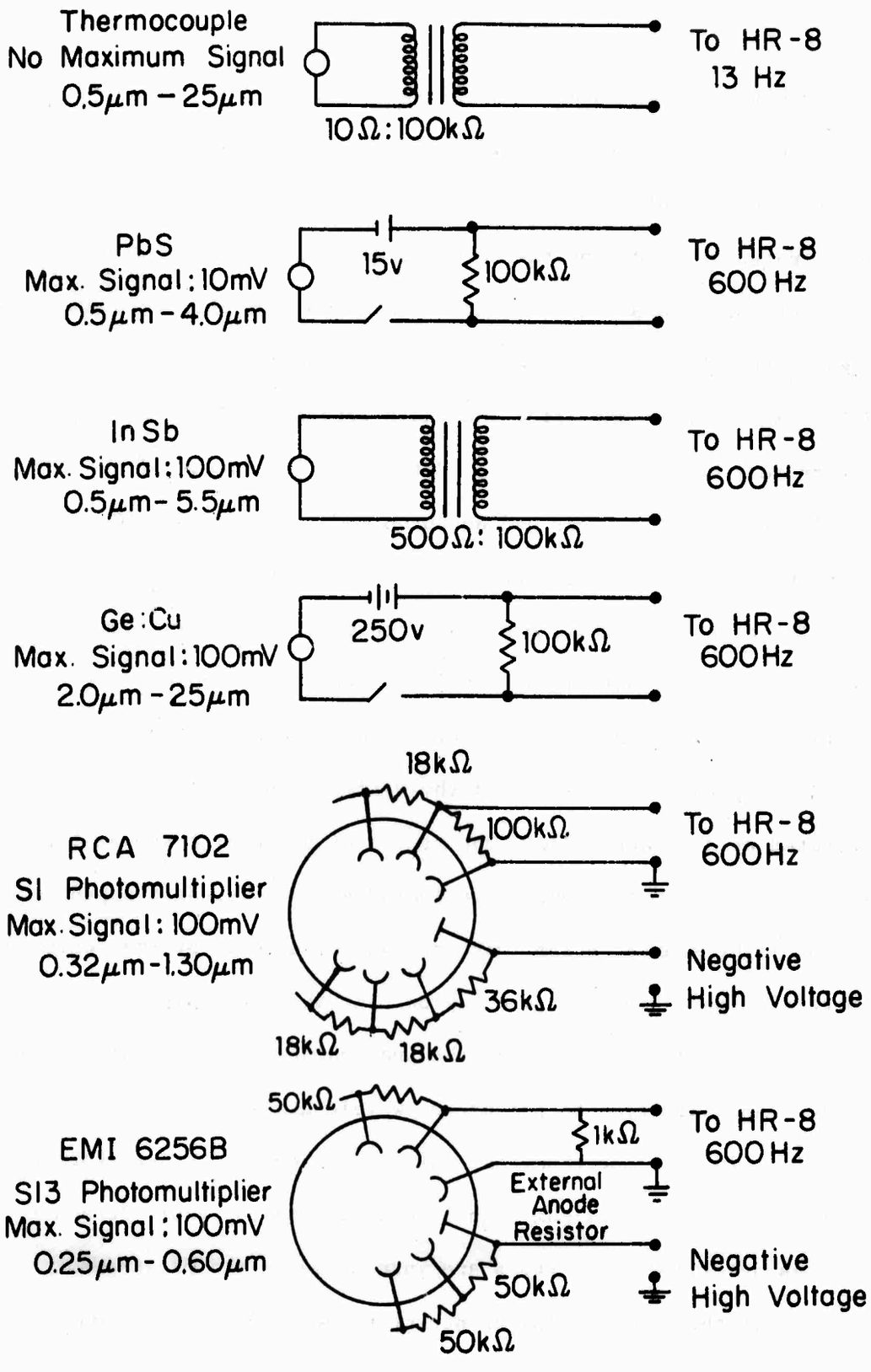

FIGURE IV-7 Circuit diagrams for detectors including chopping frequency, maximum output, and spectral response.

voltages above the maximum indicated, the tubes will be burned out due to overheating.

The thermocouple detectors were purchased from Reeder Corp. in Detroit, Michigan and operate at room temperature. Some of them have hygroscopic infrared windows and must be kept in a desiccated container. Their sensitive area is 0.1 mm X 1.0 mm, and the thermocouple element has a uniform detectivity at all wavelengths. Thus the region of spectral response as defined above is 0.5 μm to 25 μm and is determined by the transmission of the window, the dispersion of the prism, and the spectral dependence of the light source intensity. The PbS detector was purchased from Infrared Industries in Waltham, Massachusetts. This is a photoconductive device which operates at room temperature, has a sensitive area of 1 mm X 3 mm, and has a region of spectral response from 0.5 μm to 4.0 μm. The InSb detector was purchased from Philco Corporation in Spring City, Pennsylvania and is in a liquid nitrogen dewar which has a 4-hour hold time. It is a photovoltaic device and the output is transformer coupled to the model HR-8 lock-in amplifier. The sensitive area is 1 mm X 3 mm and the region of spectral response is from 0.5 μm to 5.5 μm. The copper doped germanium detector was purchased from Santa Barbara Research Center in Goleta, California and is mounted in a liquid helium dewar. This dewar is designed so that the cold shield is cooled by the escaping helium gas rather than by a liquid nitrogen jacket. It holds one liter of liquid helium when filled

and has a hold time of 6 to 8 hours. This is a photoconductive device, the sensitive area is 1 mm X 3 mm, and the region of spectral response is from 2.0 μm to 25 μm. A BaF_2 cold window can be placed in the dewar to improve the detectivity by a factor of two, but it also reduces the long wavelength cutoff to 15 μm. The RCA 7102 photomultiplier has an S1 photocathode and it is mounted in a container in which dry ice can be placed to reduce the noise level by a factor of 100. The photocathode is one inch in diameter and the light should be focused so as to nearly fill the sensitive area. The region of spectral response is from 0.32 μm to 1.30 μm. The MI 6256 B photomultiplier tube has an S13 photocathode and does not need to be cooled during operation. The photocathode is one centimeter in diameter and the light should be focused so as to nearly fill the sensitive area. The region of spectral response is from 0.25 μm to 0.60 μm. The anode resistor is not built into the wiring of the tube socket, and so an external 1 kΩ resistor must be included in the circuit between the tube and the HR-8. Precuations should be taken to shield the photomultiplier tubes from room light during operation in order to prevent burning out the tubes.

6. Spectrometer Calibration

The wavelength drive mechanism which turns the Littrow mirror is connected to an indicating drum on the spectrometer and to a cam which activates a microswitch which is connected to a pip marker on the recorder. The calibration procedure consists of making a graph which will convert drum readings into wavelengths. Since spectral

absorption and emission lines are known to great accuracy, a very precise spectral calibration can be achieved if a sufficient number of calibrating wavelengths are measured. For the measurements we planned to make, we felt that an uncertainty in the wavelength calibration of about 0.5% would be acceptable and this helped to determine the number of lines which we used for the calibration. More than thirty spectral lines from a General Electric H85A3/uv mercury vapor spectral lamp were used to calibrate the system from 0.25 μm to 2.0 μm [3]. This provides a calibration accuracy varying from 0.1% near 0.25 μm to 0.3% near 0.85 μm to 0.2% near 2 μm. More than thirty atmospheric absorption lines were used to calibrate the system from 2 μm to 7 μm [4]. The calibration accuracy in this region varies from 0.1% near 6 μm to 0.2% near 3 μm to 0.15% near 2 μm. All of our measurements were made with a CaF_2 prism, and each time the Littrow mirror was changed or the prism was taken out and then replaced again the system was recalibrated by the above procedure. One useful feature of the spectrometer is that all calibrations of the same prism will be identical except for a displacement of the drum readings. Thus different calibrations can be easily compared, and we found the different calibrations to agree to within the uncertainties quoted above.

The spectral resolution of the instrument depends upon the wavelength, slit setting, and prism used. Consider the case where the exit slits are covered by a white card and a spectral lamp is being used as a light source. As the drum is turned the Littrow

mirror rotates and the image of the spectral lines moves across the card. For our spectrometer the geometry and the gear ratio between the drum and Littrow mirror are such that the image of the spectral lines moves 2 mm for each drum rotation. Now consider the case where the slits are opened 1 mm and there is a spectral line focused at each edge of the slits. The spectral resolution of the instrument at this setting is just the difference between the wavelength of these two lines. Since the slits are 1 mm wide, we know from the above analysis that the two lines will be 0.50 drum units apart on the calibration curve. Thus the resolution of the spectrometer can be determined from the calibration curve and the slit setting. For example if the slit setting was 2 mm, the wavelength interval in the exit beam would correspond to that produced by one unit of drum rotation.

B. Optical Measurements

1. Reflection Measurements

We made reflectivity measurements on V_2O_4 crystals both above and below the transition temperature from 0.25 μm to 4.0 μm. A deuterium light source and an EMI 6256B photomultiplier detector were used for the region from 0.25 μm to 0.55 μm, and a 200 watt sun-gun light source and a PbS detector were used between 0.5 μm and 4 μm. We also used an RCA 7105 photomultiplier detector in the region from 0.4 μm to 1 μm to confirm that we were joining the curves from these two regions together properly. The optical arrangement of the spectrometer for reflectivity measurements has already been

discussed and is illustrated in Figures IV-3 and IV-4. The sample was mounted on an aluminum post which could be heated by a coil of No. 40 enameled copper wire which was wound around the middle of the post. The sample was heated to 90°C for the measurements above the transition temperature.

Figures IV-8 and IV-9 show the reflectivity data for one the crystals that was used for transmission measurements. The crystal was lapped, and polished as is described in Section 2. We found considerable variation in the reflectivity spectra from different crystals. In the semiconducting phase, for example, all samples showed a reflectivity peak near 1 eV and one near 3 eV, but the height of the 1 eV peak varied from the value shown in Figure IV-8 down to 27% for different samples and the location of the peak varied between 0.75 eV and 1.1 eV. The variation in the high energy peak was not as extreme. All of our measurements were made with unpolarized light on (110) crystal faces. Different surface preparations were tried, but the difference in reflectivity for the same sample with a natural face, a polished face, or an etched face was much less than the variation between samples. These differences are not due to errors in the measurement, since the values of reflectivity in each measurement are accurate to $\pm$ 10% as was mentioned previously.

We see from Figures IV-8 and IV-9 that there is a large change in the reflectivity as the sample is heated through the transition temperature. Below T_c there is a peak near 1 eV which is suggestive of an energy gap and above T_c there is a large free carrier like

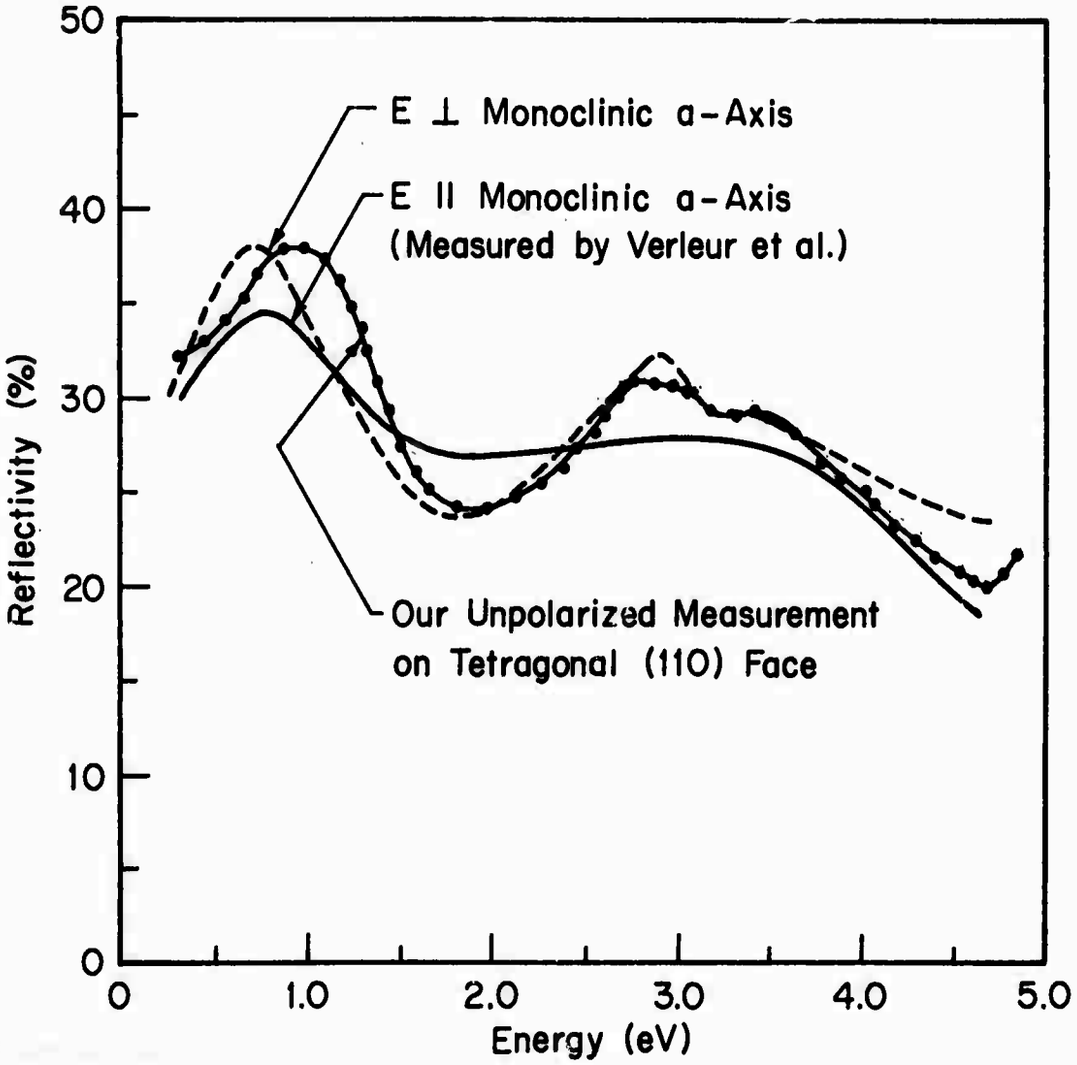

FIGURE IV-8 Our reflectivity measurement on V_2O_4 for $T > T_c$ compared with those of Verleur et al. [5].

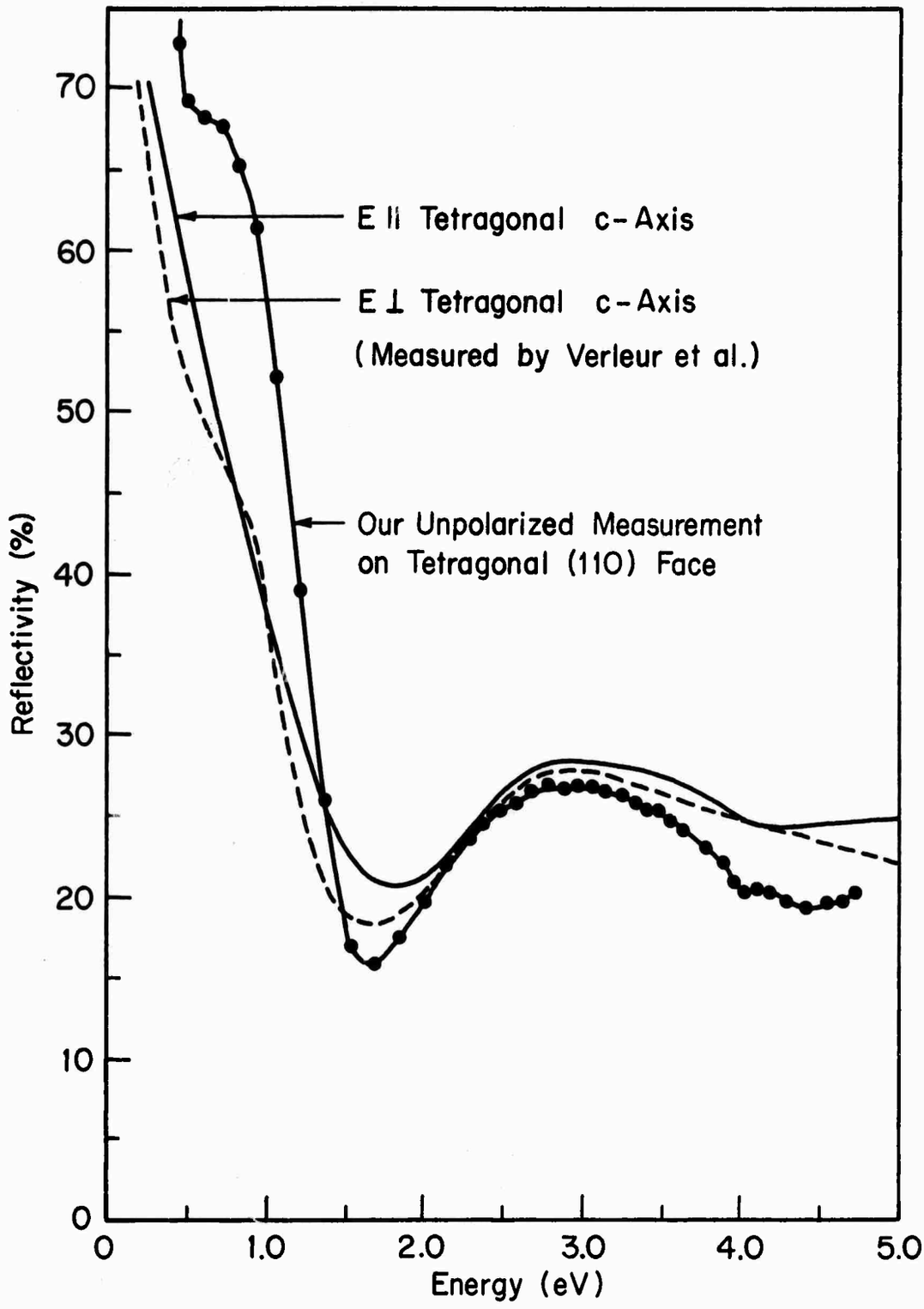

FIGURE IV-9 Our reflectivity measurement on V_2O_4 for $T > T_c$ compared with those of Verleur et al. [5].

reflectivity for energies below 1 eV. There is also some structure near 1 eV in the metallic state. A peak near 3 eV appears in both phases.

The reflectivity of V_2O_4 crystals has also been measured by Verleur et al. [5] and by Mokerov and Rakov [6]. The data of Verleur et al. are shown in Figures IV-8 and IV-9, and the date of Mokerov and Rakov have similar features except that the peak at 3 eV is larger than the 1 eV peak. Considering the large variation we have observed from sample to sample for our own crystals, we do not consider that the differences between the spectra reported by ourselves, by Verleur et al., and by Mokerov and Rakov to be significant. Verleur et al. have also measured the reflectivity and transmission of thin V_2O_4 films and their data is shown in Figures IV-10 and IV-11. These films show features in reflectivity that are similar to bulk crystal data [5]. Looking at the absorption of the films, we see that for $T < T_c$ there is an energy gap corresponding to the peak at 1 eV and there is a strong absorption corresponding to the peak at 3 eV. For $T > T_c$ there is a free carrier like absorption in the infrared and a strong absorption near 3 eV. The interpretation of the above bulk crystal and thin film measurements will be discussed in more detail in Chapter VI.

2. Transmission Measurements

It was not hard to show that V_2O_4 transmitted infrared radiation below the transition temperature, but the determination of an energy gap and its temperature dependence was quite difficult. We used very

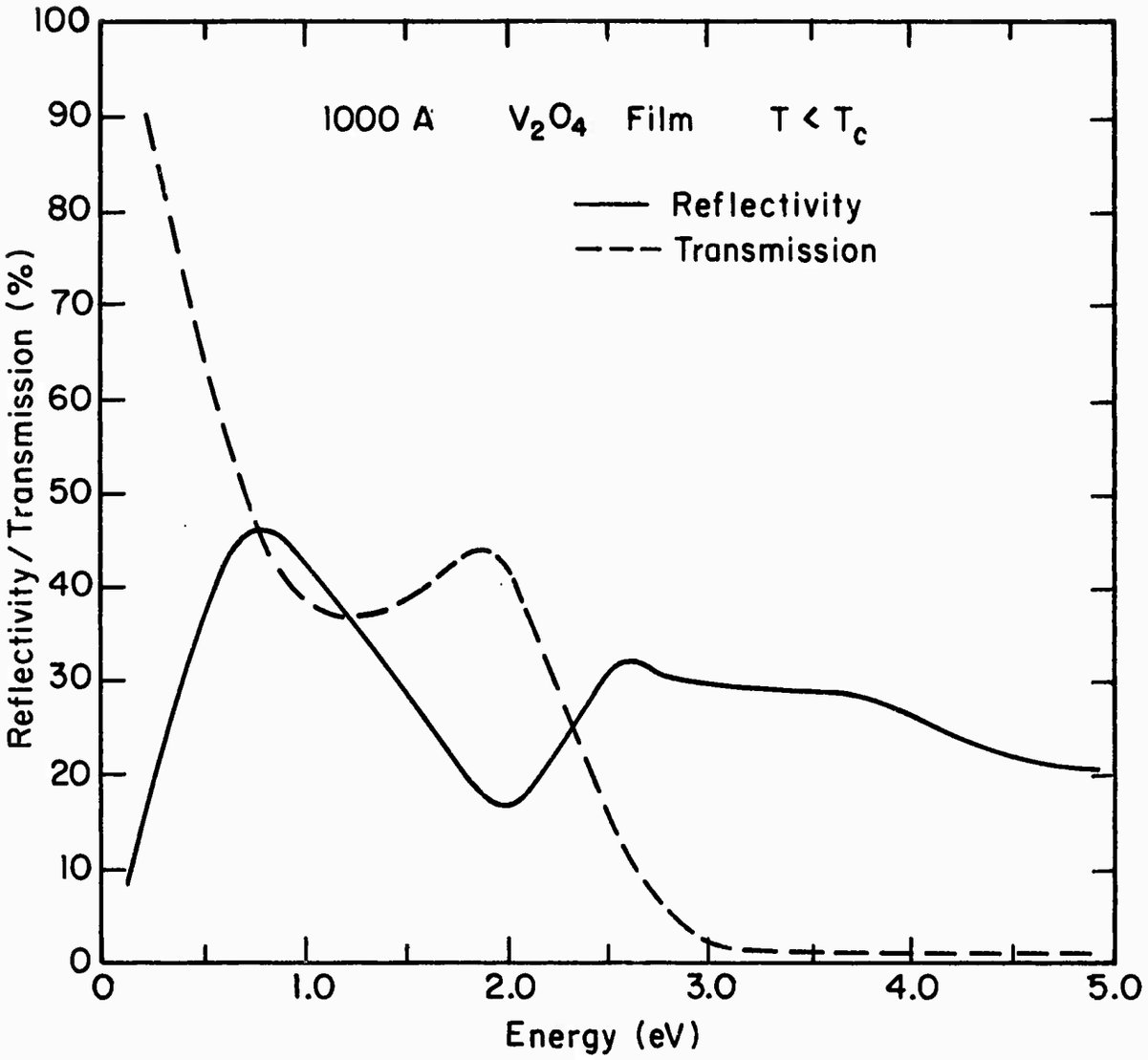

FIGURE IV-10 Reflectivity and transmission of a thin V_2O_4 film below the transition temperature as reported by Verleur et. al. [5]

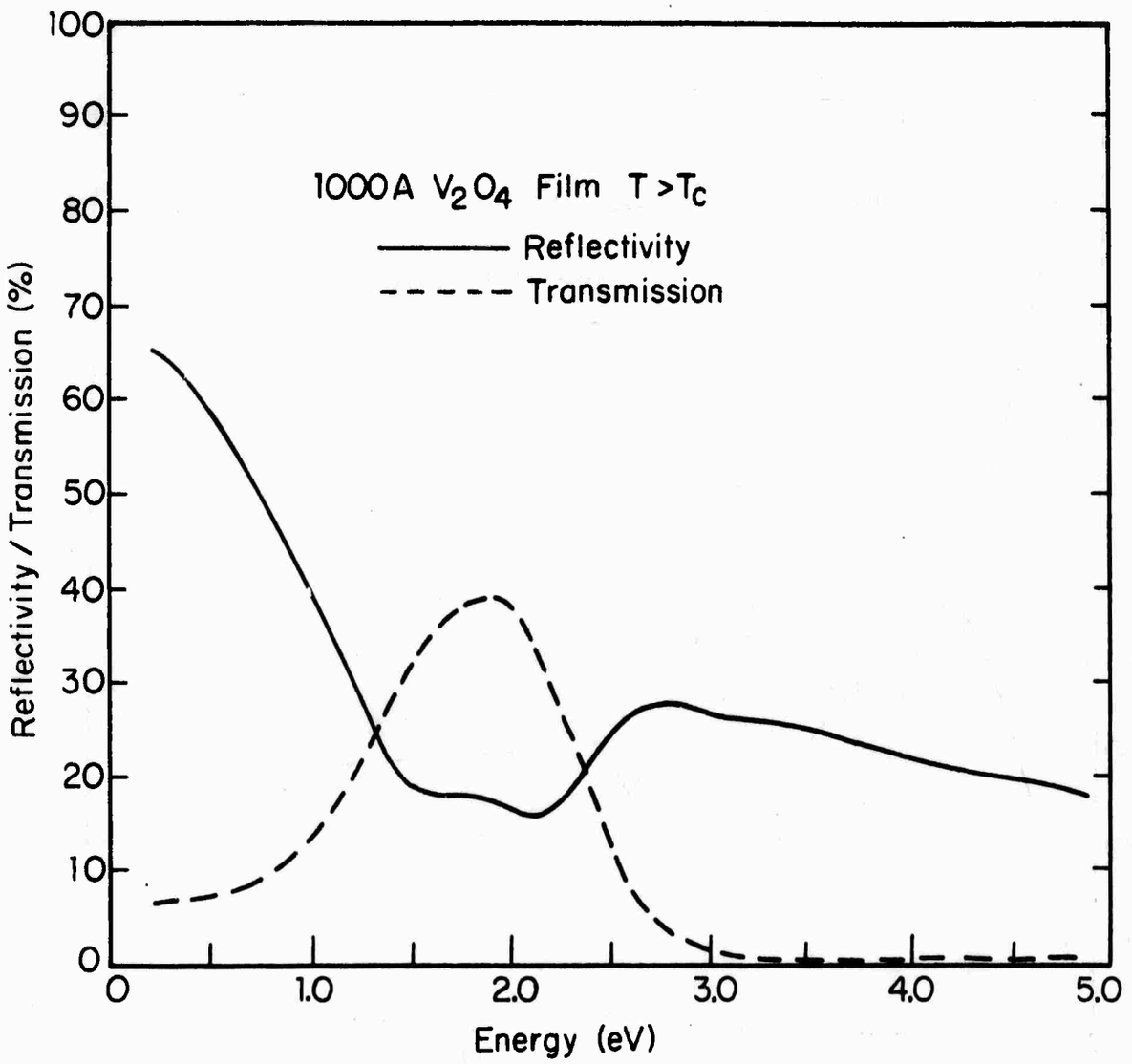

FIGURE IV-11 Reflectivity and transmission of a thin V_2O_4 film above the transition temperative as reported by Verleur et. al. [5].

thin samples so that the highest possible absorption coefficient could be measured. This allowed us to measure a portion of the absorption edge where the absorption was varying quite rapidly with energy, and consequently we could make a more accurate determination of the temperature dependence of the transmission.

Transmission samples were prepared from our better looking samples in the following manner; The crystals were first lapped flat on one side with 3 μm Al_2O_3 abrasive and then polished with 1 μm diamond paste on a silk lap. They were then turned over, lapped to the desired thickness, and polished on the same side. The lapping was always done parallel to the crystals natural (110) faces for both the transmission and reflection samples. The crystals were cemented to the lapping pedestal with Duco cement rather than wax or solder to avoid heating them through the transition temperature. Although most crystals broke during this process, we obtained five samples which were lapped to a thickness of 17 μm and three were successfully mounted and measured.

The sample thickness was determined by measuring the height of the lapping pedestal first with the sample cemented in place and then with the sample removed. We used a thickness comparator which is accurate to better than 1 μm, and we corrected for the thickness of the cement. The measurement of thickness is therefore accurate to about $\pm$ 10%. We did not attempt to make a more accurate measurement of the thickness after the sample was removed from the lapping pedestal because we were afraid of breaking the sample and because

our determination of the temperature dependence of the transmission did not depend upon exact knowledge of the sample thickness.

A typical transmission sample is 0.025" wide, 0.100" long, 0.0006" thick, and weighs about 75 μg. When cementing the sample over the hole in the sample holder, shown in Figure IV-6, we found the surface tension force from a small drop of Duco cement was large enough to pull the sample out of place. This problem was overcome by using a watch crystal cement which comes in a special tube which has an applicator shaped like a hypodermic needle [7]. This allowed us to apply a very tiny drop of cement directly to the edge of the sample, and we usually applied one small drop to each end of the sample.

Measuring a successfully mounted transmission sample was difficult due to focusing problems. We wanted to measure the energy gap as a function of temperature, so we needed to compare transmission curves for one sample which were made at different temperatures. To do this we had to have identical focussing at each temperature on both the sample and the detector. The focus at the sample was arranged so that the image of the exit slit was smaller than the hole over which the sample was mounted. Thus all of the light could pass through the sample and the hole in the sample holder when the focus was properly adjusted. The samples were mounted over slit shaped vertical holes so the most critical focusing problem was in the horizontal direction. To aid in focusing the light simultaneously on the sample and the detector, we mounted the dewar on a sliding platform which permitted the sample to be moved sideways with respect

to the light beam. The focusing procedure involved three steps: first the light was focused visually on the sample, then the sample was removed and the light was visually focused on the detector, and finally the sample was replaced and the detector signal on the recorder was maximized by adjusting the focus at the detector and by moving the sample sideways in the light beam. When the sample holder temperature was changed, however, there were small changes in the position of the sample due to thermal strains in the dewar. Thus at each temperature the dewar was moved sideways to maximize the signal on the recorder. Sometimes a slight adjustment of the vertical focus at the sample and detector was also necessary.

We used an InSb detector for measurements on two of our three samples and a PbS detector for the third sample. The InSb detector had a larger long-wavelength cutoff, but the PbS detector had a better signal to noise ratio. The response of the InSb detector was not uniform over the sensitive area, but the focusing procedure described above eliminated the possibility of errors arising from this factor. The PbS detector did have a uniform response over the sensitive area.

The data for a transmission versus temperature measurement for one sample are shown in Figure IV-12. The I_o curve was measured with the light passing through the dewar windows, and was found to be the same both before and after the transmission measurements were made at different temperatures. We could not measure a transmission

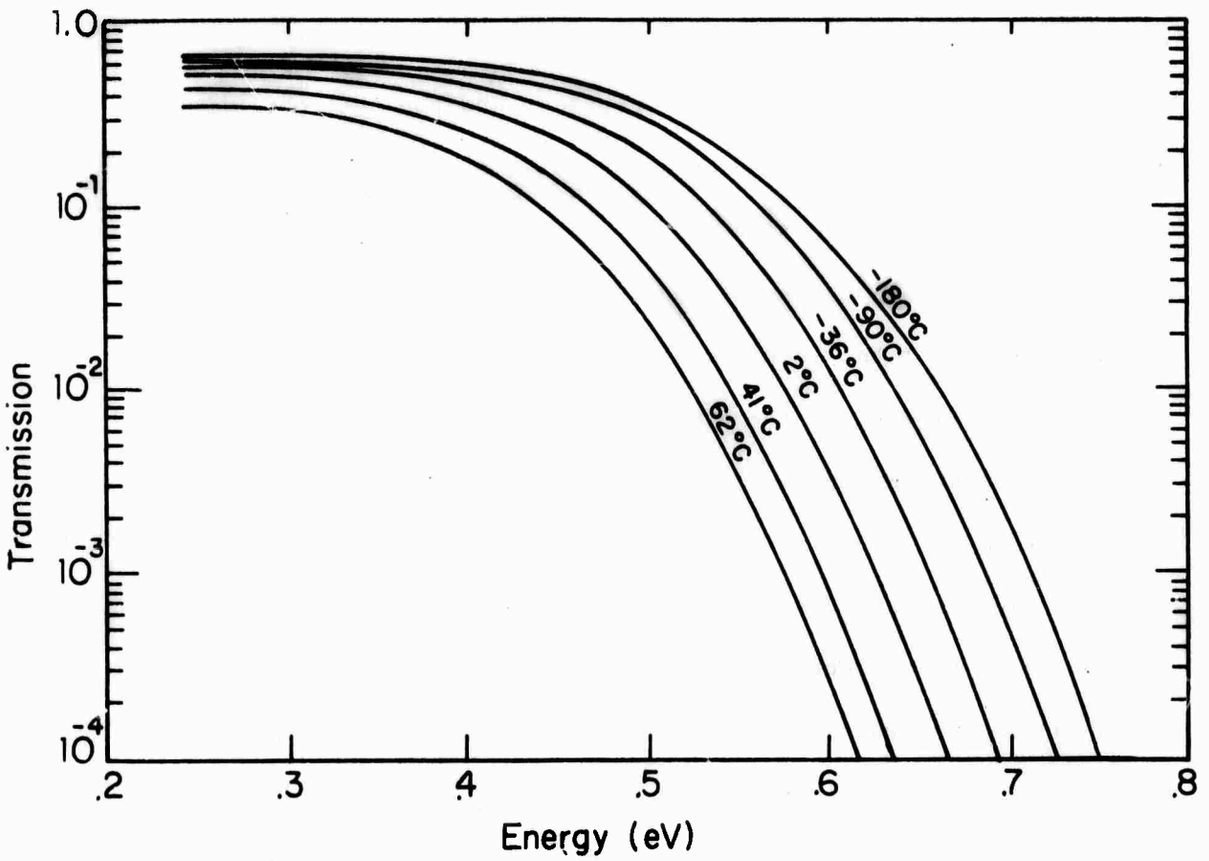

FIGURE IV-12 Transmission versus energy for a V_2O_4 crystal. at six different temperatures.

of less than 10^{-5} due to scattered light of long wavelength present in the exit beam of the monochromator. The smallest amount of transmission which could be measured accurately was 10^{-4}. Using the value of crystal transmission T shown in Figure IV-12 and the value of reflectivity R shown in Figure IV-8, we can compute the absorption coefficient by using the formula $T = (1 - R)^2 e^{-\alpha x}$ where x is the crystal thickness. For the wavelength where the transmission is 10^{-4} at room temperature, the reflectivity loss is 58% and the absorption coefficient turns out to be 5000 cm^{-1}.

The energy dependence of the absorption coefficient of V_2O_4 crystals at room temperature is shown in Figure IV-13 as measured on our samples and as calculated by Verleur et al. [5] from reflectivity data using a classical oscillator fit computer program. The crystals measured by Verleur et al. [5] have an absorption coefficient of 10^3 cm^{-1} or greater in the energy gap region which they attribute to a large density of states present in the energy gap. From the figure it can be seen that our crystals have a much sharper absorption edge. Since the reflectivity spectra of our crystals is similar to the reflectivity spectra of the crystals from which the absorption coefficient data in Figure IV-13 was calculated, we assume that the absorption coefficient of our samples rises to about 10^5 cm^{-1} near 1 eV and is similar to the data in the figure for higher values of energy.

To determine an exact value of the energy gap is impossible unless we can fit the energy dependence of the absorption coefficient to a theoretical model. Experimentally the energy dependence does

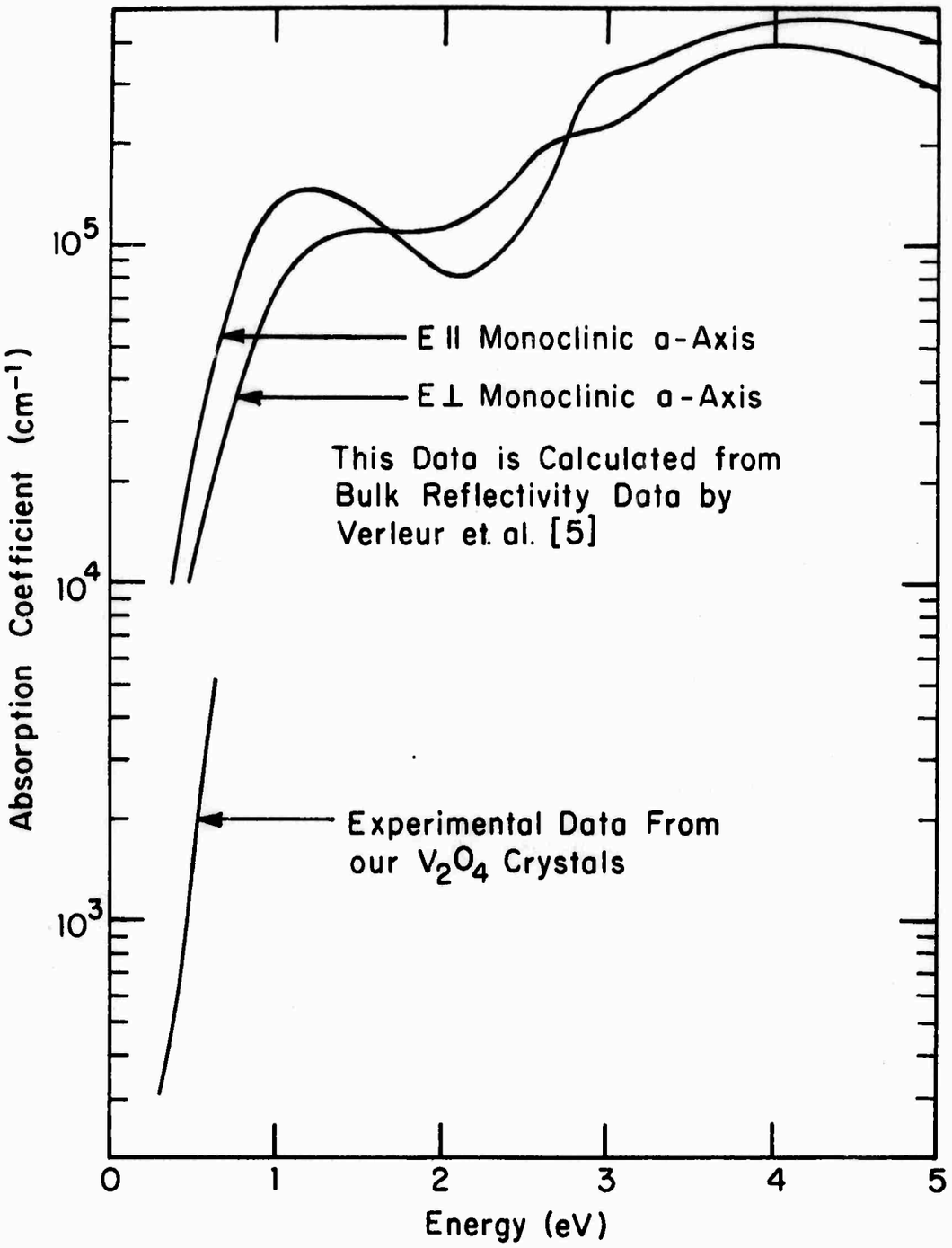

FIGURE IV-13 Calculated and experimental values of the absorption coefficient of V_2O_4 crystals at 300 °K

not fit a $(E - E_g)^{\frac{1}{2}}$ or $(E - E_g)^{\frac{3}{2}}$ dependence corresponding to a direct gap or a $(E - E_g)^2$ dependence corresponding to an indirect gap, and there are no theoretical predictions about the shape of an absorption edge for an energy gap produced by correlation effects with which the data can be compared. For our crystals the absorption coefficient of the edge varies from approximately 10^2 cm^{-1} to 10^5 cm^{-1}, and the largest value of α we can measure accurately is 5000 cm^{-1}. As can be seen from Figure IV-13 this value of α is approximately the geometric mean of the absorption coefficient of the edge, and the energy at which α = 5000 cm^{-1} can be taken to be a good first approximation to the energy gap.

Experimentally we found that the shape of the α versus E curve did not change as the temperature was varied and we thus feel that the temperature dependence of the energy at which α = 5000 cm^{-1} can be interpreted as the temperature dependence of the energy gap.

We found that as the temperature of a transmission sample was increased, the reflectivity peak near 1 eV moved to lower energy and the reflectivity increased somewhat. In order to make a plot of absorption coefficient versus energy at each temperature, the reflectivity would have to be measured at each temperature. We found, however, that the value of reflectivity at the energy E when the crystal transmission T was 10^{-4} was constant to within 1% as the sample temperature was changed from 20° to 60°C. Thus above room temperature the value of E for which α = 5000 cm^{-1} is identical to the value of E for which T = 10^{-4} and can be found from curves similar to those in Figure IV-12. Below room temperature it is hard to measure

the reflectivity accurately since the sample has to be put in the dewar and focusing becomes very difficult. Extrapolating from the measurements above room temperature, however, we will assume that the energy at which $T = 10^{-4}$ is also the energy at which $\alpha = 5000$ cm^{-1} below room temperature. If this assumption is not exact, only a small error will be introduced. For example, if the value of (1 - R) at the energy where $T = 10^{-4}$ increases by 5% below room temperature, the value of the energy at which $\alpha = 5000$ cm^{-1} would increase by 0.0015 eV. Looking ahead to Figure IV-14 we see that this would introduce only a very small error in the shape of the $E_g(T)$ curve and it would only affect the low temperature portion of the curve.

We also notice in Figure IV-12 that the crystal transmission for low energies is higher at lower temperatures. This results from the fact that at low temperatures the reflectivity loss for energies in the gap region is much less than at high temperatures. We would like to emphasize that the difference in crystal transmission at low energies for different temperatures is not the result of an experimental error and does not indicate that the value of reflectivity loss at the energy where $\alpha = 5000$ cm^{-1} is temperature dependent. The uncertainty in reading the 10^{-4} transmission point from curves similar to Figure IV-12 is $\pm$ 0.0015 eV. Errors due to focusing and changes in the reflectivity with temperature are estimated to produce an uncertainty in transmission $(\Delta T/T) = \pm$ 0.08. This gives an added uncertainty in the value of energy where the transmission equals 10^{-4} of $\pm$ 0.0015 eV. Thus the total uncertainty in each value of energy is $\pm$ 0.003 eV plus the

possible low temperature error mentioned above.

Figure IV-14 shows the temperature dependence of the energy at which the crystal transmission is equal to 10^{-4} for these samples. The curve does not show a precipitous drop near T_c and the uncertainty of $\pm$ 0.003 eV in the determination of each point does not permit a curve which is much different from the one shown in the figure to be drawn through the data points. This measurement definitely shows that a second order crystal distortion induced transition such as described by Adler and Brooks [8] is not present in V_2O_4. A first order crystal distortion induced transition, however, might still be compatible with the above data if the temperature T_c was several degrees lower than T_o. The interpretation of the above transmission measurements will be discussed further in Chapter VI.

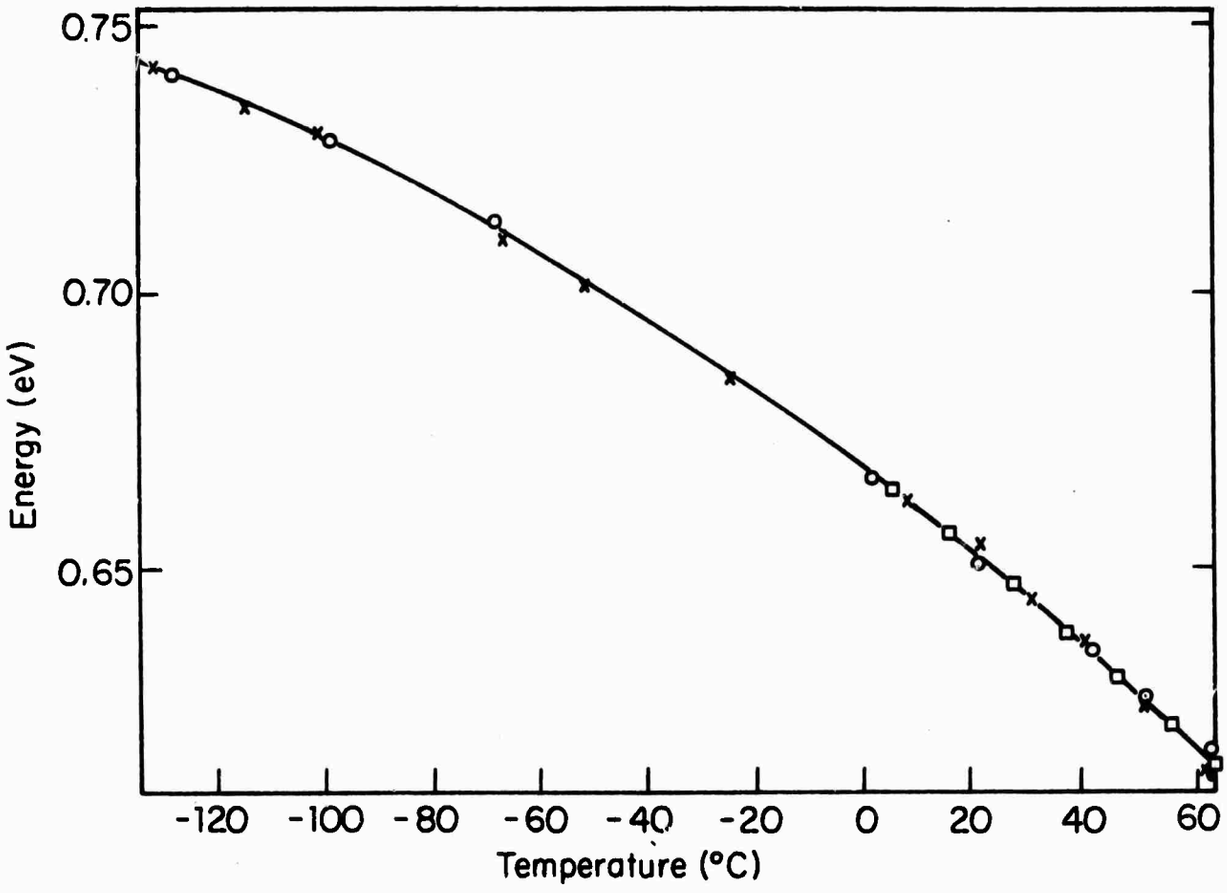

FIGURE IV-14 Energy gap versus temperature for three V_2O_4 crystals.

Chapter IV

REFERENCES

[1] M. DeMeis, Tech. Rept. No. ARPA-16, Div. of Eng. and Appl. Phys., Harvard University, 1965 (unpublished), and V. Prakash, Tech. Rept. No. HP-13, Div. of Eng. and Appl. Phys., Harvard University, 1967 (unpublished).

[2] M. Ference, H. Lemon, and R. Stephenson, Analytical Experimental Physics, Second Rev. Ed., p. 488, University of Chicago Press, Chicago, 1956.

[3] These lines can be looked up, for example, in the following: S. Zwedling and J. Theriault, Spectrochimica Acta, 17, 819 (1961).

[4] These lines can be looked up, for example, in the following: Instruction Manual, Perkin Elmer Infrared Equipment, Volume 3A, Model 112 Single Beam Double Pass Infrared Spectrometer, Perkin Elmer Corporation, Norwalk, Connecticut.

[5] H. Verleur, A. Barker, and C. Guggenheim, Phys. Rev., 172, 788 (1968).

[6] V. Mokerov and A. Rakov, Sov. Phys.-S.S., 11, 150 (1969).

[7] Tube Cement for SUC Watch Crystals, Standard Unbreakable Watch Crystals, Inc., New York, N.Y.

[8] D. Adler and H. Brooks, Phys. Rev., 155, 826 (1967).

Chapter V

UNIAXIAL STRESS MEASUREMENTS

In this chapter we will discuss the uniaxial stress measurements which we made and their interpretation. Measurements were made of the dependence of the resistivity and the transition temperature on c-axis uniaxial stress. From X-ray data it was known that the c-axis contracts by about 1% when the crystal is heated through the transition [1], and so it was expected that the transition temperature would decrease with c-axis uniaxial stress. We also attempted to make measurements with stress applied to the as grown (110) crystal faces, but the transition was broadened and the change in T_c with stress could not be determined. However, if we recall that the a-axis expands and the b-axis contracts during the transition and that below the transition temperature the crystal is composed of domains in which the a-axes and b-axes are interchanged, then we can understand this broadening of the transition in terms of a simple model: Stress applied in the basal plane of the crystal would raise the transition temperature of some domains and lower the transition temperature of others.

By comparing the decrease in the transition temperature with stress to the change in resistivity with stress and using a one band model for V_2O_4 we hoped to see if there was any simple connection between the carrier concentration in the conduction band and the transition temperature. In particular, we wanted to test the

predictions of the Adler-Brooks theory [2,3]. We found, however, that the interpretation of our uniaxial stress data was somewhat difficult and that more information could be obtained by comparing our results to hydrostatic pressure measurements on V_2O_4.

A. Uniaxial Stress Apparatus and Sample Preparation

The apparatus shown in Figure V-1 was available in the laboratory for the production of uniaxial stress [4]. The bottom of the apparatus where the sample is mounted is suspended on a foot long tube from the mounting platform which can be clamped to a table. This allows stress measurements to be made with the sample in a temperature bath or a dewar. The sample is mounted between sapphire blocks and is compressed by the piston, rod, and weights which it supports. The large bolts serve as guides for the piston which slides between them with very little clearance and very little friction. Most of the measurements were made with the bottom of the stress apparatus sitting in an American Instrument Company oil bath temperature controller [5]. The current in the oil bath heater is turned on and off by a bi-metallic strip relay which controls the bath temperature. The rated temperature regulation is $\pm$ 0.001°C, but the temperature of the oil was found to fluctuate by $\pm$ 0.01°C.

We had some difficulty in obtaining and mounting high quality samples for the stress measurements. Even our best samples broke with stresses of between 1 kbar and 2 kbar. We therefore limited the stress used to less than 1 kbar, kept the thermal cycling

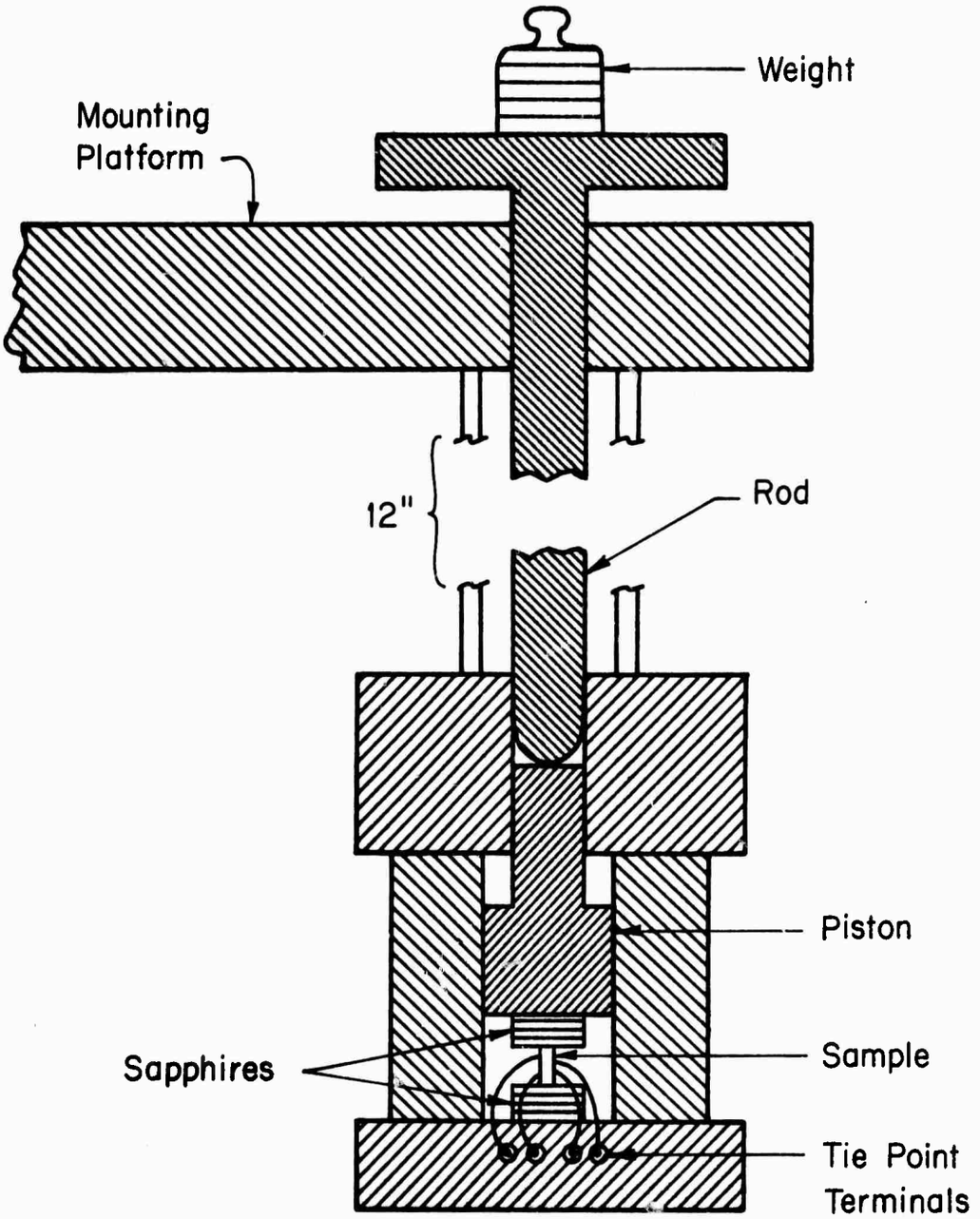

FIGURE V-1 Schematic diagram of uniaxial stress apparatus. (Not to scale).

through the transition to a minimum, and used only our smaller and stronger crystals for these measurements. A typical sample was 0.020" x 0.025" in cross section and 0.075" long. A special jig was designed so that the end of the crystal could be lapped parallel to each other and perpendicular to the length of the crystal. Four leads of 0.002" platinum wire were attached to the sides of the crystal with silver epoxy, and then the crystal was mounted vertically in the stress apparatus as shown in Figure V-1. A piece of one mil thick mylar was put between the ends of the sample and the sapphire blocks to accommodate for any irregularities in the end faces of the crystals. A magnifying telescope was used to align the crystal vertically before lowering the piston onto the sample. The lower end of the rod was hemispherically shaped so that no torque would be applied to the piston and crystal when the rod was raised or lowered or when weights were added.

B. Change of the Transition Temperature with Stress

In order to speed up data taking and simplify the determination of the transition temperature of samples under different stresses, a Mosely Autograf Model 7001A x-y recorder was used to record the sample resistance versus temperature. The x-axis was connected to a copper constantan thermocouple mounted on the piston of the stress apparatus and the y-axis recorded the voltage drop across the sample potential leads. The sample resistance was less than 10 k Ω and a 1 M Ω resistor was placed in series with the sample and a 100 volt battery to produce

a constant current through the sample. Figure V-2 shows the recorder trace that was obtained when a sample was cycled through the transition both ways at a rate of 1°C every 15 minutes. This heating and cooling rate was achieved by leaving the heater and stirrer in the oil bath turned on and adjusting the heater voltage with a variac to 85 V for heating and 45 V for cooling.

Although the configuration described above was suitable for preliminary measurements, we found that a modification of the circuitry enabled us to obtain more accurate determinations of the transition temperature. Figure V-3 shows the data that were obtained when the x-axis was swept in time at a rate of 100 sec/inch and the heating rate was the same as described above. The temperature scale on the recorder chart was determined by monitoring the voltage on the thermocouple with a Leeds and Northrup type K-3 potentiometer and a Leeds and Northrup type M galvanometer and by placing a pip mark on the recorder trace by hand each time the potential changed by 1 μV. The figure shows the change in transition temperature as the sample is heated through the transition with different amounts of c-axis stress. Notice that there is only a slight change in the shape of the curve as the stress is increased. The displacement of the curve on each of the three y-axis voltage scales is shown in the figure and the average displacement of the curve is 25 μV.

To compute a number representing the change in T_c with stress for a given sample, data similar to Figure V-3 are taken for heating and cooling without the stress, then twice with the stress, and then

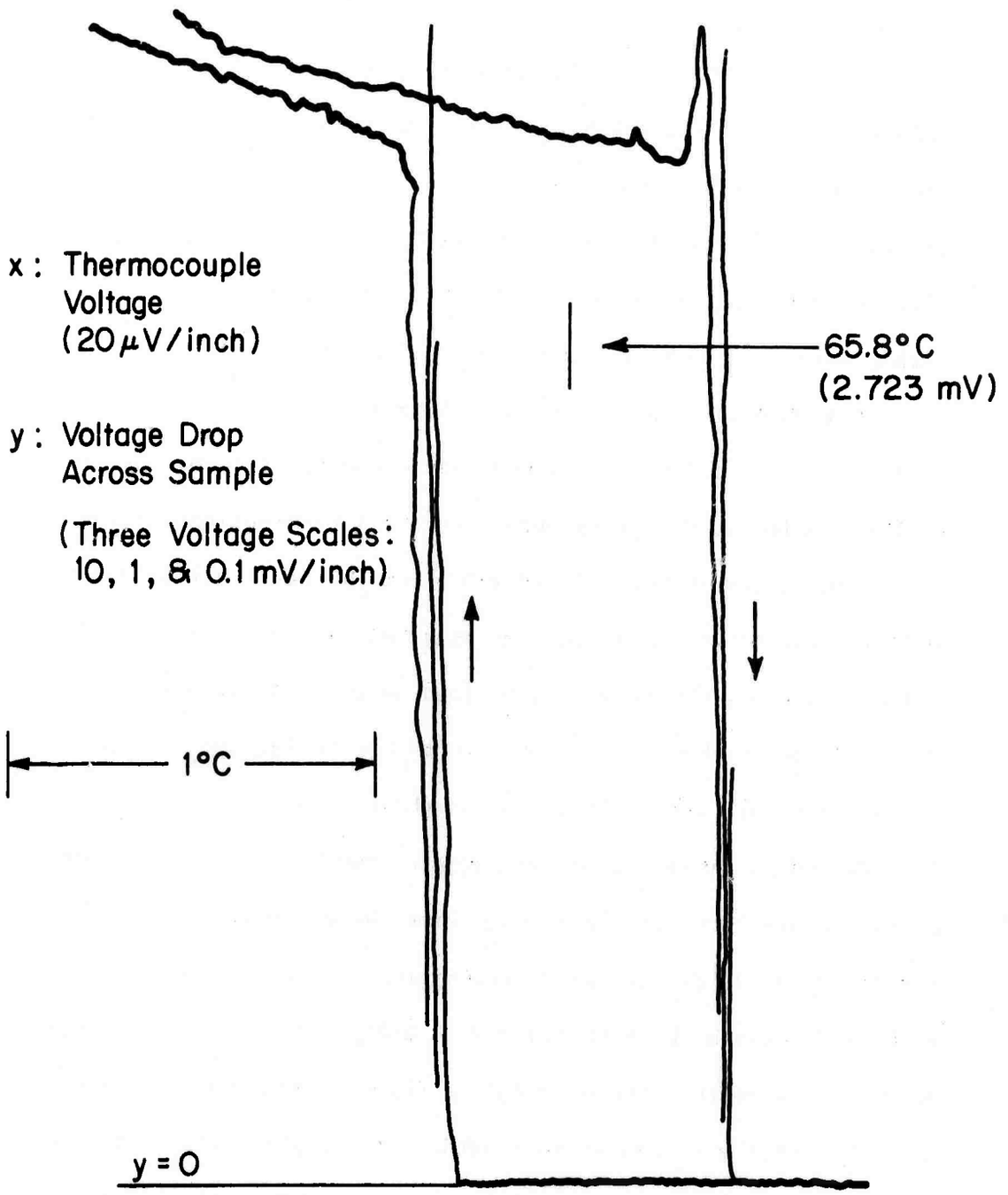

FIGURE V-2 Recorder trace of the resistance versus temperature for sample c-4 as it is cycled through the transition at a rate of 0.07°C / minute.

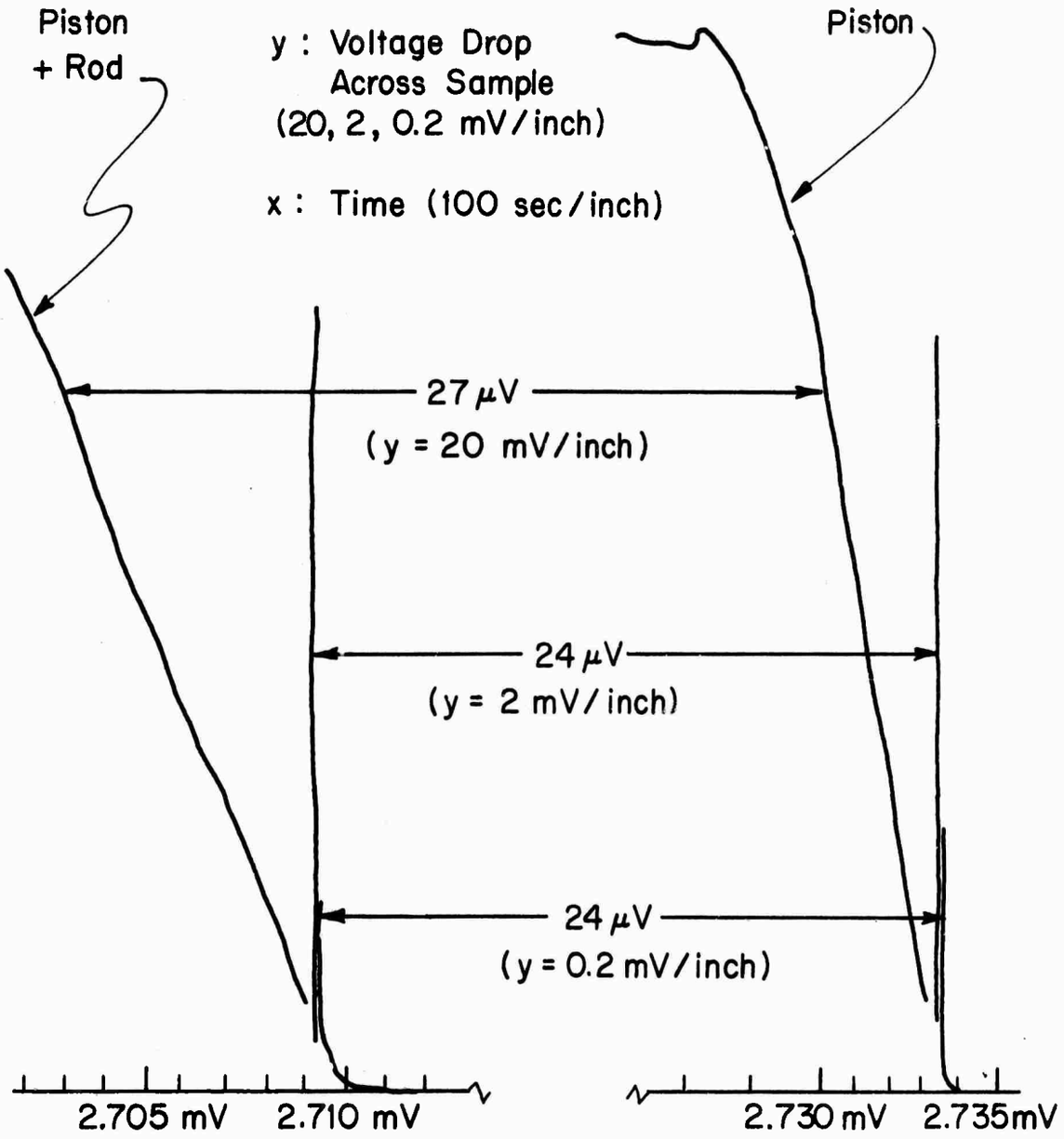

FIGURE V-3 Recorder trace of resistance versus temperature as sample c-4 is heated through the transition with different amounts of c-axis stress. The change in transition temperature is 25μV or 0.57°C for 431 bar.

once without the stress again. If the data are consistent, values of the change in T_c for heating the sample and for cooling the sample are determined and then these two values are averaged to obtain dT_c/dS. This procedure reduces errors due to a change in the amount of hysteresis with stress which was observed for some samples.

During the course of making measurements the leads sometimes came off and had to be reattached. Thus a sample would be labeled c-4-2 to denote that it was the fourth c-axis stress sample to be measured and that the leads had been put on for the second time. The following data were obtained:

Sample	Max. Stress	Displacement of T_c
c-2-1	313 bar	-57 μV/kbar
c-3-1	257 bar	-54.5 μV/kbar
c-4-1	431 bar	-58.7 μV/kbar
c-4-2	431 bar	-52.3 μV/kbar
c-5-1	380 bar	-60.8 μV/kbar

If these values are averaged we obtain a shift of -56.7 μV/kbar or $\frac{dT_c}{dS} = -1.3°K/kbar$. The error in determining this coefficient arises primarily from variations from sample to sample, variations from run to run with the same sample, and changes in the shape of the resistivity curve as stress is applied. The uncertainty in the measurement from these sources is estimated to be $\pm$ 10%.

One check on the above measurement is the Clausius-Clapeyron equation, but before we can write this expression we must determine the appropriate form of the Gibbs function. In the most general case we can write $G = U + \sum_{ij} s_{ij}c_{ij} - TS$ where s_{ij} is a tensor component of

the stress and c_{ij} is a tensor component of the strain [6]. In our experimental setup we are applying only c-axis stress and so only s_{33} is nonzero. During the transition, however, the crystal distorts and some shear stress will arrise. This shear stress, however, will be small and can be ignored since the coefficient of friction between the mylar pieces supporting the sample and the polished sapphire pieces is low. We will thus write the Gibbs function as $G = U - TS + s_{33}e_{33}$. This Gibbs function leads to a Clausius-Clapeyron equation which can be written $\frac{dT_c}{ds_{33}} = -\frac{\Delta e_{33}}{L/T_c}$ where s_{33} is the c-axis stress, Δe_{33} is the change in c-axis strain which can be expressed as $\Delta e_{33} = \left(\frac{\Delta x_c}{x_c}\right) V_{mole}$, and L is the latent heat per mole [7]. The latent heat of single crystals has been measured to be L = 1020 cal/mole [8], the change in the c-axis lattice constant has been reported to be $\Delta x_c = 3.5$ pm [1], and the molar volume can be computed from the x-ray unit cell dimensions to be $V_{mole} = 17.8$ cm^3/mole [9]. Putting these numbers together we obtain $\frac{dT_c}{dS} = -1.73$°C/kbar which is somewhat larger than the experimental value of -1.3°C/kbar. Most of the difference between these two values can be accounted for by the large uncertainty of at least $\pm$ 20% in the measurement of $\Delta x_c/x$ [1]. We thus conclude that our measured value of $\frac{dT_c}{dS}$ and the value calculated from the Clausius-Clapeyron equation agree to within the experimental uncertainties of the two values.

C. Change of the Semiconducting Resistivity with Stress

Measurements of the c-axis stress dependence of the resistivity in the semiconducting state were made at temperatures from -15°C to + 50°C on the same samples that were used to measure the stress

dependence of the transition temperature. For measurements between 10°C and 50°C the American Instrument Company oil bath which could be water cooled was used to regulate the temperature and only the measuring electronics had to be changed. For measurements between -15°C and 30°C the sample end of the stress apparatus was placed in a polystyrene tube through which cold nitrogen gas was circulated. The gas was passed through a dehumidifier and a copper coil immersed in acetone and dry ice, and the temperature of the sample was determined by adjusting the nitrogen flow rate. Care had to be taken to prevent water vapor from entering the system because it would condense on the sample and produce leakage currents.

For this measurement a constant current source was connected to the current leads of the sample and the voltage leads were connected in series with a Leeds and Northrup type K-3 potentiometer and the y-axis of a Moseley Autograf model 7001A x-y recorder. The potentiometer was used to null out most of the voltage drop across the sample and the x-axis of the recorder was swept in time. Figure V-4 shows the recorder trace that was obtained as the weight on the sample was varied. Notice that there is very little friction in the apparatus and that the readings for P+R are almost the same when the weight on the sample is being increased or decreased. Notice also that the displacements on the recorder are proportional to the weight supported by the piston. In the lower temperature measurements the sample impedance became large compared to the recorder input impedance and an electrometer had to be used to measure the voltage across the

x : Time (100 sec / inch)

y : Voltage Drop Across Sample
(10 mV / inch)

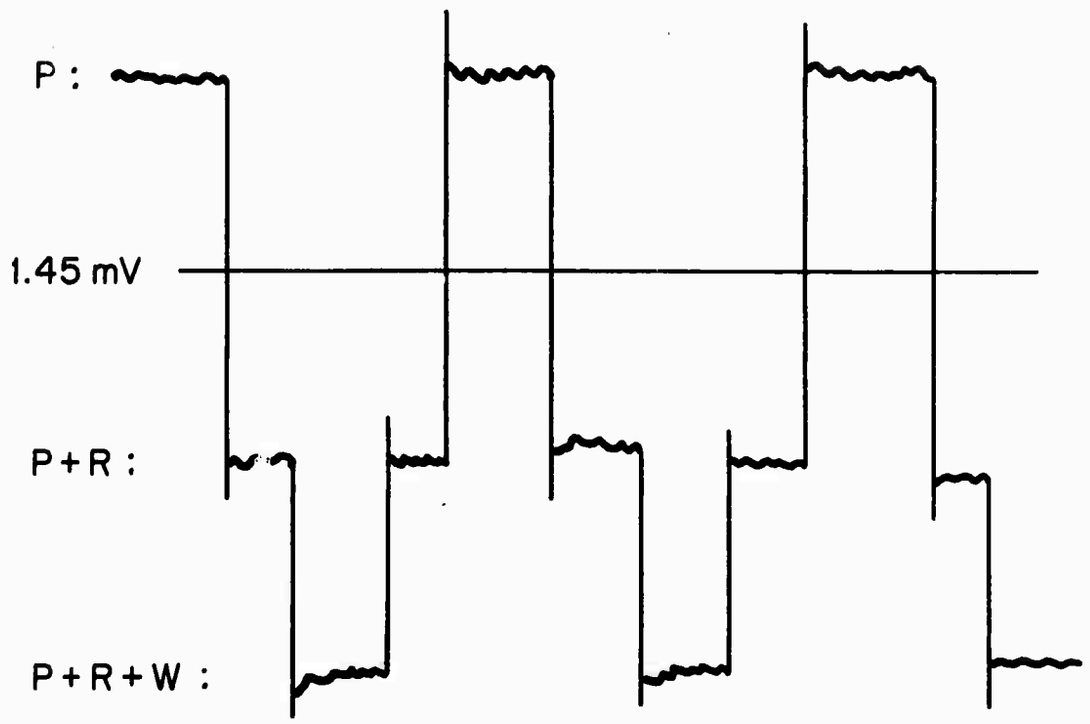

P: Piston = 275 g = 142 bar

R: Rod = 832 g = 431 bar

W: Weight = 500 g = 259 bar

FIGURE V-4 Recorder trace of resistance versus time for sample c-4 as the c-axis stress is varied at room temperature. The resistance change is 2.15 % for a stress of 690 bar.

sample voltage terminals. The electrometer output was connected to the recorder and potentiometer as above. The noise was greater for the lower temperature measurements, and the temperature control when nitrogen gas was used for cooling was not nearly as good as when the oil bath was used. The above circuit, however, allowed measurements to be made even in the presence of considerable noise and drift.

Figure V-5 shows the results of our measurements of $d\ell nR/dS$ as a function of temperature. It is clear from the figure that this coefficient decreases as the temperature is reduced, but it is impossible to tell the exact shape of curve from the data. It is possible that the variation from sample to sample may be due in part to the presence of cracks or imperfections in the crystal structure which affect the stress dependence of the resistivity. The variation from run to run could be due to the development of cracks in the sample and loosening of the contacts as the sample is thermally cycled and stressed. Data were not taken at higher temperatures since the noise became too large near the transition temperature. If the estimated average curve shown in the figure is extrapolated to T_c, then we obtain $\left(\frac{d\,\ell n\,R}{dS}\right)_{T_c} = -4.3\%/\text{kbar}$. The uncertainty in this value is about 20% and arises from the variation from sample to sample and from run to run.

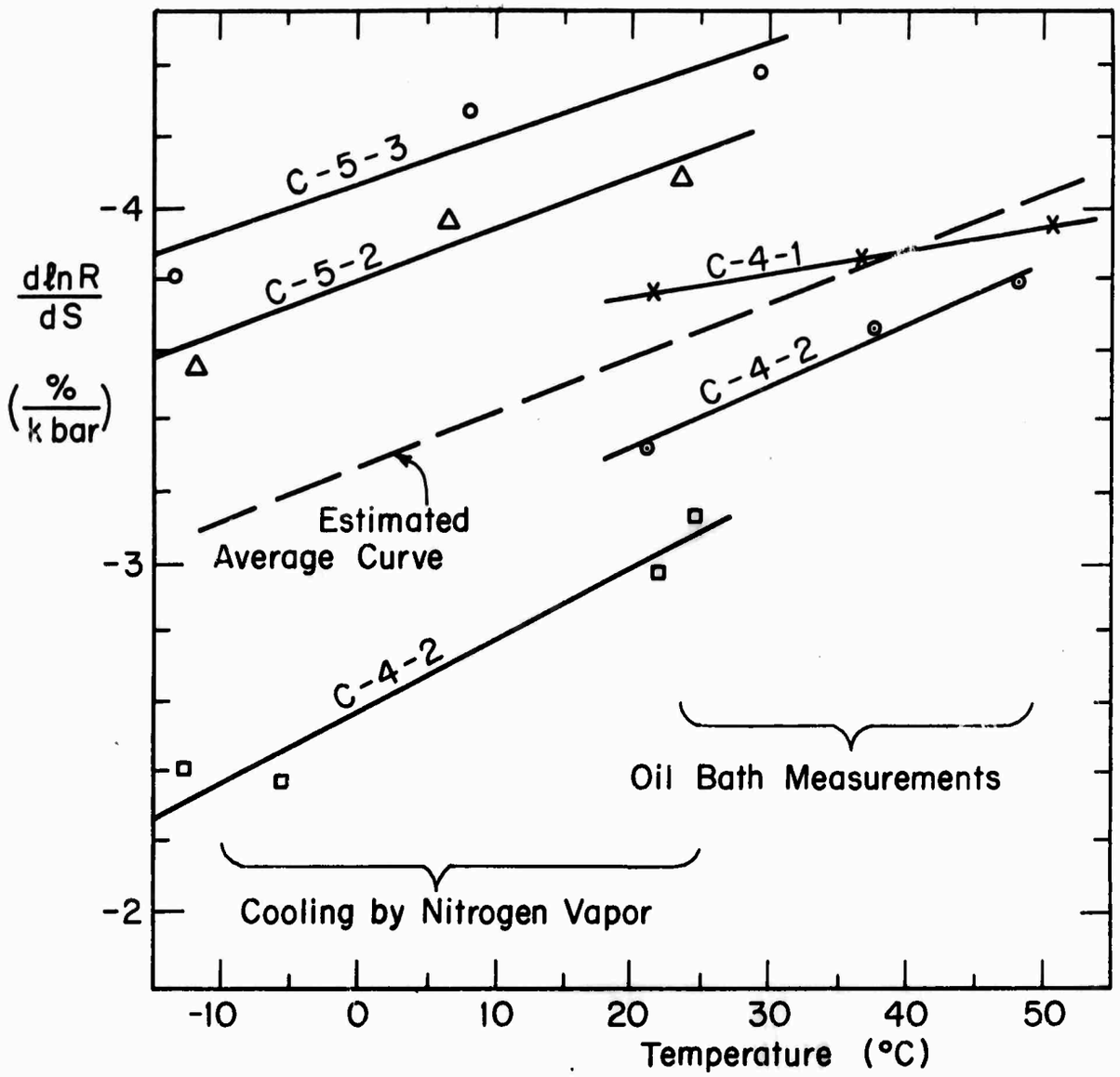

FIGURE V-5 Temperature dependence of the c-axis stress resistivity coefficient for two different samples and two different cooling methods.

D. Comparison with Hydrostatic Pressure Measurements and Interpretation

It was hoped when this research project was begun that the Adler-Brooks theory would apply to V_2O_4 and that the predicted relationship $\frac{d\,\ell n(E_g)_o}{dS} = \frac{d\,\ell n\,T_c}{dS}$ could be confirmed by uniaxial stress measurements [2,3]. The results of our optical measurements, however, indicate that the simple form of the Adler-Brooks theory in which the above relationship is derived does not apply to V_2O_4 [2]. First we found that the energy gap was between 0.7 eV and 0.8 eV and so the ratio $(E_g)_o/kT_o$ was about 25. The relationship $d\,\ell n(E_g)_o/dS = d\,\ell n\,T_o/dS$ is only valid for the narrow band approximation when $(E_g)_o/kT_o \leq 10$, and for $(E_g)_o/kT_o \sim 25$ we would expect $d\,\ell n(E_g)_o/dS$ to be somewhat smaller than $d\,\ell n\,T_o/dS$ [10]. Our measurements also showed that the energy gap did not decrease sharply near T_c, and this indicates that even if the Adler-Brooks theory applies to V_2O_4, a first order transition occurs at a temperature T_c below the second order transition temperature T_o. Thus we cannot test the Adler-Brooks theory by comparing the quantities $\frac{d\,\ell n(E_g)_o}{dS}$ and $\frac{d\,\ell n\,T_c}{dS}$ [3].

Although the Adler-Brooks theory could not be tested directly, we still considered it of interest to try and determine whether the population in the conduction band was involved in the transition mechanism. To determine whether or not the transition occurs at a particular carrier density, we felt that a knowledge of both stress and pressure measurements was necessary and our interpretation will be presented following a review of recent pressure measurements on V_2O_4.

The dependence of the transition temperature upon hydrostatic pressure has been measured on our crystals for pressures up to 9 kbar by Rosevear, and a coefficient $\frac{dT_c}{dP} = 0.061 \pm 0.012$ °C/kbar was obtained [11]. This is twenty times smaller than the c-axis stress dependence as is expected since the volume change during the transition is quite small. Berglund and Jayaraman have also measured the pressure dependence of the transition temperature for pressures up to 40 kbar and obtained the coefficient $\frac{dT_c}{dP} = 0.082 \pm 0.005 \frac{°C}{kbar}$ [12]. Although these two measurements are not quite within the experimental errors quoted, the differences between the measured values of the pressure coefficient are as likely to be due to differences between the samples measured as to errors in the measurements. Both of these recent measurements disagree with the earlier measurements of Minomura and Nagasaki who found $\frac{dT_c}{dP} = 0.46°C/kbar$ [1]. Since their measurements were made on poor quality crystals and since the coefficient is so small, it is not too surprising that their results are inconsistent with more recent data.

The Clausius-Clapeyron equation $\frac{dT_c}{dP} = \frac{(\Delta V)_{mole}}{L/T_c}$ can be used to check the measurements of $\frac{dT_c}{dP}$, but the X-ray data available for this calculation are not as accurate as one would desire. The measurements of Minomura and Nagasaki indicate that $\Delta V/V$ is less than 0.1% during the transition which means that dT_c/dP should be less than 0.14°C/kbar [1]. This is approximately twice the experimental value and so we can say that the Clausius-Clapeyron equation is satisfied, but it is not a good check of the measured values of dT_c/dP. McWhan has recently

made a measurement of the change in volume at the transition temperature and he has found that $\Delta V/V = 0.1 \pm 0.4\%$ [13]. These data clearly are in agreement with the experimentally measured values of dT_c/dP, but the error is even larger than that in the measurements of Minomura and Nagasaki. Beylund and Jayaraman [12] have stated that the Clausius-Clapeyron equation checks out using the value of dilatation measured during the trancition in sintered samples by Kawakubo and Nakagawa [14], but this is not correct since the measured value $\Delta\ell/\ell = 0.13\%$ is five times to large to satisfy the Clausius-Clapeyron equation. This disagreement is not surprising since during the transition two axes expand and one contracts and so the dilatation of ceramic samples could be expected to give an overestimate of the volume change during the transition.

The dependence of the resistivity in the semiconducting phase on hydrostatic pressure has been measured on our samples at room temperature and the resistivity has been found to decrease linearly for pressures up to 30 kbar with a coefficient $\frac{1}{R}\frac{dR}{dP} = -1.5\%/\text{kbar}$ [15]. Our measurement gives a coefficient which is slightly larger than the value of 1%/kbar measured by Neuman, Lawson, and Brown [16], and we attribute the difference to the fact that our crystals were of much higher quality. Berglund and Jayaraman have made pressure measurements on semiconducting V_2O_4, but they held the pressure constant and varied the temperature in their measurements [12]. They then computed the pressure dependence of the activation energy from the change in slope of their $\log R$ versus $1/T$ plots for different pressures. This procedure,

however, cannot be justified since their $\log R$ versus $1/T$ plots, like ours, are not straight lines and so an activation energy cannot be obtained from their data. It will be shown in Chapter VI that if band theory applies to semiconducting V_2O_4, then the shape of the resistivity versus temperature curve is determined by the change in the distance of the Fermi level from the conduction band with temperature.

We will now try and relate the change in resistivity with stress or pressure to a change in the carrier concentration in the conduction band. We will assume that the conductivity can be written $\sigma = ne\mu$ and that n changes more than μ with the application of stress or pressure. This assumption is somewhat difficult to justify since the fractional changes in resistivity measured are of the same order of magnitude as the mobility changes found in classical semiconductors such as germanium [17]. Nevertheless, for the moment we will assume that the change in mobility with stress or pressure can be ignored.

Let us now try and interpret the experimental results. The change in resistivity with stress is -3.6%/kbar and the change in resistivity with pressure is -1.5%/kbar. Thus if the change in resistivity results from a change in carrier concentration, and the transition always occurs at a particular value of carrier concentration, we would expect that the coefficients of the change in transition temperature with stress and pressure would have the ratio of 3.6/1.5. This is not observed since the transition temperature decreases at a rate of 1.3°C/kbar with stress whereas it increases

at a rate of 0.08°C/kbar with pressure. Within the limits of our model we are forced to conclude that the carrier concentration has no simple relationship to the transition temperature. Our model, however, is very crude and it is quite possible that the mobility effects are important. Whether or not the inclusion of mobility effects would change our interpretation is impossible to predict. Further discussion of the semiconductor-metal transition will be reserved for Chapter VI.

Chapter V

REFERENCES

[1] S. Minomura and H. Nagasaki, J. Phys. Soc. Jap, 19, 131 (1964).

[2] D. Adler, Tech. Rep. No. ARPA-12, Div. of Eng. and Appl. Phys., Harvard University, Unpublished (1964).

[3] D. Adler and H. Brooks, Phys. Rev., 155, 826 (1967).

[4] This apparatus was designed by our technician Dave McLoed for use in making measurements on CdTe.

[5] The American Instrument Company temperature controller consists of a three gallon water-cooled oil bath in which is located a stirring motor, a heater coil, and a Model 4-235 A "Quickset" Bimetal Thermoregulator which operates a Model 4-5300 Super-sensitive Relay which turns on and off the heater current.

[6] J.F. Nye, "Physical Properties of Crystals," Chapter X, Oxford University Press, London (1957).

[7] A.L. King, "Thermophysics," p. 68. W.H. Freeman and Co., San Francisco, 1962.

[8] C.N. Berglund and H.J. Guggenheim, Phys. Rev., 185, 1022 (1969).

[9] G. Andersson, Acta, Chem. Scand., 10, 623 (1956).

[10] D. Adler, Private Communication, Mass. Inst. of Tech., Cambridge, Massachusetts.

[11] B. Rosevear and W. Paul, to be published, Harvard University, Cambridge, Mass.

[12] C.N. Berglund and A. Jayaraman, Phys. Rev., 185, 1034 (1969).

[13] D.B. McWhan and T.M. Rice, Private Communication, Bell Telephone Laboratories, Murray Hill, New Jersey.

[14] T. Kawakubo and T. Nakagawa, J. Phys. Soc. Jap., 19, 517 (1964).

[15] L. Ladd and W. Paul, Solid State Comm., 7, 425 (1969).

[16] C.H. Neuman, A.W. Lawson, and R.A. Brown, J. Chem. Phys., 41, 1591 (1964).

[17] M.I. Nathan, H. Brooks, and W. Paul, Phys. Rev., 124, 391 (1961).

Chapter VI

SUMMARY OF OTHER RECENT WORK AND CONCLUSIONS

This chapter will first give a summary of the experimental and theoretical work completed by other investigators during the course of this research program, and then present our present understanding of the properties of the high and low temperature phases of V_2O_4 and of the mechanism of the semiconductor-metal transition. We shall see that there are still some basic questions which are unanswered and we will suggest further experimental and theoretical investigations which should lead to a better understanding of the properties of this material

A. Recent Experimental Work by Other Investigators

In this section we will review a selection of the large volume of recent experimental work which is judged to be significant because it was carefully carried out on high quality crystals. Throughout this section crystals will be said to have a sharp transition if the change in resistivity at the transition temperature occurs over a small temperature interval, and crystals with a sharp transition and a large resistance ratio will be called high quality crystals. This terminology is justified by the fact that we are primarily concerned with studying the semiconductor-metal transition and so we are most interested in examining the properties of crystals with a sharp transition and a large resistance ratio. The degree to which these

properties correlate with the purity, stoichiometry, and crystalline perfection of V_2O_4 crystals has not yet been completely determined. The section will be organized under five headings: crystal growth and analysis, electrical measurements, optical measurements, magnetic measurements and thermal measurements.

1. Crystal Growth and Analysis

It is very important to make measurements on high quality well characterized crystals when studying the semiconductor-metal transition in V_2O_4, since there is a considerable amount of variation in the measured properties reported by different authors which is probably due to differences in the crystals which were measured. There are now two methods which give large high quality single crystals: the vacuum reduction method of Sasaki and Watanabe [1], and the vapor transport method of Bando et al. [2]. Both methods are discussed in Chapter II. The vacuum reduction method has been used by Guggenheim to produce crystals up to 1 cm on an edge which have a sharp resistivity transition and a resistance ratio $R_s/R_m = 10^5$ [3]. The vapor transport method of Bando et al. has been used to make crystals which are almost as large and which have similar electrical properties. This method uses a closed tube vapor transport system and appears to be the simplest method of growing high quality crystals. The structural and optical properties of crystals grown by this method have not yet been reported. We have grown smaller crystals by the slow cooling method of Sobon and Greene [4]

which have the sharpest electrical transition reported, a resistance ratio of $R_s/R_m = 10^5$, and steeper absorption edge then the crystals grown by Guggenheim [5]. Our crystals and those grown by Guggenheim have been analyzed for chemical purity and stiochiometry and found to have similar characteristics. The impurity content was shown to be less than 10^{-6} by spectroscopic analysis, but the stoichiometry could only be analyzed to approximately one atomic percent by chemical means. Unfortunately, however, a variation in stoichiometry of one atomic percent could produce a carrier concentration of more than 10^{20} cm^{-3}, a value much higher than that usually observed in high quality crystals. Since more accurate methods of measuring the stoichiometry are not available, the contribution of variations in the stoichiometry to the carrier concentrations observed in different crystals cannot be determined. The crystal structures of our crystals and those of Guggenheim and of Bando et al. have been verified by X-ray analysis. The presence of domains in the low temperature phase which has been discussed in Chapter III has been investigated in detail by Fillingham [6]. This phenomenon complicates the measurement of the tensor properties of crystals below the transition temperature.

Several investigators have grown and measured the properties of doped V_2O_4 crystals, although the structure of the samples has not been examined very carefully. Guggenheim has grown doped samples using the vacuum evaporation growth method and measured their electrical properties [3]. Some of his crystals were analyzed with X-rays to

determine their structure, but the details were not reported [3]. The stoichiometry of these crystals was also not measured. The largest change in the transition temperature with doping was found to be -17°C/atomic percent for niobium doped crystals. Crystals with as little as 0.035% of cobalt were found to have a resistance ratio of only R_s/R_m = 100 and a very large amount of hysteresis in the resistivity. It appeared that when the vanadium was replaced by smaller cations the transition temperature decreased. Umeda et al. have reported the existence of a third phase during the transition process in polycrystalline V_2O_4 [7], and Mitsuishi has identified this phase as trichinic and shown that it occurs when the crystal is doped with certain cations such as iron which tend to favor oxygen deficiency in the crystal [8]. Thus any investigation of doped crystals should include a structural analysis of the crystals measured.

Some very interesting work has been done by Nygren and Israelsson who have shown by differential thermal analysis that the transition temperature of powdered samples of tungsten doped V_2O_4 decreases by about 80°C/atomic percent [9]. The low-temperature phase was found to have the normal monoclinic structure. Measurements were made for doping levels up to a little more than 2 atomic percent. The phase relations of the $V_xW_{1-x}O_2$ systems have been investigated further by Israelsson and Kihlborg who have found that there are five phase regions present in this pseudobinary system when x is varied from 0 to 1 at room temperature [10]. For $0.33 \leq x \leq 0.98$ the rutile

structure is the stable phase at room temperature. These measureemtns were made on powdered samples and it would be of interest to grow single crystal specimens of this material since almost any value of transition temperature below 65°C seems to be available by changing the amount of tungsten in the crystals.

Another interesting aspect of the crystal growth problem is the study of Magneli phases. These phases are structures in which the rutile lattice is periodically interrupted by a plane of interstitial atoms and which have the general formula V_nO_{2n-1} [11]. The Magneli phases for n = 3,4,5 have been grown by the vapor transport growth method of Nagasawa et al. [12]. These materials have been determined to have transitions between states with different conductivities by the electrical measurements of Okinaka et al. [13, 14,15]. Information on the V-O phase diagram and analysis of the phase boundaries has been reported by MacChesney et al. [16] and Kosuge [17]. A further investigation of transitions in the Magneli phases may give information which helps to understand the transition in V_2O_4.

Crystalline and amorphous films of V_2O_4 have been grown by several investigators. The crystalline films have not, however, been characterized very carefully and do not show as sharp an electrical transition as single crystals. Good crystalline films have been grown by Hensler by sputtering [18], by MacChesney et al. by the reduction of V_2O_5 films [16], and by Powell et al by the oxidation of vanadium films [19]. The sharpest transition was seen

by Powell whose films had a resitance ratio $R_s/R_m = 10^4$. The stoichiometry has not been checked for any of these crystalline films. Amorphous films have been grown by Kennedy and Mackenzie which do not show a transition [20]. Films grown above the transition temperature had a low resistivity and a small, negative temperature coefficient of resistivity at all temperatures, whereas films grown below the transition temperature had a resistivity which was three orders of magnitude larger and a negative temperature coefficient of resistivty at all temperatures [21]. When these films were annealed they showed a transition between two states with different values of conductivity but with similar negative temperature coefficients of resistivity. X-ray diffraction measurements showed that the annealed films were polycrystalline. Although these results are very interesting, the films have not been characterized very well and only show a resistance ratio of one hundred at the transition. The stoichiometry is only known to be correct to within three atomic per cent, and the annealing may have changed the stoichiometry by a considerable amount. The relationship between the magnitude of the resistance ratio observed and the grain size in the polycrystalline films is also unknown, whereas the properties of the observed transition could depend quite strongly on the grain size of the films [22].

2. Electrical Measurements

Electrical measurements have been made on pure and doped single crystals and on thin films of V_2O_4. Although there is considerable difference between the resistivity versus temperature curves obtained from crystals grown by different researchers as is shown in Figure III-6, the transition temperature for undoped crystals does not vary by more than 10°C. This variation in resistivity behavior underscores the need to measure high quality well characterized crystals.

Our measurements of the temperature dependence of the resistivty and the hysteresis of undoped samples are the most complete to date. The resistivity change at the transition of the crystals grown by Guggenheim [3] and Bando et al. [2] appears to be nearly as sharp as that of our crystals. The anisotropy of the resistance has been measured on high quality crystals by Everhart and MacChesney [23]. Because of the formation of domains,only the conductivity parallel and perpendicular to the rutile c-axis can be determined, and it is found that the c-axis conductivity is approximately a factor of two higher in the semiconducting state and approximately a factor of ten higher in the metallic state.

The properties of doped crystals have been measured by several investigators. MacChesney and Guggenheim have measured the conductivity of V_2O_4 crystals doped with various impurities [3]. In general, the resistance ratio of the transition is reduced whereas the transition temperature and conductivity may either be raised or

lowered. The stoichiometry of the doped crystals was not measured. Everhart and MacChesney found that in comparison to undoped crystals, a crystal grown under similar conditions which was doped with about 0.1% of iron had an anisotropy which was approximately ten times larger, a conductivity which was higher, and a resistance ratio which was much smaller. This is a rather large effect for such a small amount of impurity, and is typical of the type of results that have been observed. The stoichiometry and the crystal structure of the low temperature phase were not measured, and it is possible that the iron doped crystals have different structural properties than the undoped samples as was observed by Mitsuishi [8].

The dependence of the conductivity on frequency, stress and pressure has been measured for single crystal V_2O_4. The frequency dependence of the conductivity of high quality single crystals with a resistance ratio $R_s/R_m \sim 4\ 10^4$ has been measured for frequencies up to 24 GHz by Kabashima _et al_. [24]. The conductivity at room temperature is constant up to frequencies of $f \sim 10^8$ Hz and then increases with frequency approximately as $f^{\frac{1}{2}}$. The flat response up to 10^8 Hz is typical of band type conductivity whereas the frequency dependence above 10^8 Hz is usually associated with hopping type conductivity. The frequency at which the conductivity begins to increase is smaller at lower temperatures. Our measurements of the stress and pressure dependence of the semiconducting resistivity were discussed in Chapter V. Berglund and Jayaraman have also measured the pressure

dependence of the resistivity of high quality crystals, but their analysis of the change in activation energy with pressure in the semiconducting state is incorrect as was pointed out in Chapter V [25]. Their measurement of the change in conductivity with pressure in the metallic state shows a slight conductivity increase and then saturation above about 15 to 20 kbar. This is consistent with a model which postulates overlapping conduction bands.

Other electrical measurements such as Hall effect and thermoelectric power have been made on high quality crystals. Rosevear and Paul have measured the temperature dependence of the Hall effect in the semiconducting state for crystals grown in our laboratory and found a Hall mobility $\mu_H = 0.5$ cm^2/Vsec which decreases slowly and linearly with increasing temperature [26]. This is the most precise Hall data now available. Barker *et al.* have also measured the Hall effect and obtained Hall mobilities of $\mu_H \sim 0.6$ cm^2/Vsec in the semiconducting state and $\mu_H \sim 16$ cm^2/Vsec in the metallic state [27]. These data are for three small crystals with resistivity ratio $R_s/R_m \sim 10^4$ and the experimental uncertainty is quite large. The thermoelectric power of high quality crystals has been measured by Bongers [28] and by Kitahiro and Watanabe [29]. In the semiconducting state the thermoelectric power α of high quality crystals is about -900 μV/°C and decreases with temperature. Above the transition temperature, α is approximately - 30 μV/°C. The sign corresponds to conductivity by electrons in both phases. Berglund

and Guggenheim report that the thermoelectric power increases with temperature in the metallic state [30], and they and other researchers have reported values as low as $\alpha \sim -100\ \mu V/^{\circ}C$ in the semiconducting state. The lower values of α are usually observed for crystals with smaller values of resistance ratio.

Electrical measurements have been made on thin films of V_2O_4 by several investigators. Hensler has measured the resistance, Hall voltage, and thermoelectric power of crystalline films which have a resistance ratio of 10^3 [18]. The stoichiometry and impurity content of these films have not been measured, and there are variations of an order of magnitude between the properties of different films. The Hall mobility was about an order of magnitude lower than the bulk crystal values measured by Rosevear and Paul [26]. The thermoelectric power measurements were about an order of magnitude smaller in the metallic state and approximately the same in the low temperature phase as bulk crystal data. The measurements made by Mackenzie on amorphous V_2O_4 films were mentioned in the last section. None of the films used in the measurements described above have been characterized sufficiently well so that they can be taken to represent the properties of pure, stoichiometric V_2O_4 and films with large values of resistance ratio have not yet been grown. Thus greater emphasis in this review is being placed on single crystal measurements than film measurements.

3. Optical Measurements

Our optical measurements and the reflection and transmission measurements of other investigators were discussed in Chapter IV. This section will deal with the photoemission measurements of Powell et al. [19,30] and the infrared reflectivity measurements of Barker et al. [27].

Photoemission quantum efficiency and energy distribution curves were obtained by Powell et al. for polycrystalline films which had a resistivity ratio $R_s/R_m = 10^4$. In both the semiconducting and metallic states there is evidence of a high density of states band approximately 2.5 eV below the Fermi level. This band is believed to be the filled oxygen 2p band. In the semiconducting state there is a band gap of approximately 0.7 eV around the Fermi level and in the metallic state a high density of states is observed at the Fermi level. Details of the density of states could not be resolved because of broadening effects. Figures IV-1 and VI-2 show the density of states information obtained from this measurement.

Infrared reflectivity has been measured by Barker et al. from 1 μm to 100 μm, but the crystals used were not of the best quality and cracked during the measurements [27]. A classical oscillator fit computer analysis of the reflectivity data was also used to determine the dielectric constant and the frequencies of the strongest optically actives modes. Measurements were made with polarized light parallel and perpendicular to the tetragonal c-axis. This measurement gives an

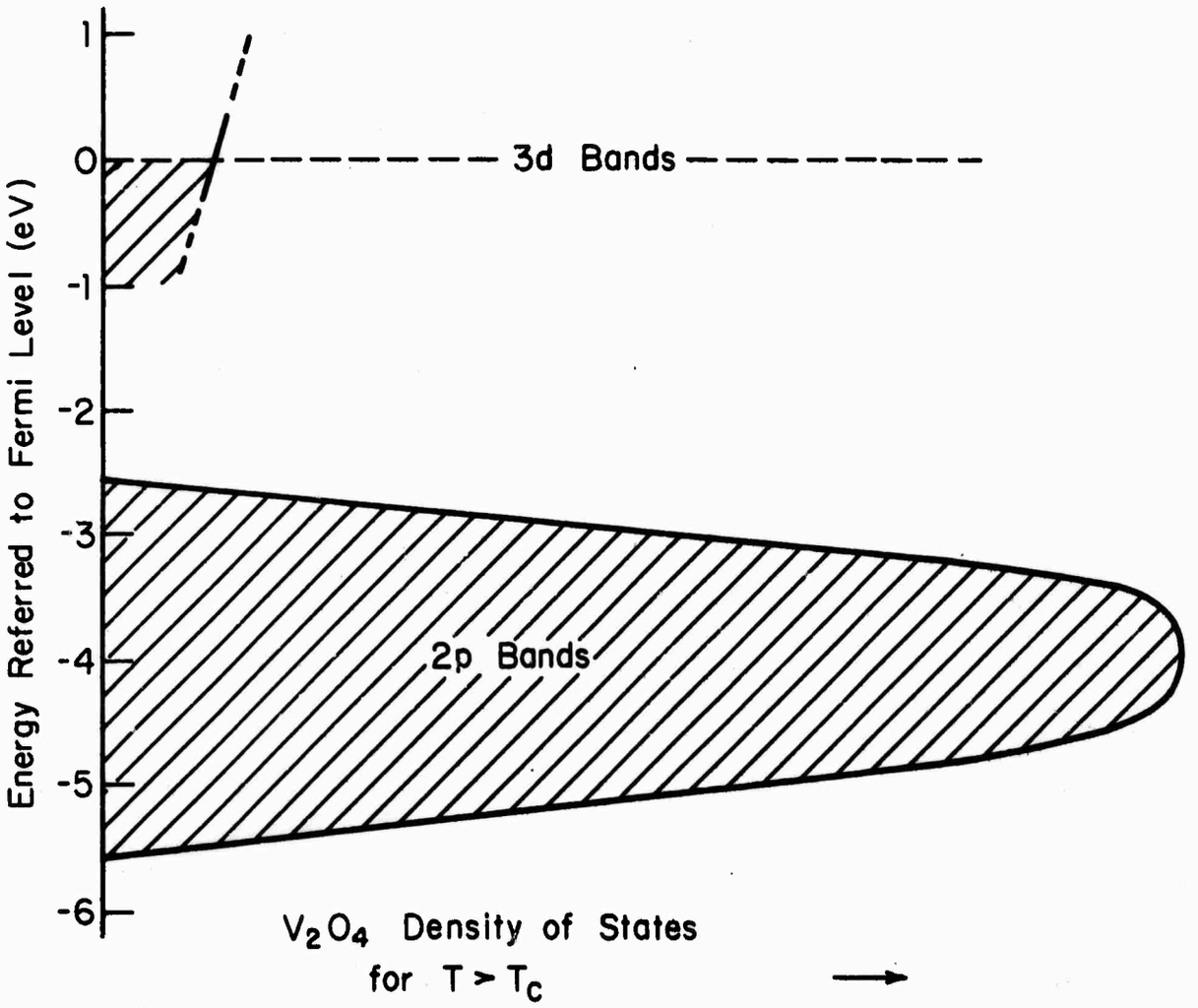

FIGURE VI-1 V_2O_4 density of states as determined by Powell et. al. from electron photoemission measurements [19,30].

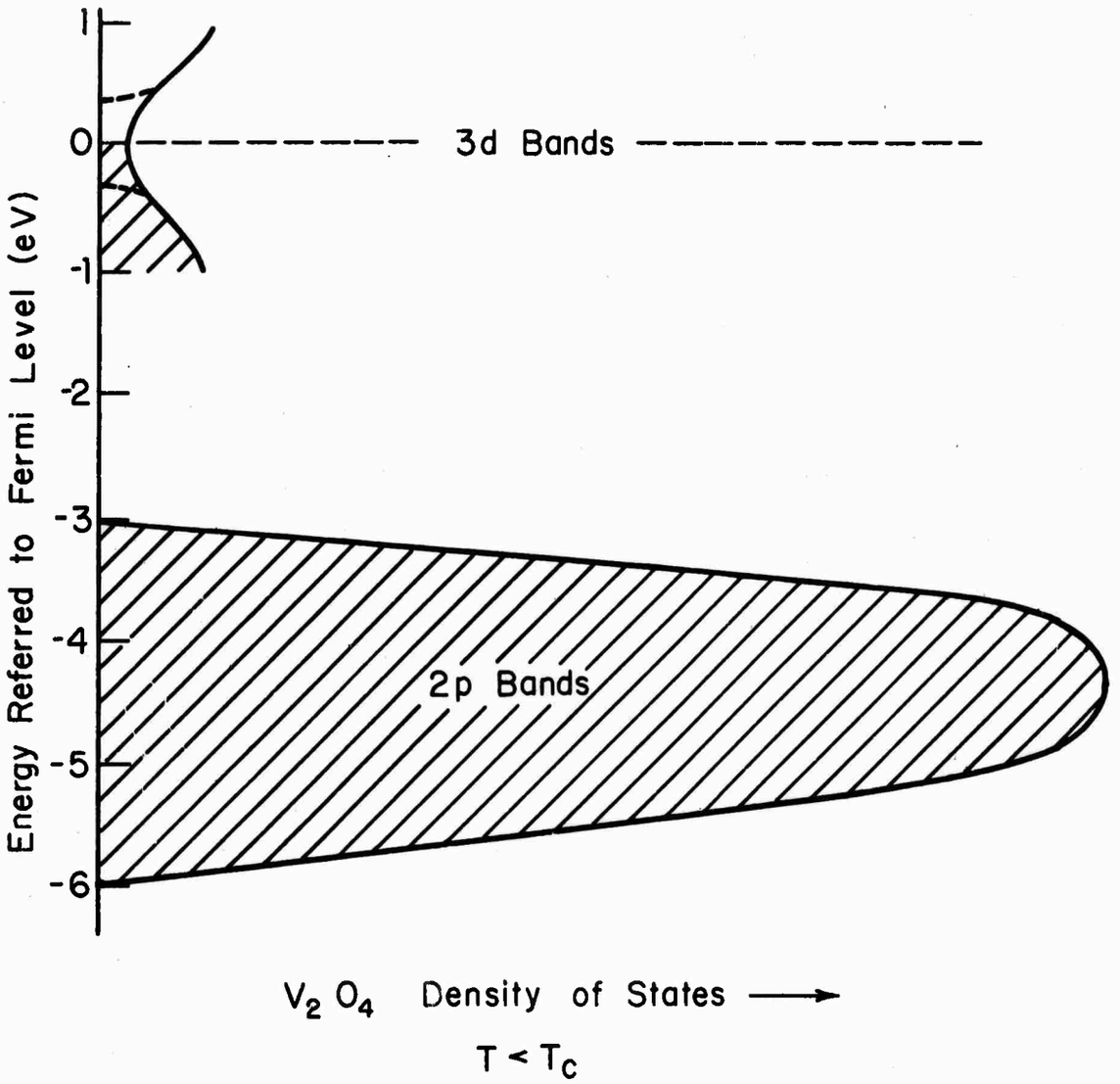

FIGURE VI-2 V_2O_4 density of states as determined by Powell et.al. from electron photoemission measurements [19,30].

approximate value of the low and high frequency dielectric constants which can be used to help evaluate whether or not polarons are present in V_2O_4. This topic will be discussed in Section C.

4. Magnetic Measurements

This section will summarize the recent measurements of Mössbauer effect, magnetic susceptibility, nuclear magnetic resonance, and electron spin resonance. The Mössbauer measurements made by Kosuge on powered samples showed that there is not antiferromagnetism in the low temperature phase [17,31]. This is in contrast to the case of V_2O_3 where Mössbauer measurements made by Singo et al. clearly show that there is an internal field present in the low temperature state which disappears suddenly at the transition temperature [32]. The estimated Neel temperature for the V_2O_3 crystals measured is 200°K which is considerably higher than the transition temperature of about 150°K. In these measurements the materials were doped with about 1% of Fe^{57} which was necessary in order to obtain the Mössbauer effect. The presence of this impurity affected the structure of the V_2O_4 somewhat, but this effect does not alter the conclusion that V_2O_4 is not antiferromagnetic in the low-temperature phase.

Magnetic resonance measurements have been made on pure and doped V_2O_4 crystals and powder. Umeda et al have measured the NMR spectrum of V^{51} in powdered V_2O_4 and shown that a new phase is present in a small temperature region near the transition [33]. Umeda et al. have also shown that this third phase only occurs in crystals which are

impure [34]. The NMR measurements also indicate that V_2O_4 is not antiferromagnetic below the transition temperature. The Knight shift was found to be positive below the transition temperature and negative above. The negative shift in the metallic state indicates that the contribution from the core polarization is larger than the Van Vleck paramagnetic contribution. The positive shift below the transition can be explained by assuming that the 3d electrons are paired up in chemical bonds on the closely spaced cations, thus eliminating the core polarization contribution. Electron spin resonance measurements made by Umeda et al. [34] and by Goto et al. [35] also suggest that the electrons in the low temperature phase are paired up. The measurements of Goto et al. are on Ti doped single crystals and the strength of the absorption and the line shapes suggest that each Ti ion introduces one unpaired and localized electron into the crystal. This is exactly the result one would expect if the electrons were localized in pair bonds below the transition temperature. As the concentration of Ti ions increases, the holes become more mobile and the absorption lines broaden.

Magnetic susceptibility measurements have been made on single crystals and powdered samples. The best single crystal measurements are those reported by Berglund and Guggenheim [30]. Figure VI-3 shows the magnetic susceptibility of high quality single crystals of V_2O_4 both parallel and perpendicular to the

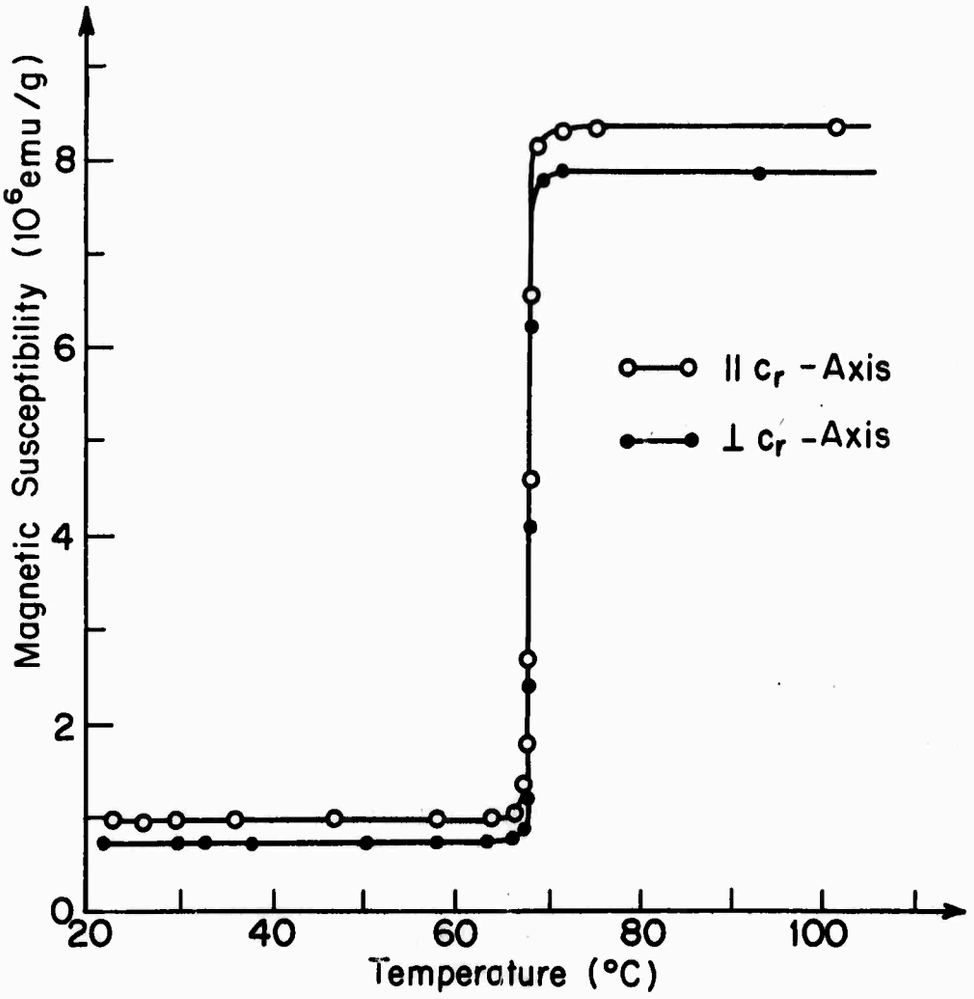

FIGURE VI-3 Magnetic susceptibility of single crystal V_2O_4 as reported by Berglund and Guggenheim [30].

tetragonal c-axis. The higher susceptibility in the metallic state can be attributed at least in part to a high density of states at the Fermi level. If a calculation based on a one band effective mass approximation is used, the density of states required to produce the observed magnetic susceptibility implies a bandwidth of about 0.1 eV which is inconsistent with the optical data. Thus correlation or exchange effects may be involved in producing the large susceptibility. The susceptibility at higher temperatures up to 440°K was measured on poor crystals by Hill and Martin [36]. The susceptibility curve which they obtained has been interpreted as resulting from a combination of spin paramagnetism and Kubo temperature independent paramagnetism [37]. The paramagnetic susceptibility of doped crystals has been measured by Kosuge who has shown that the susceptibility of the metallic state does not depend strongly upon doping [17]. If we assume that the susceptibility depends mostly upon the density of states at the Fermi surface, this measurement indicates that the Fermi surface density of states is not a strong function of doping. Below the transition temperature Kosuge has shown that the susceptibility can be approximated by the relationship $\chi - \chi_o + \frac{C}{T - \theta}$ [17]. The factor χ_o is the temperature independent part which is characteristic of undoped material, and the other term represents the contribution from unpaired spins resulting from doping. Since the added term obyes the Curie-Weiss law, we know that there are localized states present in doped material. The constant C is proportional to the doping level which means that the

number of localized states is proportional to the doping density. If the electrons are localized in pair bonds below the transition temperature, then each impurity cation would result in a localized unpaired elution. Alternately localized states could be due to the presence of localized levels on impurity cations or defect states which result from doping.

Kosuge has also measured the magnetic susceptibility of all the phases of the V_2O_3 - V_2O_5 system as a function of temperature [17]. This allows the susceptibilities of the different phases to be correlated with their electrical properties and structures. Mössbauer measurements show that V_2O_3 is the only one of the phases which is antiferromagnetic at low temperatures [17]. The Magneli phases which have transitions are paramagnetic both above and below their transition temperatures.

5. Thermal Measurements

This section will discuss the recent measurements of the specific heat and the thermal conductivity of single crystal V_2O_4 which were reported by Berglund and Guggenheim [30]. The specific heat measurement was done by Ryder and the data are shown in Figure VI-4. The latent heat is 1020 cal/mole of VO_2 and the Debye temperature is 750°K. It is unfortunate that no data were taken at higher temperatures, since it is of interest to see if there is any change in the Debye temperature at the transition. The data indicate that there is a slight increase in the specific heat at

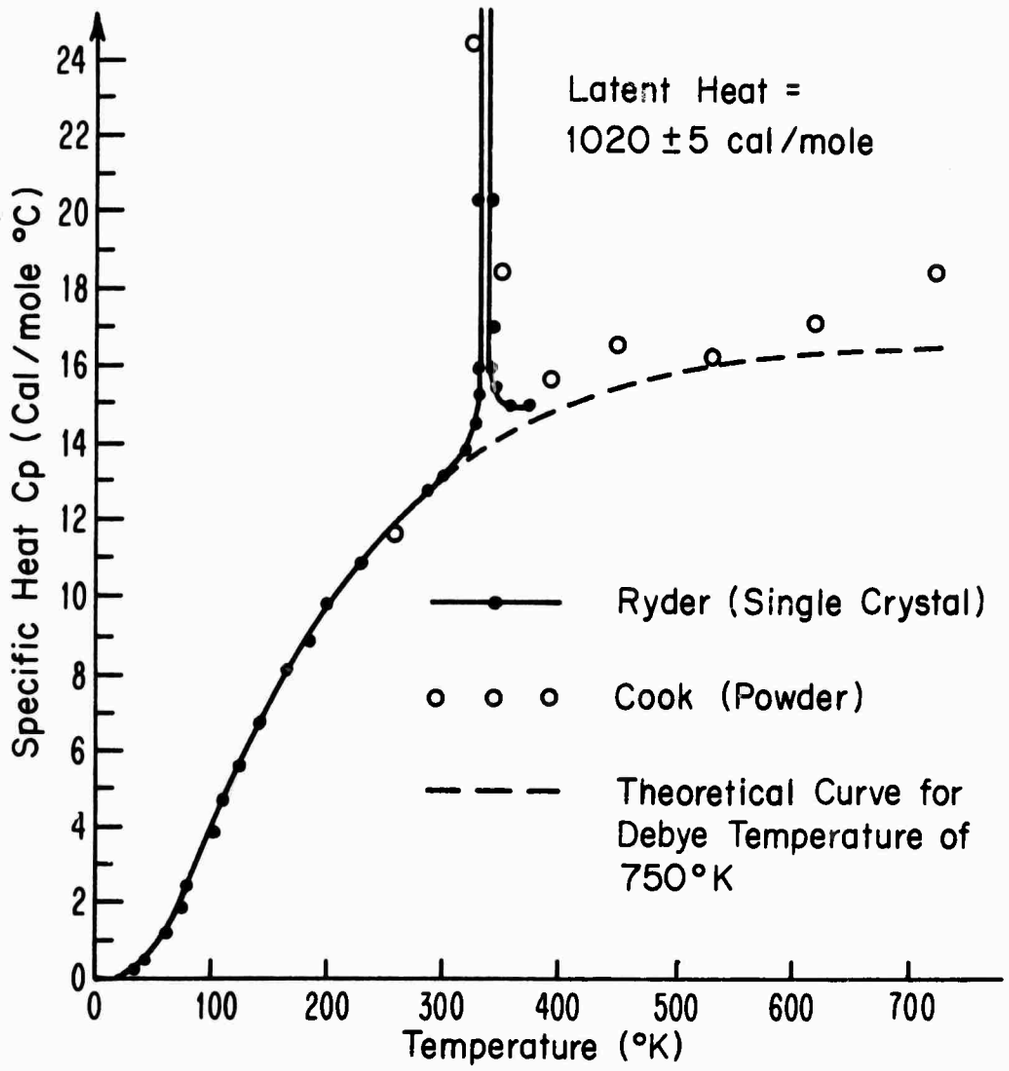

FIGURE VI-4 Specific heat of V_2O_4 as measured by Ryder [30] and Cook [38].

the transition, but measurements at higher temperature are necessary before the exact amount of this change can be determined. The figure shows that the specific heat data of Ryder are not too much different from the older data of Cook [38]. Older values of the latent heat for powder samples are Cook: 800 cal/mole [38], Klemm and Grimm: 1025 cal/mole [39], and Kawakubo and Nakagawa: 750 cal/mole [40]. Berglund and Jayaraman [25] have reported that the latent heat data, pressure dependence of the transition, and the X-ray data of Kawakubo and Nakagawa [40] satisfy the Clausius-Clapeyron equation, but their analysis is incorrect as was discussed in Chapter V. A correct analysis using improved experimental data, also given in Chapter V, leads to agreement with the Clausius-Clapeyron equation to within the uncertainties of the measurements involved.

The temperature dependence of the thermal conductivity has been reported by Berglund and Guggenheim for good quality single crystals [30]. From 25°C to 85°C the thermal conductivity is constant with a value of 66 mwatt/cm°C. This indicates that there is no appreciable heat conductivity by the electrons in contradiction to the Wiedemann-Franz law which predicts an increase of about 35 mW/cm°C at the transition. The Wiedemann-Franz law, however, only applies when the electron scattering is elastic and can be represented by a scattering time and these conditions may not be satisfied for V_2O_4. The very low electron mobility suggests that a scattering time approximation

may not be appropriate since it leads to a very short mean free path as is discussed in Section C. In addition, the electrons should be strongly scattered from longitudinal optical phonons since the lattice is quite polar. This scattering process is not elastic at room temperature since the phonon energies are greater than kT as is also discussed in Section C. The thermal conductivity, then, must be attributed entirely to the lattice. A perfect crystal would be expected to have a conductivity which varies as $\frac{1}{T}$ or stronger, and the lack of a temperature variation in the conductivity of the crystals measured indicates a high level of imperfections. This result is consistent with the optical measurements of Verleur et al. on crystals grown by Guggenheim which also indicated a large number of defects in the crystal structure [30].

B. Recent Theoretical Work by Other Investigators

This section will be divided into two parts: the recent theoretical work on the semiconductor-metal transition will be discussed in the first section, and the theories which have been suggested to explain the properties of V_2O_4, including the transition, will be discussed in the second section.

1. The Semiconductor-Metal Transition

In this section we will first report some of the recent developments of the theories which were introduced in Chapter I and then we will discuss the theories which have been developed more recently.

The band overlap theory has been applied to explain the properties of Ti_2O_3 by Van Zandt et al. [41]. The increase in resistance of Ti_1O_3 that occurs near 450°K is spread out over an interval of several degrees and there is no change in the lattice structure, although there is some change in the lattice constants. The model of a transition which results from antiferromagnetism as suggested by Slater [42] and developed by Adler and Brooks [43] has been applied to hexagonal NiS by Sparks and Komoto [44]. This material has a transition at the Neel temperature of 264°K during which the resistivity of powdered samples drops by a factor of about 100. More recent work, however, suggests that there may be a structural distortion present during the transition which may invalidate the above interpretation [45].

There have been many improvements in the approximations used to analyze the Hubbard Hamiltonian, and correlation theory may soon be developed to the point that experimental transport and optical measurements can be compared to theoretical predictions. The developments through 1968 are summarized by Adler [46], and only some of the more recent results will be mentioned here.

Brinkman and Rice have calculated the bandwidth and mobility of an extra carrier in a Mott insulator [47]. They used the Hubbard Hamiltonian in the atomic limit where the transfer energy t is less than the Coulomb repulsion energy U and considered the case of one electron per atom in a simple cubic lattice. A one particle Green's function calculation is used which gives different results for the

ferromagnetic, antiferromagnetic, and random spin cases. A ferromagnetic configuration was found to have the same bandwidthas calculated in the tight binding approximation, whereas the other two configurations were found to have somewhat smaller bandwidths. When reasonable experimental parameters were substituted into the results, bandwidths of approximately 1 eV and mobilities of approximately 1 $cm^1/Vsec$ at 1000°K were obtained. It was also found that the conductivity seems to be due to a diffusive type of Brownian motion rather than to be the result of scattering of mobile carriers. These results are quite significant and indicate that correlation effects do not necessarily produce bandwidths of less than 1 eV and mobilities of less than 1 $cm^2/Vsec$.

Some very interesting results have also been obtained by Langer et al. who have solved the Hubbard Hamiltonian for the case of one electron per atom in a simple cubic structure using a one particle Green's function [48]. They found that when the Coulomb interaction U is greater than about 0.27 of the bandwidth Δ in three dimensions there are two critical temperatures: the Neel temperature T_N, and the temperature $T_M > T_N$ at which the localized magnetic moments disappear and the insulator-metal transition occurs. For $U < 0.27\ \Delta$ there is only one transition temperature T_M. This calculation is significant in that it predicts a sharp insulator-metal transition to occur as a result of temperature change and because it shows that there may be two transition temperatures for the case of narrow bandwidth. The authors have pointed out, however, that the situation

specified in the calculation is one which is inherently unstable with respect to antiferromagnetism and so the validity of the latter conclusion is questionable. In any case the derivation of a temperature induced semiconductor-metal transition from the Hubbard Hamiltonian is an important theoretical result.

The experimental observation of a Mott transition in chromium doped V_2O_3 has been reported by McWhan et al. [49]. They have found that there are three phases present in doped V_2O_3 samples: a low temperature antiferromagnetic phase, and two high temperature phases which they denote as insulator and metal and which differ in conductivity by a factor of about 10^3. The phase which they term metallic also exists at low temperature in Ti doped crystals. The phase diagram is shown in Figure VI-5 and shows the equivalence of pressure and doping. In both of the high temperature phases the resistivity of chromium doped samples decreases with increasing temperature. When a $(V_{0.96}\ Cr_{0.04})_2O_3$ sample is subjected to 47 kbar of pressure the transition is suppressed and the temperature coefficient of resistivity becomes positive. Both high temperature phases have the corundum structure, whereas the antiferromagnetic phase has a monoclinic structure. When 13 kbar of pressure was applied to a $(V_{0.96}\ Cr_{0.04})_2O_3$ sample, a transition between the insulating and metallic phases with a resistance ratio of 150 was observed. The c/a ratio also increased sharply during this transition, but there was no change in the long range magnetic order. The authors thus suggest

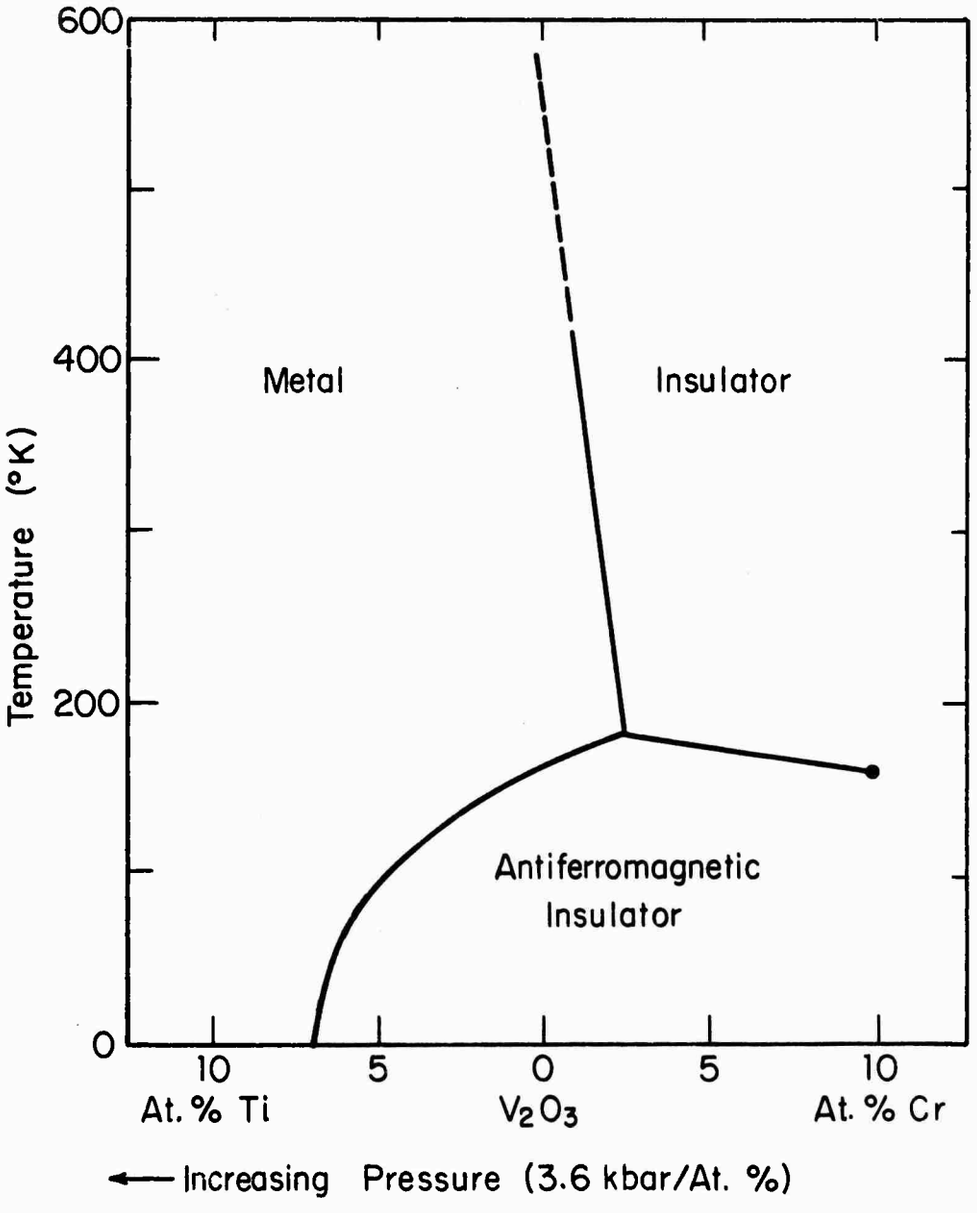

FIGURE VI-5 Phase diagram of V_2O_3 doped with Ti or Cr as determined by McWhan et. al. [49]. The equivalence of pressure and doping is shown.

that this phase change is of the type originally described by Mott [50] -- a correlation induced transition brought about by a change in the lattice constant. This conclusion may be a little premature, however, and would have to be substantiated by further investigations before it can be accepted. The crystals used in these measurements only had a resistance ratio of 3×10^3 in comparison to the value of 10^7 measured by Feinleib and Paul [51]. This if doped crystals with higher values of resistance ratio are grown, significantly different shaped resistivity versus temperature curves might be obtained.

Fröhlich has attempted to introduce screening effects into the Hubbard Hamiltonian [52]. He suggested that thermal excitation of free carriers from the filled to the empty quasiparticle band would create mobile carriers which would effectively screen the intra-atomic Coulomb repulsion U. Thus as the temperature is increased, the value of U and the quasiparticle band gap would decrease until at a critical temperature a phase change would occur and the material would change discontinuously from a Mott insulator to a metal. This model requires that more than one band be present in order for U to be screened, and it also requires that the quasiparticle band gap be sufficiently small that a sufficient number of electrons are excited at the transition temperature to produce appreciable screening. At the International Conference on the Metal-Nonmetal Transition at San Francisco in 1968 there was considerable controversy as to whether or not sufficient screening could be introduced by the above mechanism to produce a transition of this type [53]. This model is duscussed in more detail in the next section.

Falicov and Kimball have proposed a model for the semiconductor-metal transition which is based on the existence of localized and itinerant states in a material which are closely spaced in energy [54]. They begin with the Hubbard Hamiltonian and at low temperatures they assume the existence of localized states which are filled with electrons. It is also assumed that mobile states exist at an energy Δ above the localized quasiparticle band. The localized holes and itinerant electrons are supposed to have an attractive U. The intra-atomic interaction between electrons is neglected, and in the zero bandwidth approximation, the energy necessary to excite n electron hole pairs is

$$E(n) = n\Delta - n^2U$$

since all the free electrons feel the presence of all the bound holes. This leads to an effective energy gap of magnitude

$$E_g(n) = \frac{dE(n)}{dn} = \Delta - (2U)n \ .$$

This is analogous to the Adler-Brooks relation discussed in Chapter I, and the temperature dependence of the energy gap and the mobile carrier concentration is similar to that obtained in the Adler-Brooks theory. An insulator-metal transition occurs when U is finite and $\Delta/U < 1$. For $\Delta/U < 0.63$ the transition is first order. There are some objections to this theory, principally that U will decrease when n is large due to screening effects, but the model cannot be ruled out in general provided that the initial assumptions are satisfied.

Another theory of the insulator-metal transition is the excitonic insulator theory which has been reviewed by Halperin and Rice [55]. Consider the case of a semimetal with a small band overlap in which the attraction between an electron and a hole produces a bound state with a binding energy larger than the amount of overlap. It can be shown in the limit of weak electron-hole coupling that below a critical temperature condensation of excitons occurs which produces a low conductivity state known as an excitonic insulator. Although this is often called a Bose condensation in the literature, it has been pointed out by Kohn that this terminology is misleading [56]. Above the critical temperature the excitons break up which results in a second order excitonic insulator-semimetal transition. Although this model shows no large discontinuity in resistivity [57] there exists the possibility in the limit of strong electron-hole coupling that such a transition could produce a large jump in resistivity [58]. This model has been applied by McWhan and Rice to explain the properties of V_2O_3 [59], but it has since been withdrawn in favor of a model based on correlation effects which was discussed above [49]. Since the excitonic insulator model is based on the existence of a condensation of excitons in the insulating state, it should only be considered for materials which have a transition temperature well below room temperature. It also should only be applied to materials with a small band gap. Both of these considerations prevent its application to explain the properties of V_2O_4.

Berglund and Guggenheim have suggested that the transition in V_2O_4 may be simply the result of a change in the band structure which results from the distortion which occurs at the transition [30]. They assume that band theory applies to both the high and low temperature phases and that the distortion is caused by lattice effects. This theory is discussed in more detail in the next section.

Mott has recently proposed a complex model which also exhibits a conductivity discontinuity [60]. The necessary condition for his model is that a crystalline distortion occurs at a critical temperature and that the dielectric constant of the high temperature phase is much larger than that of the low temperature phase. Below the transition temperature the material is a Mott insulator with localized states arising from correlation effects, and above the transition temperature the material is composed of small polarons. This can occur when the binding energy of the small polarons is larger than the quasiparticle energy gap. The lattice transformation brings about the transition, and the transition temperature must be below one half the Debye temperature Θ in order that the polarons form a band [61]. Thus another transition is expected at a temperature around $\frac{1}{2}\,\Theta$ above which polaron conductivity is by hopping and the conductivity of the material is greatly reduced. This model requires the coincidence of a large number of particular material properties and therefore is unlikely to be observed experimentally.

Another model of the transition which is based on the electron-phonon interaction has been suggested by W. Paul and C. Hearn [62]. They speculate that the 3d electrons are critically intermediate in character between localized and band electrons so that they are easily excited yet sufficiently localized so that their excitation produces considerable local fluctuation in charge. It is argued that the phonon spectrum in the metallic state is softened more than the spectrum in the insulating state. Thus, although the latter is the stable phase at low temperature, increasing temperature raises the entropy of the metallic state preferentially, until at a critical temperature the free energy of the metallic state becomes equal to that of the insulator.

In summary, there are several theories which are capable of explaining semiconductor-metal transitions, and it appears that different materials may be described by different theories. Those theories which have been applied to V_2O_4 are discussed in the next section.

2. Recent Interpretations of V_2O_4

There are two theories which have recently been applied in detail to V_2O_4: the Fröhlich theory and the lattice induced transition theory. These theories will be analyzed in this section, and the properties of V_2O_4 will be discussed in detail in the next section.

Hyland [37] has attempted to show that the electrical, optical, magnetic, and thermodynamic properties and the insulator-metal

transition can be explained in terms of the Fröhlich theory [52] discussed in Section 1. There are three facts that must be demonstrated in order to show that this theory applies: (1) The high temperature state must be an ordinary metal with non-localized electrons; (2) the electrons in the low temperature state must be localized by correlation effects; and (3) the transition must be induced by an avalanche-like increase in the number of electrons and decrease in the electron activation energy just before the transition. This activation energy does not arise from a band gap, rather it is the amount of energy necessary to excite an electron from a localized ground state to a band like excited state. We will now briefly review and analyze Hyland's arguments for these three points.

To show that the electrons are not localized in the high temperature state, Hyland notes that the conductivity is high and that a plasma absorption edge is present in the infrared. He also notes that the magnetic susceptibility is larger than in the low temperature state. To show that the electrons are localized in the low temperature state, he notes that there is no plasma absorption edge in the infrared, that the magnetic susceptibility is constant and small, and that there is evidence from NMR measurements that the electrons are paired up. The argument that the electrons are not localized above T_c is reasonable even though the conductivity is much lower than that of a good metal. The argument that the electrons are localized in pair bonds below T_c is also reasonable.

Hyland does not offer any evidence that the transition is by an avalanche like process such as is required by the Fröhlich model. He says that there is some evidence that the conductivity activation energy decreases just before the transition, but that there is not enough data to prove or disprove this condition. Hyland's analysis, however, was written before our optical data on the temperature dependence of the energy gap was published [63]. Our data clearly shows that an avalanche like process does not occur. We can thus conclude from condition (3) alone that the Fröhlich model does not apply to V_2O_4.

Berglund and Guggenheim have attempted to show that ordinary band theory can be used to explain the properties of V_2O_4 [30]. They cite the photoemission data of Powell et al. [19] which shows that the 3d bands have bandwidths $\Delta \gtrsim 1$ eV as evidence that the semiconducting state need not be due to correlation effects. They also try to interpret the electrical, optical, magnetic, and thermal behavior of V_2O_4 in terms of ordinary band theory. They show that the latent heat of 1020 cal/mole must come largely from the lattice and they speculate that the distortion is caused by lattice effects similar to those observed in ferroelectrics. They then note that the lattice distortion causes a doubling of the number of bands which could lead to the formation of an energy gap in the low temperature state. They also note that the transition temperature does not depend much upon doping or upon the activation energy in the semiconducting state.

They thus attribute the semiconductor-metal transition to be the result of a change in the band structure which results from the lattice distortion at the transition temperature. Their analysis can be criticized in several respects. First their calculations of the properties of V_2O_4 in terms of band theory are not very convincing since they are only order of magnitude type calculations, and in particular the low mobility of both phases and the high magnetic susceptibility of the metallic phase are not readily explained in terms of band theory.

Berglund and Guggenheim's analysis also does not consider the magnetic, ESR, and NMR data mentioned in Section A which indicate that the electrons are paired up and localized below the transition temperature. Their speculation that correlation effects are not present because the bands are wide is also inconsistent with the recent results of Brinkman and Rice which were mentioned earlier in this section [47]. Their analysis also does not include a microscopic model of the transition. These points will be discussed in more detail in the next section.

We thus see that neither of the two explanations which have been presented to explain the properties of V_2O_4 is entirely satisfactory. In the next section we will present our interpretation of the properties of V_2O_4 and we will suggest some experiments which should lead to a resolution of some of the problems which are still unsolved.

C. Conclusions and Suggestions for Further Work

Our presentation of the work which we have done and the recent work done by other investigators is now complete and we are ready to discuss our interpretation of the properties of V_2O_4. We find that although a considerable amount of data has been amassed about the properties of V_2O_4, there are still many unresolved questions. In the first two sections the high and low temperature states will be considered, and the mechanism of the transition will be discussed in the next section. Finally, a short summary of the results of this research project and suggestions for further work will be presented in the last section.

1. Interpretation of the High Temperature State

The high conductivity and large infrared reflectivity suggest that above the transition temperature V_2O_4 has metallic properties due to the presence of a partly filled conduction band. In this section we will attempt to interpret the optical, transport, and magnetic properties of the high temperature state in terms of ordinary one electron band theory to see if this hypothesis is acceptable.

The crystal field splitting calculation of Hyland is a convenient starting place for analysis of the structure of the 3d bands of the high temperature phase [37]. Since V_2O_4 is considered to be an ionic crystal, we expect that there will be one unbonded electron per vanadium ion. This electron will be strongly attracted to the vanadium ions and repelled by the oxygen ions and we expect the tight

binding approximation to be more suitable than the free electron approximation. In this approximation the crystal field levels correspond to the band structure at k = 0. Hyland has shown that the orthorhombic crystal field splits the V^{4+} $(3d)^1$ level of the one unbounded electron per vanadium ion into five levels. By using electron spin resonance data from V doped TiO_2 and other spectroscopic data, he has calculated the results shown in Figure VI-6. There are two sites for vanadium ions in the crystal lattice which have local environments which are identical except for a 90° rotation about the crystal c-axis which corresponds to the y-axis in the figure. The levels are doubly degenerate for this reason and they are also doubly degenerate due to Kramer's theorem. Thus the band structure at k = 0 consists of five levels which are each fourfold degenerate. Away from k = 0 each of these bands will split into two bands which are identical except for a 90° rotation about the c-axis. Since there are two unbonded electrons per unit cell, the bottom band or bands will be partly filled. This simple band analysis thus predicts that V_2O_4 should be a metal above the transition temperature. Although this analysis ignores hybridization between the 3d and 2p levels, such hybridization does not affect the degeneracy of the levels at k = 0.

Let us now consider the optical properties of the high temperature phase. The measurements of Powell et al. [19] suggest that the Fermi level is about 2.5 eV above the top of the 2p bands and thus support our assumption that the conductivity is due to the 3d electrons.

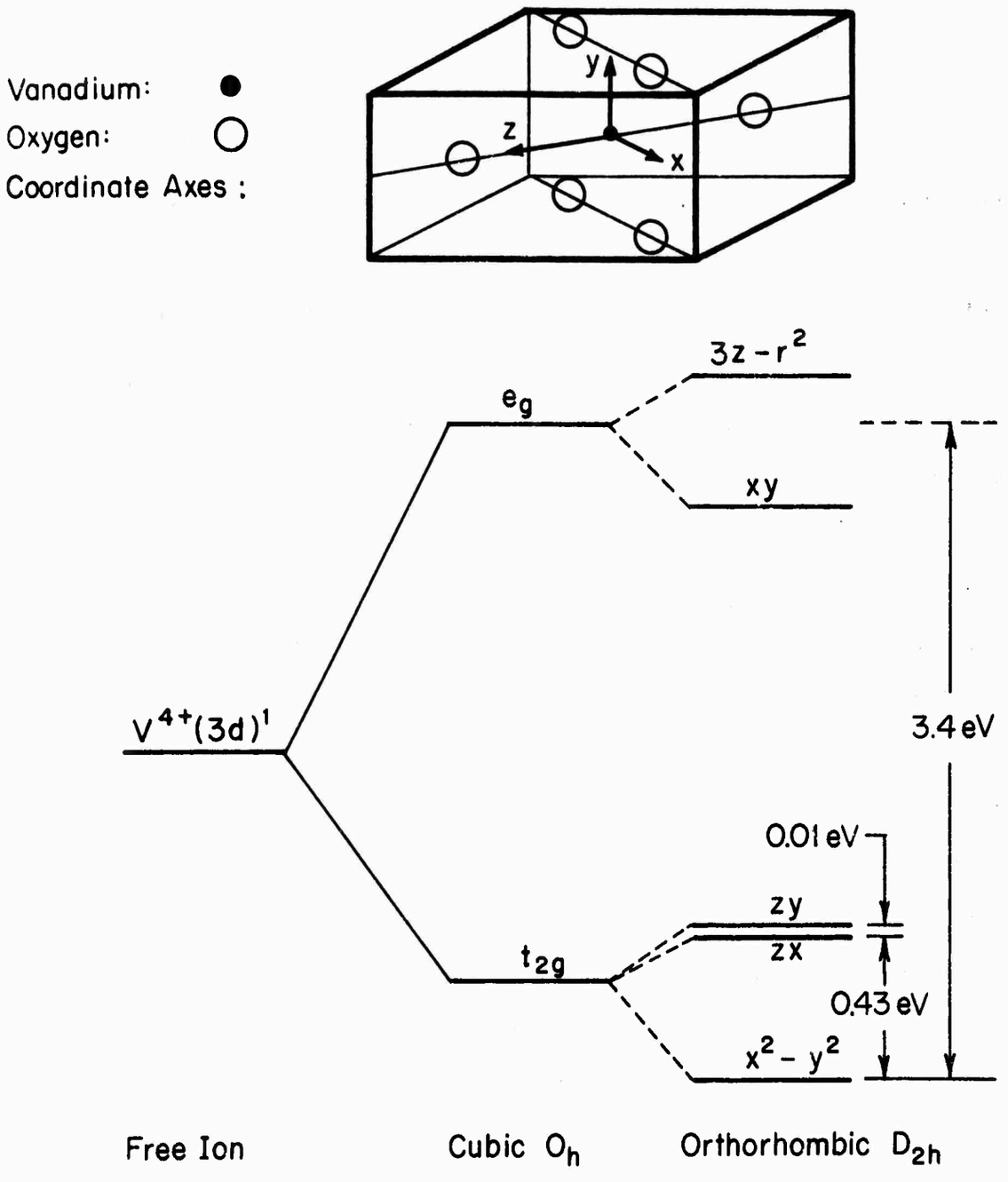

FIGURE VI-6 The crystal field splitting of the vanadium (3d) orbitals in tetragonal V_2O_4 as calculated by Hyland [37].

These measurements also indicate that the Fermi level lies in the middle of a partly filled conduction band. There are no sharp features in the reflectivity spectrum which would indicate bandwidths of less than 1 eV. There is a strong reflectivity peak at about 3 eV which is probably a 2p to 3d transition, but might also be a 3d to 3d transition.

Analysis of the infrared reflectivity spectrum can be used to determine some of the properties of the conduction band. The dielectric constant of a metal can be represented as $\epsilon(\omega) = 1 - \frac{\omega_p^2}{\omega(\omega + i/\tau_c)}$ [64], where $\omega_p^2 = \frac{4\pi n_c e^2}{m_a}$, n_c is the density of conduction electrons, τ_c is the relaxation time for the conduction electrons, and m_a is the average effective mass of the conduction electron:

$$\frac{1}{m_a} = \frac{1}{4\pi^3 n_c \hbar^2} \int d^3k \, \tfrac{1}{3} \nabla_k^2 E_c(k).$$

Although the free carrier absorption depends on the properties of the electrons at the Fermi surface, the above formulas were obtained by transforming a surface integral into a volume integral, and so the value of m_a represents an average over the entire occupied conduction band. A classical oscillator fit interpretation of the reflectivity such as was done by Verleur, Barker, and Guggenheim gives values of ω_p and τ_c [5]. In their analysis they used n_c = 0.1 electron per vanadium ion in accord with their interpretation of their Hall measurements, but as will be shown this is incorrect. If we assume that there is one electron per vanadium ion or $n_c = 3.4\ 10^{22}$ cm^{-3}, we

obtain $\omega_p = 4.2$ eV, $\tau_c = 5.3\ 10^{-16}$ sec, and $m_a = 3.2\ m_e$ for $E \parallel$ c-axis and $\omega_p = 3.56$ eV, $\tau_c = 6.2\ 10^{-16}$ sec, and $m_a = 3.2$ for $E \perp$ c-axis. These small values of τ_c give a large uncertainty in the energy of each state. Using the uncertainty principle we obtain that $\Delta E \sim \hbar/\tau_c \sim 1$ eV so that we do not expect the bandwidth to be less than 1 eV. If we use the effective mass approximation with the above values of $n_c = 3.4\ 10^{22}$ cm^{-3} and $m_a \sim 2m_e$ for a fourfold degenerate band, we obtain that $E_F = 1.2$ eV. This is a reasonable value since it corresponds to the bottom of the 3d band being approximately 1.3 eV above the top of the 2p band. Although we know the effective mass approximation is not valid, the above calculation gives us an idea of the bandwidth and relaxation time.

Let us now calculate the transport properties which would result from the above values of m_a and τ_c in the effective mass approximation. The mobility can be calculated as $\mu_{opt} = \frac{e\,\tau_c}{m_a} \sim 0.5$ cm^2/Vsec. The mean free path is $\Lambda = v_F \tau_F$, and we can assume that $\tau_F \sim \tau_c$ since in the calculation of m_a the Fermi surface relaxation time was involved. In the effective mass approximation $v_F = \frac{\hbar k_F}{m_a}$ and for $n_c = 3.4\ 10^{22}$ cm^{-3} in a fourfold degenerate band, $k_F = 0.8\ 10^8$ cm^{-1} and $v_F = 2.28\ 10^8$ cm/sec. We thus obtain $\Lambda = 1.35$ nm which is 3 to 5 times the nearest neighbor distance for vanadium cations in the crystal. Although this very short mean free path is not inconsistent with one electron band theory, it suggests that correlation effects may be present and responsible for the low mobility.

Let us now calculate the transport properties from transport data. If we set $\sigma = n e \mu$, then $n = 3.4\ 10^{22}\ cm^{-3}$ gives us that $\mu = 1.84\ cm^2/Vsec$. This is somewhat larger than the value μ_{opt} calculated above, but of the same order of magnitude. To compute the mobility from the Hall effect data is more difficult. The Hall constant is defined as $R_H = \frac{E_H}{HJ}$ and in the effective mass approximation $R_H = \frac{-1}{ne}$. Barker et al. measured the Hall voltage of three medium quality crystals and concluded that $n = \frac{-1}{R_H e} \sim 2.3\ 10^{21}\ cm^{-3}$ [21]. Hensler has measured the Hall constant of poor quality sputtered films and concluded that $n = \frac{-1}{R_H e} \sim 1.5\ 10^{23}\ cm^{-3}$ [18]. The big difference between these values shows us that the Hall constant depends upon crystal quality. In analyzing these data we must first realize that the interpretation of Barker et al. and of Hensler is misleading. Since the effective mass approximation is not valid then $R_H \neq \frac{-1}{ne}$ and so n cannot be computed. It is more reasonable to assume that there is one mobile electron per vanadium ion and that R_H is greater or lesser than $\frac{-1}{ne}$ depending upon the shape and properties of the Fermi surface. The sign of R_H indicates that the Fermi surface is mostly composed of portions that have positive effective mass. We thus see that no quantitative interpretation of the Hall effect data is possible since we do not know the shape of the Fermi surface. Similarly a quantitative interpretation of the thermoelectric power measurements is not possible and they will not be discussed here.

We will now consider the magnetic properties of the high temperature phase. The susceptibility is very large and nearly isotropic.

There are four contributions to the magnetic susceptibility: core diamagnetism, Landau diamagnetism, spin paramagnetism and Kubo temperature independent paramagnetism. The core diamagnetism is probably much smaller than the observed value of $\chi \simeq 8\ 10^{-6}$ emu/gram and will be ignored. In the effective mass approximation the ratio of the Landau diamagnetism to the spin paramagnetism is $|\chi_d/\chi_s| = (\frac{1}{3})(m_e/m^*)^2$ [37]. Thus if $m^* \gtrsim 2\ m_e$, we can also ignore the Landau diamagnetism. The Kubo temperature independent paramagnetism arises from the contribution of the orbital magnetic moment in metals with non s-like bands and is only present in narrow bands or when the density of states at the Fermi surface is quite large [65]. If we ignore the Kubo contribution for a moment and calculate the susceptibility based on a free electron approximation for a fourfold degenerate band with $m^* = 2m_e$, we obtain that $\chi \sim 2$ emu/gram. This is only 20% of the experimental value and suggests that the density of states at the Fermi level is somewhat larger than in the above model. If the effective mass is large at E_F or if there are overlapping bands at E_F, then the density of states would be large. Also if the density of states if fairly large, then there will be a contribution to the susceptibility from the Kubo paramagnetism. Thus the large susceptibility can probably be explained in terms of band theory, but correlation or exchange effects may also be present. The susceptibility falls off somewhat at higher temperatures, but good single crystal data which could be quantitatively interpreted is not available above 100°C.

Thus in summary we can say that there is strong evidence that the 3d bands are at least 1 eV wide in the high temperature state and that the conductivity occurs in a 3d band with an effective mass $m^* \sim 2\ m_e$ and an electron mobility $\mu \sim 1\ cm^2/Vsec$. The relaxation time and mean free path are probably quite short, but not inconsistent with band theory. The shape of the Fermi surface is not known and Hall effect and Seebeck effect data cannot therefore be easily interpreted. There is some anisotropy in the electrical properties which is to be expected since the crystal structure is anisotropic. The magnetic susceptibility is quite large, but not inconsistent with band theory. Thus the main features of the high temperature phase are consistent with a band theory model, but correlation and exchange effects may be present and responsible for the large magnetic susceptibility and low mobility.

2. Interpretation of the Low Temperature State

At the transition temperature the conductivity of our crystals changes by a factor of 10^5. The lower conductivity below the transition temperature can be explained by a reduction in the number of carriers or the mobility of the carriers or both. A lower mobility could arise from correlation effects or from polaron effects. A lower carrier concentration would occur if the ground state became non-conducting and there were an activation energy for the production of mobile electrons. Such a situation might arise if there were a gap in the one electron density of states, if the carriers were localized

in pair bands, or if the electrons were localized by correlation effects. In this section we will try and determine which of these effects are present. We will discuss the possible one electron band structure and the optical, transport, and magnetic properties. A model which is consistent with the properties of the low temperature state will then be presented.

In applying one electron band theory to the low temperature state we must take into account the distortion of the crystal structure which occurs at the transition. Below the transition temperature the unit cell doubles in size and there are four non-equivalent vanadium sites per unit cell. Thus there are twenty two-fold degenerate 3d bands in the first Brillouin zone. Since there are four unbonded electrons per unit cell, if there is a gap between the bottom two bands and the other eighteen bands the material would have a gap in the one electron density of states. This could give rise to an activation energy for the production of mobile carriers and a lowering of the number of carriers below the transition temperature.

Our optical measurements on the low temperature phase show that there is an energy gap at room temperature. The absorption coefficient rises to approximately 10^5 cm^{-1} near 1 eV as is shown in Figure IV-13. The photoemission measurements of Powell _et al._ also indicate a gap in the electronic density of states at the Fermi level [19]. Thus the optical data are consistent with a model of the low temperature

phase in which there is a gap in the electronic density of states which would produce an activation energy for carrier production. Such a gap in the density of states could arise in terms of an ordinary one-electron band model, a model in which the electrons are localized by correlation, or a model in which the electrons are localized in pair bonds. In both of the last two cases there are excited states for the system whose energy is greater than the ground state energy by an amount which corresponds to individual electrons being excited across an energy gap equal to that found in the density of states measurement.

If we assume that band theory applies to V_2O_4, then we can calculate ξ, the distance of the Fermi level from the conduction band. Using the effective mass approximation, the measured Hall mobility of $\mu = 0.5\ cm^2/V\ sec$, and assuming that $m^* \sim 2\ m_e$, we obtain that $\xi \sim 0.15$ eV near the transition temperature. At 100^oK ξ increases to ~ 0.25 eV. If the energy gap is assumed to be 0.6 eV at room temperature then the conductivity is clearly not intrinsic. Looking back at Figure IV-13, however, we see that the absorption edge is not very sharp. Thus a lower value of the energy gap is also consistent with the optical data. If the energy gap is assumed to be ~ 0.3 eV near the transition temperature then the conductivity would be intrinsic. This would explain the consistency from sample to sample of the low temperature resistivity data shown in Figure III-8. More variation would be expected from non-intrinsic conductivity.

We will now consider the interpretation of the transport measurements. First we will consider whether or not the Hall data are compatible with one electron band theory. Using a one band model Rosevear and Paul have obtained a mobility $\mu_H = 0.5\ cm^2/Vsec$ which is almost independent of temperature [26]. In order to compute the electron scattering time τ, we will set $\mu_H = \frac{e\tau}{m^*}$ where e is the charge on the electron and m* is the electron effective mass. If we assume that the effective mass is approximately twice the free electron mass in accord with the free carrier absorption measurements of Verleur et al. [5], we obtain that $\tau = 5.7\ 10^{-16}$ sec which is quite small. Although this effective mass measurement may not be very accurate, it will serve for a first approximation. The mean free path Λ is given by $\Lambda = v\tau$ where v is the carrier velocity in the conduction band. If we set $\frac{1}{2}\ m^*v^2 = kT$, this will give the statistically most probable velocity of a conduction electron and we obtain that $\Lambda = 60$ pm. This distance is only 20% of the average vanadium-vanadium spacing, making the application of the usual theory of an itinerant electron suffering occasional scattering inappropriate. This short mean free path cannot be attributed to polaron effects. Using the optical measurements of Barker et al. [27] Berglund and Guggenheim have calculated that the electron phonon coupling costant $\alpha \simeq 2$ which means that the polaron effective mass is only twice the normal effective mass [30].

A two band model could explain the low value of the Hall constant. In this case the electron and hole contributions to the Hall voltage would be nearly equal and of opposite polarity and the mobility and mean free path of each type of carrier could be many times the value calculated above. The mean free path, however, would still be quite short and correlation effects can be assumed to be present. A two band model is much more likely to be applicable if the conductivity is intrinsic since the product $R_H\sigma$ is nearly independent of temperature. This means that the electron hole ratio must be independent of temperature which is quite unlikely for the case of extrinsic conductivity. An implicit result of the above analysis is that the conductivity can be written $\sigma = ne\mu$ and that the carrier concentration is determined by an activation energy. The $\sigma(\omega)$ measurements of Kabashima *et al.* [24] indicate that both band and hopping conductivity are present and suggest that a simple model with only one type of conductivity may not be appropriate. In summary the transport measurements indicate that the number of carries is governed by an activation energy, that correlation effects are responsible for the low mobility, and that more than one type of conductivity may be present.

We will now consider the interpretation of the magnetic properties. NMR [33] and ESR [34,35] measurements indicate that

the electrons are paired up below the transition temperature. Magnetic susceptibility measurements [17] indicate that there are localized states present in doped crystals and suggest that the electrons may be paired up in undoped crystals. The magnetic data reported by Rudorff et al. for the mixed oxide system $V_{1-x}\ Ti_x\ O_2$ [66] has recently been interpreted by Rice et al. [67], as indicating that the electrons are paired up in non-magnetic bonds. They have further suggested that the lack of magnetic ordering in the low temperature phase shows that one electron band theory is applicable. They have also presented a calculation which shows that the ground state energy of a state with paired up cations and electrons trapped in pair bonds on these cation pairs can be lower than the ground state energy of a Mott insulator [67]. Thus the magnetic measurements suggest that the electrons are trapped in pair bonds and that one electron band theory applies.

In conclusion we will present a model which is consistent with the above experimental data and analysis. The electrons appear to be localized in non-magnetic pair bonds on the paired cations, and their properties appear to be describable by one electron band theory. The Hall mobility and the mean free path is quite short, however, which indicates that correlation effects are also probably present. The bandwidth of the conduction band is approximately 1 eV and there is a band gap at room temperature.

3. Interpretation of the Transition Mechanism

Before we consider the possible mechanisms of the transition we will analyze the thermodynamics of the transition. We will consider the free energy of the low and high temperature phases and show that the latent heat must arise largely from an increase in the lattice entropy at the transition. The different possible mechanisms of the transition and their compatibility with thermodynamic data will then be discussed and a model which is consistent with the thermodynamic data will be presented.

We will begin our thermodynamic analysis by trying to account for the large latent heat L = 1020 cal/mole (VO_2) [30]. We know from elementary thermodynamic considerations that the latent heat L is equal to the difference in the entropy of the two phases times the temperature. In estimating the entropy of the two phases we have to consider both electronic and lattice contributions.

The entropy of the electrons can be calculated from the formula

$$TS = kT \sum \left[n \log \left(\frac{1}{n} - 1 \right) - \log (1 - n) \right]$$

which is valid for Fermi statistics if the sum is over all the electron states and $n = \frac{1}{e^x + 1}$ where $x = \frac{E - E_F}{kT}$ [68]. For the low temperature phase we know that the material has a bandgap and so we can use the formula for a semiconductor:

$$TS = kT\left[\tfrac{5}{2}(N+P) + N\frac{E_c - E_F}{kT} + P\frac{E_F - E_v}{kT}\right]$$

where N and P are the number of electrons and holes per mole [69]. If we assume that the carriers are electrons with a mobility $\mu \sim 0.5$ cm^2/Vsec and an effective mass $m^* \sim 2\ m_e$, we obtain $E_c - E_F \sim 0.15$ eV, $N = n\ V_{mole} = 3.38\ 10^{-17}$ electrons/mole (VO_2), and $TS \sim 0.3$ cal/mole (VO_2). This value of entropy is negligible compared to the latent heat of 1 kcal/mole (VO_2).

We have already shown in Section 1 that one electron band theory appears to be applicable to the high temperature state. When $T \ll T_F$ we have that

$$TS = \tfrac{1}{2}\pi^2 NkT\left(\frac{kT}{E_F}\right) \qquad [70].$$

If we use the effective mass approximation with $m^* \sim 2\ m_e$, we obtain that $TS \sim 100$ cal/mole (VO_2). Although the effective mass approximation will not be valid, the entropy only depends upon the density of states at the Fermi surface. In Section 1 we mentioned that magnetic susceptibility measurements suggest that the density of states at the Fermi level may be higher than the above estimate. There is, however, a maximum value of the electronic entropy for narrow bands which is 0.69 k per electron. Thus the maximum

electronic entropy contribution is TS = 460 cal/mole (VO_2) which is less than half of the latent heat. Thus most of the latent heat must be supplied by the lattice.

The thermodynamic properties of the lattice are determined by Bose statistics and the entropy is given by

$$TS = kT \int_0^\infty \sigma(\omega) dw [n \log \left(1 + \frac{1}{n}\right) + \log (1+ n)]$$

where $\int_0^\infty \sigma(\omega) dw = 3N$, N is the number of atoms per mole, $n = \frac{1}{e^x - 1}$, and $x = \frac{\hbar\omega}{kT}$ [68]. We will use the Debye approximation to estimate $\sigma(\omega)$ and write

$$\sigma(\omega) = \begin{cases} \frac{3\ V_{mole}}{2\ \pi^2 c^3}\ \omega^2 & \omega < \omega_D \\ 0 & \omega > \omega_D \end{cases}$$

where V_{mole} is the volume/mole and c is the average speed of sound [71]. For V_2O_4, V_{mole}=18.7 cm^3, and $\Theta = \frac{\hbar\omega_D}{k}$ = 750°K [30] so that c = 5.4 10^5 cm/sec. We also have $x_D = \frac{\hbar\omega_D}{kT_c}$ = 2.22 and so at 338°K

$$TS = 2.12\ \frac{kcal}{mole\ (VO_2)} \int_0^{2.22} x^2 dx\ [nx + \log\ (1+ n)]\ .$$

A graphical integration of this formula gives TS = 4.87 kcal/mole (VO_2) which is approximately five times the latent heat. Thus a 20% change in the lattice entropy would account for the entire latent heat.

Let us now consider in some detail the lattice modes and how they differ from the Debye approximation. In the low temperature phase there are twelve atoms per unit cell and so there are 12

branches of the phonon spectrum including 12 longitudinal and 24 transverse modes. The volume of the Brillouin zone can be used to calculate an average $k_{BZ} = 0.79\ 10^8\ cm^{-1}$ from the relation (volume of B.Z.) $= \frac{4}{3}\pi\ (k_{BZ})^3$. In the high temperature phase there are 6 atoms per unit cell and one half as many branches and modes of the phonon spectrum and $k_{BZ} = 10^8\ cm^{-1}$. We know the approximate range of the transverse optical modes in the low temperature phase from the infrared reflectivity measurements of Barker et al. [27]. The values of the longitudinal modes can be estimated from the generalized Lyddane-Sachs-Teller relationship which is

$$\left|\frac{\epsilon(0)}{\epsilon(\infty)}\right|^{\frac{1}{2}} = \frac{\omega_{\ell_1}\ \omega_{\ell_2}\ \cdots\ \omega_{\ell_n}}{\omega_{t_1}\ \omega_{t_2}\ \cdots\ \omega_{t_n}}$$

when there are n optical branches of the phonon spectrum [72]. The ratio $\sqrt{[\epsilon(0)/\epsilon(\infty)]}$ is about three [27], and there are eleven optical branches in the low temperature phonon spectrum, thus we estimate $\omega_{\ell_1} \sim \omega_{t_1}$ and $\omega_{\ell_{11}} \sim 1.3\ \omega_{t_{11}}$ If we assume typical shapes for the acoustic modes, we obtain the spectrum shown in Figure VI-7.

The phonon spectrum of the high temperature phase cannot be estimated as readily since the free carrier absorption masks the optical properties of the phonons. Above the transition temperature there are 18 modes in the phonon spectrum. Since we estimate that the electron latent heat is around 200 cal/mole (VO_2), the lattice latent heat must be around 800 cal/mole (VO_2). Thus some or all of the lattice modes must soften. If they all soften equally, then

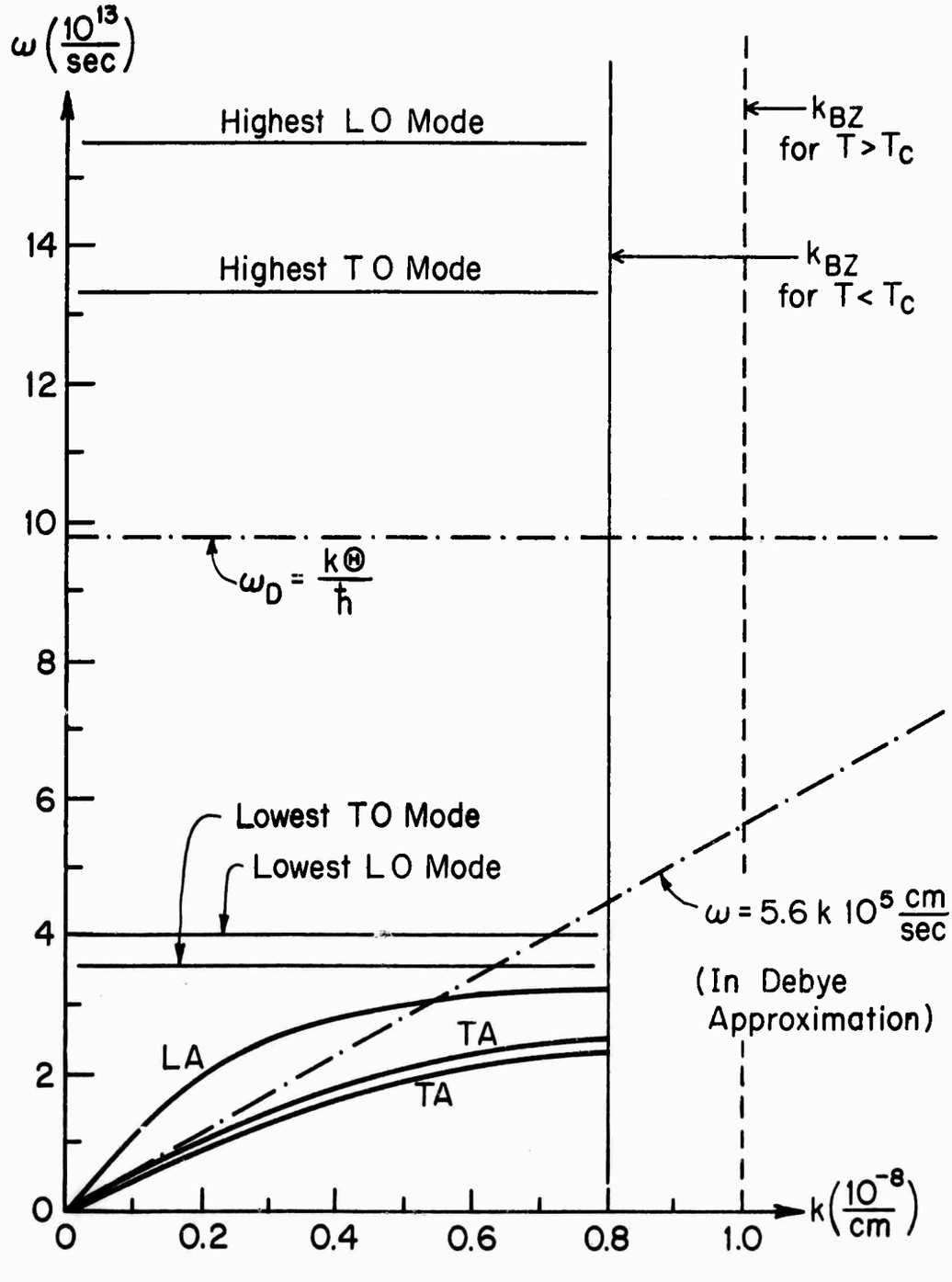

FIGURE VI-7 Estimated phonon spectrum of V_2O_4 in the low temperature phase.

the average phonon energy would be 16% lower in the metallic state. If one acoustic or optical mode softened from an average value of $x = \frac{\hbar\omega}{kT_c} = 1.0$ to $x = 0.3$ this would produce a latent heat of 500 cal/mole (VO_2). The lattice share of the latent heat can thus be contributed by the softening of one mode or several modes or all of the modes. These different possibilities will be discussed in more detail later in this section.

Let us now consider the internal energy change of the crystal during the transition. Since $F = U - TS$ is the same for both phases at the transition temperature, $\Delta U = -\Delta(TS)$ and the internal energy is smaller by 1 kcal/mole (VO_2) in the metallic state. The internal energy is contributed by both the electrons and the lattice. The lattice energy consists of the zero point energy and the phonon energy. Using the Debye approximation we can estimate the zero point energy to be $U_o = \Sigma_i \frac{1}{2}\hbar\omega_i \sim 6.5$ kcal/mole (VO_2) and the phonon energy to be $U_{ph} = \int_o^{\omega_D} \sigma(\omega) n \hbar\omega d\omega \sim 7.5$ cal/mole (VO_2). A softening of the phonon spectrum by 16% would result in a 5% decrease in the internal energy or ΔU_{ph} 700 cal/mole (VO_2). Thus the increase in the electronic energy of the metallic state is approximately 1.7 kcal/mole (VO_2). This however only amounts to about 0.1 eV/vanadium ion which is smaller than the band gap energy.

The above analysis shows that the transition temperature is determined by the value of the Helmholtz function $F = U - TS$ in the low and high temperature phases. The entropy of the metallic state is higher than the entropy of the semiconducting state mostly as a result of a

softening of some of the lattice modes. The internal energy of the semiconducting state is smaller than the internal energy of the metallic state as a result of both electronic and lattice contributions. Thus at low temperatures F = U - TS is smallest for the semiconducting state, whereas as the temperature increases the contribution of the TS term becomes more important and above the transition temperature F is smallest for the metallic state.

From the above analysis we see that any theory of the transition must include both lattice and electronic contributions. In fact at the transition several important phenomenon occur which must be accounted for: the lattice distorts, the conductivity changes, the phonon spectrum changes, the crystal internal energy changes, an energy gap opens up in the density of states, the magnetic properties change, and the optical properties change. It is very difficult to attribute all of these changes to be the result of any one mechanism such as correlation effects, the formation of pair bonds as described by Adler and Brooks [43] or by Rice et al. [67], or the distortion of the lattice as a result of some unspecified mechanism as described by Berglund and Guggenheim [30]. It is most likely that a combination of effects occur which results in the semiconductor-metal transition.

Let us consider a composite model which is in accord with the interpretation of the high and low temperature states presented in the last two sections and the above thermodynamic analysis. Above

the transition temperature V_2O_4 can be considered to be a metal with itinerant electrons whose mobility is very possibly reduced by correlation effects. Below the transition temperature it appears that the electrons are localized in pair bonds, and that some correlation effects are present and responsible for the low mobility. The distortion of the lattice can be considered to be responsible for changing the band structure and producing an energy gap. The distortion also can be considered to favor the localization of the electrons in pair bands. The change in the optical, magnetic, and electrical behavior can be considered to be due to the change in the band structure and the pairing of the electrons. To complete this model, a mechanism which results in a softening of the lattice modes in the metallic state must be found. The explanation of this phenomenon is probably related to the fact that the electron lattice interaction is quite large in V_2O_4. Paul has suggested that the unbonded electrons in V_2O_4 are critically intermediate in nature between localized and itinerant states and that this results in a very large electron lattice interaction [62]. One mechanism for the softening of the lattice modes in the metallic state which has not been mentioned before is a reduction of the dielectric constant by screening. The longitudinal acoustic mode in particular will be reduced in energy by the presence of a large number of conduction electrons [73]. As was shown above, if this mode softens from an average value of $x = \frac{\hbar\omega}{kT_c} = 1.0$ to $x = 0.3$ this would contribute one

half of the latent heat. The rest of the latent heat could be contributed by softening of other modes and the electronic contribution. Another possible mechanism might involve the softening of modes which correspond to optical vibrations of the paired cations.

We feel that the model described above is consistent with all of the experimental information now available and is more satisfactory than any of the other models which so far have been presented. There is, of course, still some uncertainty concerning the reason for the softening of the lattice modes in the metallic state, and suggestions for further work are discussed in the next section.

4. Summary of the Results of this Investigation and Suggestions for Further Work

This investigation has resulted in several new experimental results and in a better understanding of some of the properties of V_2O_4. In this section we will review these results and then suggest further work which would help to clarify some of the problems which are still outstanding.

One of the results of this investigation has been the growth of better crystals with a higher resistivity ratio than had been previously available. The conductivity, reflectivity and transmission of these crystals was measured both above and below the transition temperature. Conductivity measurements were also made during the transition process. An optical absorption edge was found in the low temperature state and its temperature dependence was carefully measured

near the transition temperature. The dependence of the semiconducting conductivity and the transition temperature on uniaxial stress was also determined.

These measurements and the recent experimental and theoretical work of other investigators has resulted in a better understanding of the properties of V_2O_4. The high temperature state appears to have a partly filled conduction band and metallic conductivity. The mean free path is short, however, and correlation effects are probably present. The low temperature state is probably described by one electron band theory and is characterized by the fact that the 3d electrons are localized in pair bands. Correlation effects are probably present and account for the extremely low mean free path. The measurement of the temperature dependence of the energy gap shows that a transition in which the number of carriers avalanches such as is described in the second order Adler-Brooks theory [43], in the theory of Falicov and Kimball [54], or in the Fröhlich theory as discussed by Hyland [37] is not present. A thermodynamic analysis was performed which suggests that the transition is best characterized as being due to the difference in Helmholtz function $F = U - TS$ between two phases with different crystal structures, band structures, and phonon spectrums. The change in the phonon spectra and the change in the band structure were said to be related since the electron-phonon interaction is large, and a model relating the change in the phonon spectrum to the change in the number of carriers via screening effects was suggested.

We will now present some suggestions for further work which would help resolve some of the outstanding problems. We can not think of any experiments which would make a big difference in our understanding of the metallic state. There are two areas of investigation that would help in understanding the properties of the low temperature phase. First, a better theoretical understanding of the properties of materials with low values of mobility would help in interpretation of the experimental data. Second, the growth and measurement of high quality doped crystals would also be quite informative. A systematic investigation of the electrical, magnetic, and optical properties of such crystals should give some insight into the behavior of V_2O_4 below the transition temperature and might reveal whether or not the conductivity is intrinsic. There are two main areas of investigation which would contribute to a better understanding of the transition mechanism. First, the properties of the phonon spectrum above and below the transition temperature should be investigated using techniques such as Raman scattering, speed of sound, X-ray diffraction, neutron scattering, and high temperature specific heat measurements. This would help to reveal what part the lattice plays in the transition. Second, the transition should be studied in tungsten doped V_2O_4 and in the Magneli phases. One percent of tungsten lowers the transition temperature by 80°C and the reason for this large effect should be determined. The Magneli phases are crystal structures which are very closely related to the rutile structure and many of them have transitions. A comparison of the properties of these phases to the properties of V_2O_4 might help to clarify the transition mechanism.

Chapter VI

REFERENCES

[1] H. Sasaki and A. Watanabe, J. Phys. Soc. Jap., 19, 1748 (1964).

[2] Y. Bando, K. Nagasawa, Y. Kato, and T. Takada, Jap. J. Appl. Phys., 8, 633 (1969).

[3] J.B. MacChesney and H.J. Guggenheim, J. Phys. Chem. Solids, 30, 225 (1969).

[4] L.E. Sobon and P.E. Greene, J. Am. Ceram. Soc., 49, 106 (1966).

[5] H. Verleur, A. Barker, and C. Guggenheim, Phys. Rev., 172, 788 (1968).

[6] P.J. Fillingham, J. Appl. Phys., 38, 4823 (1967).

[7] J. Umeda, S. Ashida, H. Kusumoto, and K. Narita, J. Phys. Soc. Japan, 21, 1461 (1966).

[8] T. Mitsuishi, Jap. J. Appl. Phys., 6, 1060 (1967).

[9] N. Nygren and M. Israelsson, Matl. Res. Bull., 4, 881 (1969).

[10] M. Israelsson and L. Kihlborg, Matl. Res. Bull., 5, 19 (1970).

[11] G. Andersson, Acta Chem. Scand., 8, 1599 (1954).

[12] K. Nagasawa, Y. Bando, and T. Takada, Jap. J. Appl. Phys., 8, 1262 (1969).

[13] H. Okinaka, K. Nagasawa, K. Kosuge, Y. Bando, T. Takada, and S. Kachi, J. Phys. Soc. Jap., 27, 1366 (1969).

[14] H. Okinaka, K. Nagasawa, K. Kosuge, Y. Bando, S. Kachi and T. Takada, J. Phys. Soc. Jap., 28, 798 (1970).

[15] H. Okinaka, K. Nagasawa, K. Kosuge, Y. Bando, S. Kachi, and T. Takada, J. Phys. Soc. Jap., 28, 803 (1970).

[16] J.B. MacChesney, J.F. Potter, H.J. Guggenheim, J. Electrochem. Soc., 115, 52 (1968).

[17] K. Kosuge, J. Phys. Chem. Solids, 28, 1613 (1967).

[18] D.H. Hensler, J. Appl. Phys., 39, 2354 (1968).

[19] R.J. Powell, C.N. Berglund, and W.E. Spicer, Phys. Rev., 178, 1410 (1969).

[20] T.N. Kennedy and J.D. Mackenzie, J. Non-Cryst. Solids, 1, 326 (1969).

[21] J.D. Mackenzie, J. Vac. Sci. Tech., 6, 658 (1969).

[22] W. Paul, Matl. Res. Bull., 5, 691 (1970).

[23] C.R. Everhart and J.B. MacChesney, J. Appl. Phys., 39, 2872 (1968).

[24] S. Kabashima, Y. Tsuchiya, and T. Kawakubo, J. Phys. Soc. Japan, 22, 923 (1967).

[25] C.N. Berglund and A. Jayaraman, Phys. Rev., 185, 1034 (1969).

[26] W. Rosevear and W. Paul, Bull. Am. Phys. Soc., Ser. II, 15, 316 (1970).

[27] A.S. Barker, H.W. Verleur, and H.J. Guggenheim, Phys. Rev. Lett., 17, 1286 (1966).

[28] P.F. Bongers, Solid State Comm., 3, 275 (1965).

[29] I. Kitahiro and A. Watanabe, J. Phys. Soc. Jap., 21, 2423 (1966).

[30] C.N. Berglund and H.J. Guggenheim, Phys. Rev., 185, 1022 (1969).

[31] K. Kosuge, J. Phys. Soc. Jap., 22, 551 (1967).

[32] T. Shinjo, K. Kosuge, S. Kachi, and H. Takada, J. Phys. Soc. Jap., 21, 193 (1966).

[33] J. Umeda, S. Ashida, H. Kusumoto, and K. Narita, J. Phys. Soc. Jap., 21, 1461 (1966).

[34] J. Umeda, K. Kusumoto, and K. Narita, J. Phys. Soc. Jap., 21, Suppl., 619 (1966).

[35] T. Goto, K. Nishimura, S. Kabashima, and T. Kawakubo, J. Phys. Soc. Jap. 28, 993 (1970).

[36] G.J. Hill and R.H. Martin, Phys. Lett., 27A, 34 (1968).

[37] G.J. Hyland, J. Phys. C 1, 189 (1968).

[38] O.A. Cook, J. Am. Chem. Soc., 69, 331 (1947).

[39] W. Klemm and L. Grimm, Naturwiss., 27, 787 (1939).

[40] T. Kawakubo and T. Nakagawa, J. Phys. Soc. Jap., 19, 517 (1964).

[41] L.L. Van Zandt, J.M. Honig, and J.B. Goodenough, J. Appl. Phys., 39, 593 (1968).

[42] J.C. Slater, Phys. Rev., 82, 538 (1951).

[43] D. Adler and H. Brooks, Phys. Rev., 155, 826 (1967).

[44] J.T. Sparks and T. Komoto, Rev. Mod. Phys., 40, 752 (1968).

[45] J. Trahan, R.G. Goodrich, and S.F. Watkins, Phys. Rev., B 2, 2859 (1970).

[46] D. Adler, Solid State Phys., 21, 1 (1968).

[47] W.F. Brinkman and T.M. Rice, Phys. Rev., B 2, 1324 (1970).

[48] W. Langer, M. Plischke, and D. Mattis, Phys. Rev. Lett., 23, 1448 (1969).

[49] D.B. McWhan, T.M. Rice, and J.P. Remeika, Phys. Rev. Lett., 23, 1384 (1969).

[50] N.F. Mott, Proc. Phys. Soc (London), A62, 416 (1949).

[51] J. Feinleib and W. Paul, Phys. Rev., 155, 841 (1967).

[52] H. Fröhlich, Contribution to Quantum Theory of Atoms, Molecules, and the Solid State, pp. 465-468, Academic Press, Inc., New York, 1966.

[53] G.J. Hyland, Rev. Mod. Phys., 40, 739 (1968).

[54] L.F. Falicov and J. Kimball, Phys. Rev. Lett., 22, 997 (1969).

[55] B.I. Halperin and T.M. Rice, Solid State Phys., 21, 115 (1968).

[56] See discussion following the paper by B.I. Halperin and T.M. Rice, Rev. Mod. Phys., 40, 755 (1968).

[57] D. Jerome, T. Rice, and W. Kohn, Phys. Rev., 158, 462 (1967).

[58] B.I. Halperin and T.M. Rice, Rev. Mod. Phys., 40, 755 (1968).

[59] D.B. McWhan and T.M. Rice, Phys. Rev. Lett., 22, 887 (1969).

[60] N.F. Mott., Phil. Mag., 20, 1 (1969).

[61] T. Holstein, Ann. Phys., 8, 343 (1959).

[62] Private communication from W. Paul, Harvard University, Cambridge, Mass.

[63] L. Ladd and W. Paul, Solid State Comm., 7, 425 (1969).

[64] M.H. Cohen, Phil. Mag., 3, 762 (1958).

[65] R. Kubo and Y. Obata, J. Phys. Soc. Jap., 11, 537 (1956).

[66] W. Rudorff, G. Walters, and S. Stadler, Z. anorg. allg. Chemie, Bd. 297, 1 (1958).

[67] T.M. Rice, D.B. McWhan, and W.F. Brinkman, Proc. Tenth International Conference on Physics of Semiconductors, Cambridge, Mass., 1970.

[68] K. Huang, Statistical Mechanics, p. 196, John Wiley and Sons, Inc., New York, 1963.

[69] P.M. Morse, Thermal Physics, Prelim. Edition, p. 189, W.A. Benjamin, Inc., New York, 1962.

[70] P.M. Morse, Thermal Physics, Prelim. Edition, p. 235, W.A. Benjamin, Inc., New York, 1962.

[71] C. Kittel, Introduction to Solid State Physics, Third Ed., p. 164, John Wiley and Sons, Inc., New York, 1966.

[72] A.S. Barker, Phys. Rev., 136, 1240 (1964).

[73] J.M. Ziman, Principles of the Theory of Solids, p. 173, Cambridge University Press, Cambridge, 1964.

ACKNOWLEDGMENTS

I would like to thank Professor William Paul for suggesting this research topic, for directing this research, and especially for his helpful editorial comments and the discussions we had during the preparation of this manuscript.

This research has benefited greatly from the careful work of Dave McLeod in preparing and mounting fragile samples for measurements and the assistance and advice of James Inglis and Albert Manning in making some of the apparatus and equipment which was used in the measurements.

I have received a considerable amount of help and advice from Professor Paul's past and present students and past doctoral fellows. In particular, I would like to thank John Fan for checking one of my optical measurements and Bill Rosevear, John Fan and Nigel Shevchik for help in getting this manuscript prepared while I was working at Raytheon.

This work was supported by the Advanced Research Projects Agency and the Office of Naval Research.